FPGA IMPLEMENTATION OF WAVELET BASED TECHNIQUES FOR MEASUREMENT OF POWER QUALITY PARAMETERS

Ph.D. Thesis

By

VINAY KUMAR TIWARI

DISCIPLINE OF ELECTRICAL ENGINEERING

INDIAN INSTITUTE OF TECHNOLOGY INDORE

AUGUST, 2020

FPGA IMPLEMENTATION OF WAVELET BASED TECHNIQUES FOR MEASUREMENT OF POWER QUALITY PARAMETERS

A THESIS

Submitted in partial fulfillment of the
requirements for the award of the degree
of
DOCTOR OF PHILOSOPHY

by

VINAY KUMAR TIWARI

DISCIPLINE OF ELECTRICAL ENGINEERING
INDIAN INSTITUTE OF TECHNOLOGY INDORE

AUGUST, 2020

INDIAN INSTITUTE OF TECHNOLOGY INDORE

CANDIDATE'S DECLARATION

I hereby certify that the work which is being presented in the thesis entitled "**FPGA Implementation of Wavelet Based Techniques for Measurement of Power Quality Parameters**" in the partial fulfillment of the requirements for the award of the degree of **DOCTOR OF PHILOSOPHY** and submitted in the **DISCIPLINE OF ELECTRICAL ENGINEERING, Indian Institute of Technology Indore**, is an authentic record of my own work carried out during the time period from September 2015 to August 2020 under the supervision of Dr. Amod C. Umarikar, Associate Professor, Indian Institute of Technology Indore, India and Dr. Trapti Jain, Associate Professor, Indian Institute of Technology Indore, India .

The matter presented in this thesis has not been submitted by me for the award of any other degree of this or any other institute.

Vinay kumar tiwari 24/08/2020
Signature of the student with date
(VINAY KUMAR TIWARI)

This is to certify that the above statement made by the candidate is correct to the best of our knowledge.

24/08/2020
Signature of Thesis Supervisor #1 with date
(Dr. AMOD C. UMARIKAR)

Jain 24/08/2020
Signature of Thesis Supervisor #2 with date
(Dr. TRAPTI JAIN)

VINAY KUMAR TIWARI has successfully given his Ph.D. Oral Examination held on 08 March 2021.

Dr. Aruna Tiwari
Signature of Chairperson (OEB)
Date: 8/3/2021

Signature of External Examiner
Date: 08/03/2021

Dr. Amod C. Umarikar
Signature of Thesis Supervisor #1
Date: 08/03/2021

Jain
Signature of Thesis Supervisor #2
Date: 08/03/2021

Dr. S. K. Vishvakarma
08/03/2021
Signature of PSPC Member #1
Date:

(Dr. Surya Prakash)
Signature of PSPC Member #2
Date: 08-Mar-2021

(Swaminathan R)
Signature of Convener, DPGC
Date: 08/03/2021

(Dr. Vipul Singh)
08/03/2021
Signature of Head of Discipline
Date:

ACKNOWLEDGEMENTS

I take this opportunity to acknowledge my heartfelt gratitude to many people who have directly or indirectly helped me throughout my Ph.D. candidature.

On the completion of this work, I feel immense pleasure in expressing my deep sense of gratitude to my supervisor Dr. Amod C. Umarikar and co-supervisor Dr. Trapti Jain. Dr. Amod C. Umarikar is always there to motivate and encourage me. His inspiring guidance, constructive suggestions, practical skills, and logical thinking have been helpful for me throughout my doctoral work. I would also like to express my gratitude to Dr. Trapti Jain for her valuable suggestions, technical writing skills, timely help and bilateral discussions to improve the quality of work. I am truly indebted for their valuable guidance, directions, coordination, positive criticism and the support given throughout the work.

I am extremely grateful to my doctoral progress committee members, Dr. Santosh K Vishvakarma and Dr. Surya Prakash, for their encouragement, insightful suggestions and valuable comments, which helped me in improving my research work.

I express my profound appreciation to my colleagues Ajinkya J. Sonawane, Suvamit Chakraborty, Dr. Karthik Thirumula, Dr. Joice Philip, Dr. Prateek Jain, Dr. P. Raju and Dr. T. Venkatesh for their trustworthy help, constant encouragement and moral support during the tough time and research work.

I would like to thank IIT Indore for providing the essential research facilities for my research work. Also, I would like to express my sincere gratitude to Ministry of Human Resource Development (MHRD), Government of India for providing the teaching Assistantship during the Ph.D.

I express my gratitude to Dr. Sachin K. Jain (Assistant Professor, IIITDM Jabalpur) who inspired and motivated me to carry out research since my post-graduation.

Last but not least, I would like to thank my parents and elder brother, who educated me, for always believing in my capabilities and encouraging me to pursue my dreams. My special thanks go to my beloved wife for her loving support, care and always being there for me during good and bad times. Without them, I would not be in the position, where I am today.

Vinay Kumar Tiwari

Dedicated to my

Parents and Teachers

ABSTRACT

Rapid growth in high-power semiconductor devices and electronic converters technologies facilitates the efficient and economical utilization of distributed and renewable energy sources in the emerging power system. Local power control equipment, power electronic-based equipment and protection circuits are also being used in domestic and industrial sectors. The high proliferation of these non-linear loads has led to the deterioration of power supply quality from the transmission to distribution level. Power quality monitoring is a procedure of gathering, investigating and interpreting raw electrical measurement data into useful information. The power quality monitoring helps in energy management, preventive maintenance, quality control and the design and development of metering instruments. Therefore, continuous monitoring of power supply is an essential step for improving power quality. In the actual power system, voltage and current signals are dynamic and highly unpredictable. Hence, the time-varying nature of the power signal requires a technique that can analyze all sorts of disturbances accurately. In the last few decades, several techniques have been reported in the literature to analyze time-varying distortions. Still, only a few methods are suitable for real-time estimation of harmonics and power quality indices. Further, these methods need improvements concerning the accuracy, implementation complexity, response time and resource utilization.

The primary objective of this thesis is to estimate harmonics and power quality indices in real-time while maintaining reasonable accuracy. Hardware efficient algorithms have been developed in this thesis based on the signal processing techniques to fulfill this objective. The Undecimated Wavelet Packet Transform (UWPT) is a multiresolution technique with additional features of redundancy and time invariance. Further, this technique can be easily implemented on the hardware platforms because of its low implementation complexity. This thesis utilizes the potential of UWPT and customizes it to measure harmonics and power quality indices.

The work carried out in this thesis is segregated into four parts. The first two work develops a simple and efficient method based on UWPT for accurate estimation of harmonics and power quality indices of time-varying power signal in only one fundamental

cycle. The main emphasis of these works is on designing and developing suitable hardware architectures for the implementation of algorithms on the Xilinx Virtex-6 FPGA ML-605 Board. The results of simulated and practical signals are presented to show the advantages of these methods. In third work, the time-invariant property of the UWPT has been exploited for visualization of electrical disturbances in the power system.

Further, a measurement technique based on UWPT and Hilbert transform is proposed to estimate instantaneous power quality indices. The simple nature of this method and capability of parallel processing make it feasible to implement on Virtex-6 FPGA ML-605 Board. Results reveal that this method performs better than similar techniques in the literature.

LIST OF PUBLICATIONS

Journal publications:

1. V. K. Tiwari, A. C. Umarikar and T. Jain, "Fast Amplitude Estimation of Harmonics Using Undecimated Wavelet Packet Transform and Its Hardware Implementation," in *IEEE Transactions on Instrumentation and Measurement*, vol. 67, no. 1, pp. 65-77, Jan. 2018, doi: 10.1109/TIM.2017.2759358.

2. V. K. Tiwari, A. C. Umarikar and T. Jain, "Field Programmable Gate Array-Based Measurement System for Real-Time Estimation of Single-Phase Electric Power Quantities," in *IEEE Sensors Journal*, vol. 19, no. 13, pp. 5086-5097, 1 July1, 2019. doi: 10.1109/JSEN.2019.2903855.

3. V. K. Tiwari, A. C. Umarikar and T. Jain, "Measurement of Instantaneous Power Quality Parameters Using UWPT and Hilbert Transform and Its FPGA Implementation," in IEEE Transactions on Instrumentation and Measurement, vol. 70, pp. 1-13, 2021, Art no. 9000213, doi: 10.1109/TIM.2020.3021769.

Conference publication:

1. V. K. Tiwari, H. B. Sandhibigraha, A. C. Umarikar and T. Jain, "Undecimated Wavelet Packet Transform Based Visualization of Time-Varying Power Quality Disturbance," *2018 20th National Power Systems Conference (NPSC)*, Tiruchirappalli, India, 2018, pp. 1-5. doi: 10.1109/NPSC.2018.8771721.

TABLE OF CONTENTS

LIST OF FIGURES

LIST OF TABLES

ACRONYMS

ANN Artificial Neural Network.

DFT Discrete Fourier Transform.

DSP Digital Signal Processor.

DWPT Discrete Wavelet Packet Transform.

DWT Discrete Wavelet Transform.

EMC Electromagnetic Compatibility.

EMD Empirical Mode Decomposition.

ESPRIT Estimation of Signal Parameters via Rotational Invariance Technique.

EWT Empirical Wavelet Transform.

FFT Fast Fourier Transform.

FIR Finite Impulse Response.

FPGA Field Programming Gate Array.

HHT Hilbert Huang Transform.

IEC International Electrotechnical Commission.

MAC Multiply Accumulate.

MUSIC Multiple Signal Classification.

RMS Root Mean Square.

ST S-Transform.

UWPT Undecimated Wavelet Packet Transform.

XSG Xilinx System Generator.

Chapter 1

Introduction

1.1 Background

The primary function of power systems is to generate, transmit and distribute electrical energy to end-users. Over the past few decades, many initiatives have been taken in the energy sector to increase the overall efficiency of the power system. At the generation side, the focus has been placed towards increasing the utilization of renewable energy sources due to the rising environmental concerns. The advancement in power electronics technology made it feasible to integrate small scale renewable energy sources, often called Distributed Generators (DGs), with the traditional power grid. These small-scale generators consist of high-power semiconductor devices and power electronic converters. The developments in recent technologies such as High-Voltage DC transmission (HVDC), Flexible AC Transmission System (FACTS), variable-speed drives, etc. have enhanced the efficiency of power networks. The use of process control equipment, protection circuit and microprocessor-based controller provides fast and easier control of the industrial process. Personal Computers (PCs) and automated electronic appliances are also being used in the industrial and commercial sectors to increase human productivity. All these developments at generation, transmission and distribution levels have changed the structure and operation of power systems. As a result, the increased use of renewable energy sources, high power semiconductor devices and other non-linear loads in the power system have led to the deterioration of the quality of power supply to very severe levels.

During the past few years, researchers have shown considerable interest in power quality monitoring and control due to significant rise in non-linear loads and solid-state power electronics technology [1]-[4]. The term power quality can be defined as the wide variety of electromagnetic phenomena that characterize the voltage, current and frequency at a given time and a particular location on the power system [5]. Presently, power quality has become a significant concern for both power utilities as well as consumers because of increased consumer awareness and stringent regulations. In one of the reports of the smart grid, power quality has been identified as one of the seven principle characteristics of the modern grid [6]. In general power Quality monitoring is the measurement of the parameters (amplitude, phase and frequency) of the electric supply. According to [7], power quality problem can be defined as “any power problem manifested in voltage, current or frequency deviation that results in failure or mal-operation of end-user equipment.” Therefore, for better interpretation of power quality, it is essential to analyze the deviation of voltage, current and frequency waveforms from the ideal sinusoidal waveforms.

1.1.1 Power Quality Disturbances

Power signals can be classified into two categories, i.e., stationary signal and non-stationary signal. For stationary signal, mean and variance of the signal do not vary with respect to time, whereas either of them or both may vary in case of the non-stationary signal. The power quality disturbances, which occur in stationary conditions, are harmonics, interharmonics and noise. Root Mean Square (RMS) voltage variations such as sag, swell and momentary interruption along with transient and fluctuation are called non-stationary disturbances. Details about each power quality disturbance are given below.

Harmonics

Nowadays, there is significant use of power electronic equipment, arc furnaces, fluorescent lamps, variable speed drives and industrial control equipment, which have the nonlinear characteristics. These equipment’s generate harmonic distortions in the power supply waveform [1], [8]. Harmonics could be defined as an undesirable component of the distorted power supply waveform.

According to Fourier series, a distorted waveform can be represented by the summation of various higher frequency components known as harmonics, which are integer multiple of the fundamental frequency component. It can be defined mathematically as

$$f(t) = a_0 + \sum_{n=1,2,3...} a_n \cos(\mathrm{n}\,\omega_0 t + \phi_n) \tag{1.1}$$

Here a_n is the magnitude of n^{th} harmonic frequency, $\emptyset_n$ is the phase angle of n^{th} harmonic frequency and ω_0 is the fundamental frequency. A distorted signal may have some components that are not integer multiple of the fundamental frequency; these are known as inter-harmonic. The subharmonics are the sinusoidal components with the frequency below the fundamental frequency. The distorted waveform is shown in Figure 1.1 (a).

Voltage sag

Voltage sag is a fall in RMS voltage for durations from 0.5 cycles of the fundamental frequency to one minute. The decrease in voltage is any value between 0.1 pu to 0.9 pu. Voltage sag occurs due to load variations, starting up of large motors and faults in the electrical power system. Voltage sag is characterized by sag magnitude, duration and phase angle jump. The distorted waveform for voltage sag is shown in Figure 1.1 (b).

Voltage swell

Voltage swell is an increase in RMS voltage above 1.1 pu and below 1.8 pu. The duration of voltage swell can be between from 10 ms to one minute. Voltage swell is generally caused by the single-line-to-ground fault, switching of a large load and energizing of a large capacitor bank. Voltage swell disturbance is depicted in Figure 1.1 (c).

Momentary interruption

The voltage drops of 90% to 100% of the rated RMS voltage lasting from ½ cycles of fundamental power frequency to a few minutes is known as a momentary interruption. It occurs due to switching operations and faulty working of reclosers. Momentary interruption is shown in Figure 1.1 (d).

Voltage fluctuation

Voltage fluctuations occur when there is cyclic variation in the voltage envelope for the long duration and the amplitude varies in the range ±10% of the rated RMS voltage. Generally, voltage fluctuations are the result of the modulation of fundamental power frequency, as depicted in Figure 1.1 (e). The main causes of the voltage fluctuations are load variation at the end-user installations, change in operating conditions and connecting of arc furnaces or welding equipment.

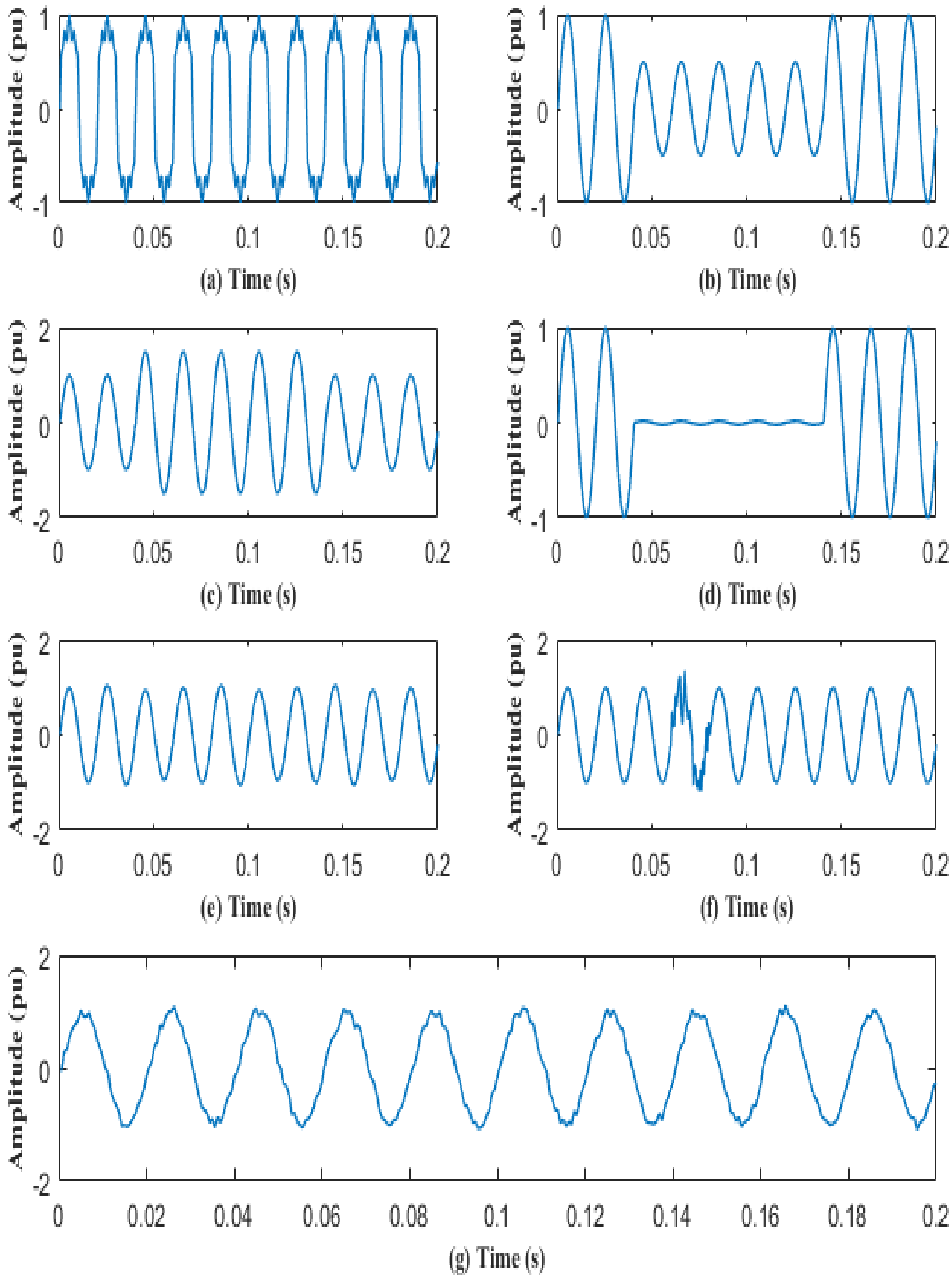

Figure 1.1: Disturbance signals (a) Harmonic distortion (b) Voltage sag (c) Voltage swell (d) Momentary interruption (e) Voltage fluctuation (f) Transients (g) Noise

Transients

An impulsive transient is defined as a sudden, non–power frequency change in the steady-state condition of voltage, current, or both that is unidirectional in polarity [5]. The main characterization properties of impulsive transients are rise time, decay time and frequency content. The primary reason for the impulsive transient is a lightning strike. Impulsive transients disturb the power resonance circuit and generate oscillatory transients. There is not much difference in impulsive and oscillatory transient. In oscillatory transient, polarity changes rapidly in positive and negative polarities, as shown in Figure 1.1 (f). The oscillatory transients can be characterized by magnitude, duration and spectral content. Back-to-back capacitor energization, snubber circuit and the commutation of power semiconductor devices are the main causes of oscillatory transients. Oscillatory transients with a primary frequency component greater than 500 kHz and duration measured in microsecond are considered as high-frequency transients.

Noise

Noise is high-frequency distortion in power signal with broadband spectral content typically lower than 200 kHz as shown in Figure 1.1 (g). It is mainly caused by equipment such as welders, switchgear, control circuit, improper grounding and transmitters.

Generally, the voltage disturbances originate in the distribution system and affect the end-users. While the reason for current disturbances is customers' installation and affect the network components and other devices. Therefore, maintaining the quality of the current is the primary responsibility of end-users, whereas voltage quality is the primary responsibility of network operators.

1.1.2 Effects of Power Quality Disturbances

Even though power quality disturbances occur for only short duration, they cause long-term issues, huge economic losses and hours of manufacturing downtime in industry. Hence, power quality problems have become an important issue for utility, equipment manufacturers and end-user customers. One of the reports provided by Wartsila India in

August 2009 stated that India suffers a staggering loss of INR 100,000 Crore (1000 Billion) because of power quality disturbances [9]. Due to the low quality of power supply, the economic loss of Europe is 10 billion Euros and 24 billion USD in the USA every year [10]. When a voltage source is connected to a non-linear load, it draws current that differs in shape from the applied pure sinusoidal voltage. This distorted current flows through distribution equipment and increases losses in conductors, cables, transformers and machines. Generation of harmonics due to non-linear load can create many other problems such as mal-operation of protection devices, torsional oscillations in AC motors, failure of electronic devices, metering inaccuracies and interference with communication line [3].

The most common problem with voltage sag, voltage swell, and momentary interruption are reduced lifetime of rotating machines, transformers, switchgear, CTs and PTs, process shut down and equipment trips. The voltage fluctuation causes flicker in incandescent lamp and gas discharge lighting equipment. Transients result in control system resetting, insulation breakdown of electrical equipment, damage to sensitive electronic components and dielectric failure. Power frequency variation can cause cascading outages of interconnected systems, de-tuning of harmonic filters and severe damage to generator and turbine shafts due to the subsequent large torques developed. Also, sophisticated power electronics-based devices and modern control equipment, which are used for control and system stability and to increase the efficiency of the grid are more sensitive to power quality disturbances and variations in comparison to the equipment used in the past.

Measurement and monitoring of power quality disturbances are important aspects. It is often difficult to determine from the observable effects on end-user devices which power quality disturbances caused the disruption [5]. Further, in the deregulated electricity industry and the competitive market, the cost of electricity directly varies with the quality of power supply. Hence, electricity utilities are putting their effort into maintaining the quality of power supply in order to satisfy their customer. Therefore, as a requirement of smart electricity transmission and distribution systems, accurate measurement, monitoring, and control of power supply distortion are very important.

1.2 International Standards on Power Quality

The guidelines and standards for power quality monitoring need to be persistent with the existing and developing international practices. Proper standardization provides an important recommendation for the implementation of technical solutions. The Institute of Electrical and Electronics Engineers (IEEE) and the International Electrotechnical Commission (IEC) have proposed their sets of power quality standards, which are given below.

IEC-61000-4-7

IEC standards on electromagnetic compatibility are divided into six parts and IEC standard 61000-4-7 [11] is a part of this standard. This deals specifically with measurement of harmonics and interharmonics of up to 9 kHz frequency. According to IEC-61000-4-7, distorted power supply waveform of a voltage or current signal can be assessed by applying the Discrete Fourier Transform (DFT). The width of the window for 50 Hz and 60 Hz system is 10 and 12 cycles, respectively, i.e., 200 ms for both cases. Therefore, the frequency resolution of DFT at the output is 5 Hz and then evaluating the groups/subgroups of adjacent spectral components, as shown in Figure 1.2.

IEEE-1459-2010

The traditional way to evaluate the quality of power supply is to estimate the power components (Harmonic distortion, active, reactive and apparent powers, power factor, etc.) from the measured voltages and currents, as suggested in IEEE Standard 1459-2010 [12]. This standard gives a set of definitions for the estimation of power components under the sinusoidal, nonsinusoidal, balanced, or unbalanced conditions. It also provides some guidelines for designing and development of the metering instrument for billing and revenue purposes. The estimation accuracy of power components is entirely dependent on the applied technique, which is used to separate fundamental and harmonic components from the measured waveforms. However, IEEE Standard 1459-2010 does not specify any technique for the spectral analysis.

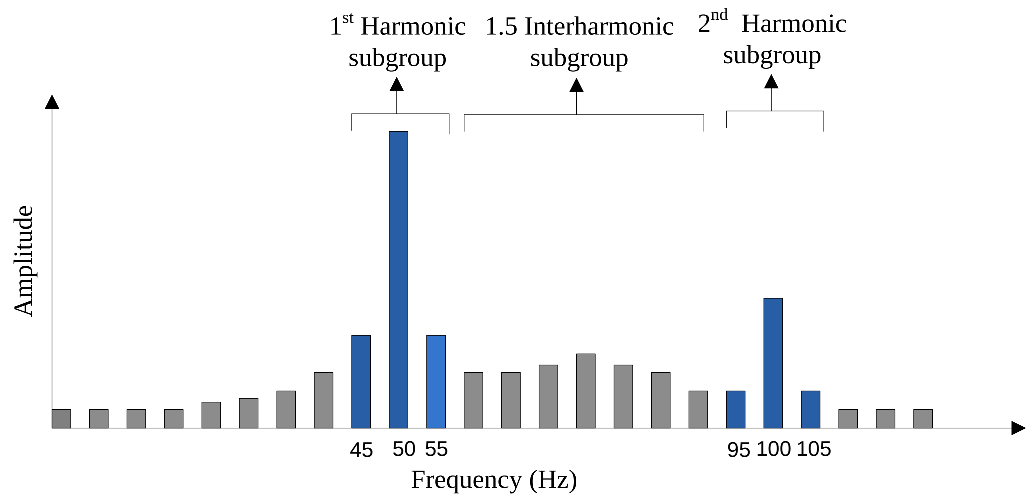

Figure 1.2: Illustration of harmonic and interharmonic subgroups

1.3 A Brief Review of Some Existing Techniques on Power Quality Monitoring

Several techniques are available in the literature for power quality monitoring, [1], [13], [14] these are broadly categorized into two classes, namely, parametric and non-parametric methods. Figure 1.3 shows some of these methods. In non-parametric methods, we find spectrum directly from the signal, usually in terms of some coefficients of a set of known functions, referred to as a basis function. In the parametric methods, we use an appropriate model to represent the signal and then estimate the power quality parameters such as amplitude, phase and frequency.

Discrete Fourier Transform

Discrete Fourier Transform (DFT) is a technique to transform a periodic, discrete time-domain signal into the frequency domain. The DFT of a discrete-time sequence $x(n)$ is calculated as follows,

$$X(k) = \sum_{n=0}^{N-1} x(n) e^{\left(-j\frac{2\pi nk}{N}\right)} \quad \forall k = 0,1,2,......,N-1, \tag{1.2}$$

where $x(n)$ is the n^{th} sample of the data, k is the frequency index and N is the total number of samples. The resolution of the signal in the frequency domain depends on the number of samples in the window. Direct calculation of DFT using 1.2 is not an efficient technique due to high computational complexity. Therefore, a computationally efficient method called Fast Fourier Transform (FFT) is developed for its evaluation, which reduces the computation complexity of the DFT significantly from $O\,(n^2)$ to $O\,(n \log n)$.

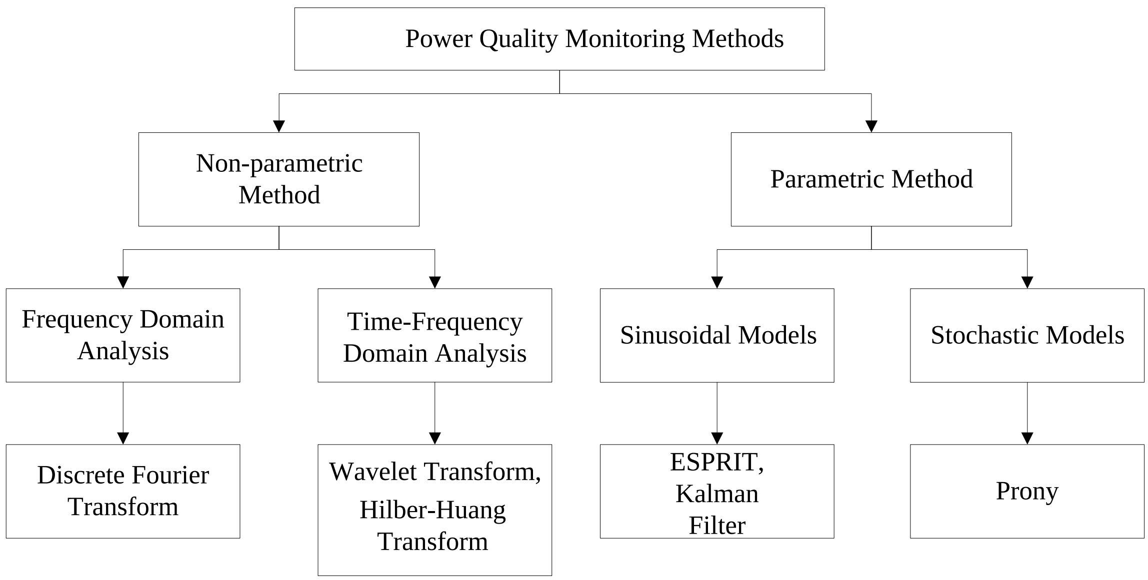

Figure 1.3: Power quality measurement techniques

Short-Time Fourier Transform

The Short-Time Fourier Transform (STFT) is an extension of DFT. The difference between STFT and DFT is that in STFT signal is multiplied by a window. In STFT, the window moves along the time axis and the signal is assumed to be stationary within this window. The STFT can be defined as,

$$X(m,k) = \sum_{n=0}^{N-1} w(n-m)x(n)e^{\left(-j\frac{2\pi nk}{N}\right)} \quad \forall k = 0,1,2,......,N-1, \tag{1.3}$$

where *m* is an integer representing window position on the time scale. Limitation of STFT includes fixed window width, which compels to compromise between time and frequency resolution. According to the Heisenberg uncertainty principle, it is not possible to obtain high time resolution and frequency resolution for a signal simultaneously. Uncertainty is defined by following equation [15],

$$\Delta t.\Delta f \geq \frac{1}{4\pi}, \tag{1.4}$$

where, Δt and Δf are time and frequency resolutions, respectively.

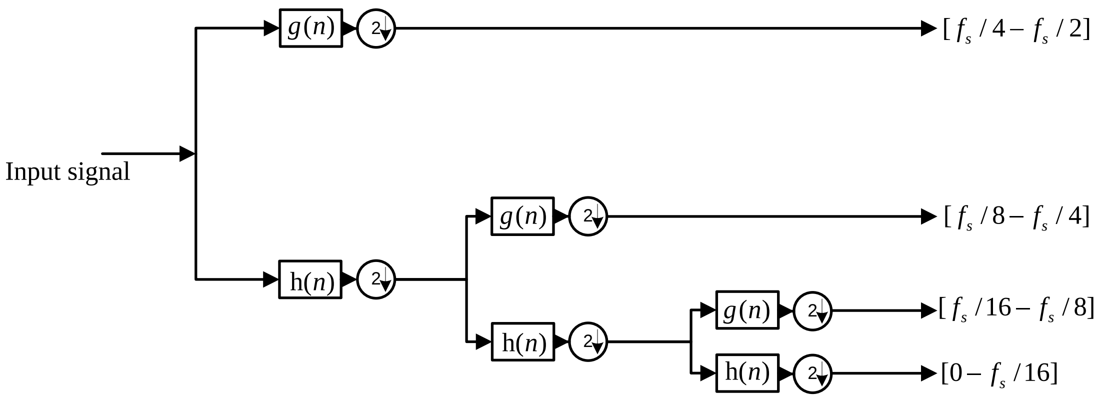

Figure 1.4: Three-level DWT decomposition tree

Discrete Wavelet Transform

Wavelet analysis is the earliest mathematical tool, which is used for the time-frequency analysis of non–stationary signals. Wavelet is a fast oscillating wave with zero average value. Wavelets are dilated and shifted for getting adequate time-frequency resolution. Wavelet analysis is suitable for the signals, which contain stationary components along with transients. Hence, the wavelet transform is more suitable for the analysis of the power signal. Discrete Wavelet Transform (DWT) can be defined as,

$$w_m[k] = \sum_n x(n) g^*_{a,b}(k), \tag{1.5}$$

where,

$$g_{a,b}(k) = \frac{1}{\sqrt{a}} g\left(\frac{k-b}{a}\right), \tag{1.6}$$

is a mother wavelet. k is the number of samples in the input signal and scale parameter $a = a_0^m$, translational parameter $b = nb_0 a_0^m$, and m and n are integers. DWT can be implemented using a multistage filter bank, as shown in Figure 1.4. The filter bank consists of wavelet function as the low- pass filters and its dual high-pass filters. An input sequence is fed into the low-pass filter ($h(n)$) and its dual high-pass filter ($g(n)$) and then downsampled by a factor of two. The output from the low-pass filter provides approximation coefficients, while the output from the high-pass filter provides detail coefficients. DWT divides the signal into a logarithmic frequency band, as shown in Figure 1.5, where *fs* is the sampling frequency.

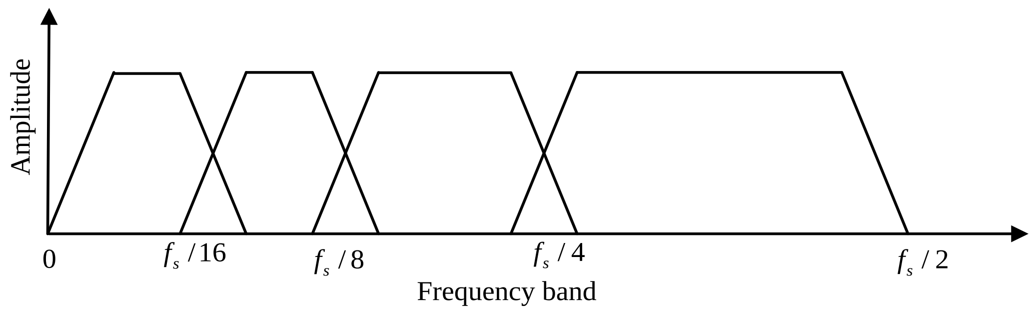

Figure 1.5: Frequency bandwidth for a DWT

Discrete Wavelet Packet Transform

The Discrete Wavelet Packet Transform (DWPT), a more general form of the discrete wavelet transform, is the preferred technique for power quality indices estimation as it provides uniform frequency bands and can be easily implemented using a multistage filter bank. With adequate sampling frequency and wavelet decomposition tree, output frequency band from a DWPT can be aligned to the specific frequency components for measuring their magnitudes [16]. Figure 1.6 depicts a three-level decomposition tree that provides eight frequency bands.

The decomposition is performed on both the approximation coefficient and the detail coefficient of the input signal at any level. The wavelet coefficients of the input signal at the l^{th} level, k^{th} point and $2i^{th}$ node can be represented as:

$$D_l^{2i}(k) = \sum_n h(n) D_{l-1}^i (2k-n), \tag{1.7}$$

$$D_l^{2i+1}(k) = \sum_n g(n) D_{l-1}^i (2k-n), \tag{1.8}$$

where, i = 0, 1. . . ($2^{(l-1)}$ -1), $h(n)$and $g(n)$ are low-pass and high-pass filters, respectively. The wavelet coefficient at any level is retrieved from the convolution of the input signal sequence at the previous level with the low-pass/high-pass filter and then downsampling by a factor of two. This scheme divides the signal into the linear frequency spectrum, as shown in Figure 1.7.

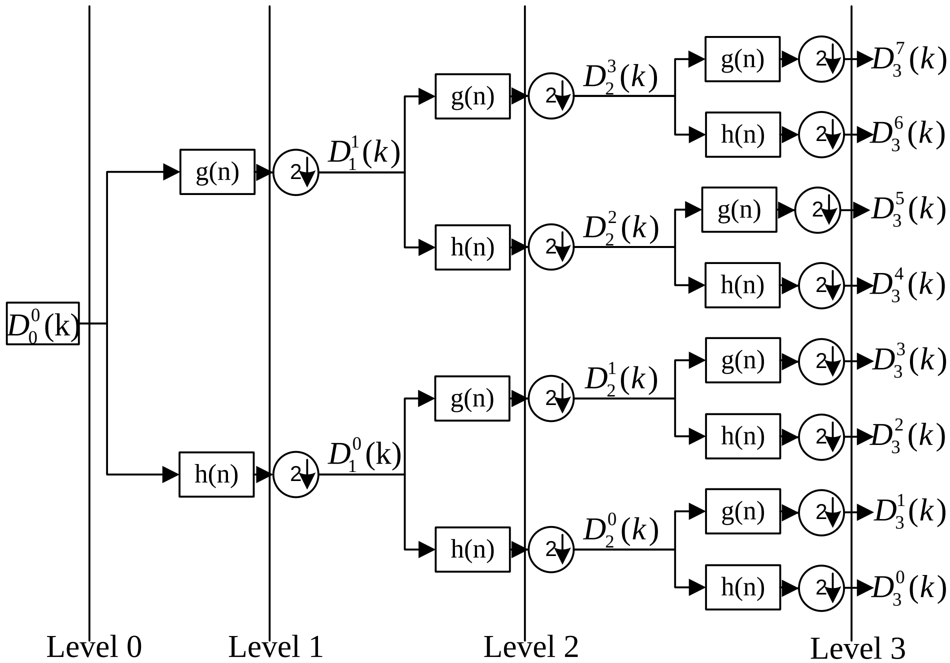

Figure 1.6: Three-level DWPT decomposition tree

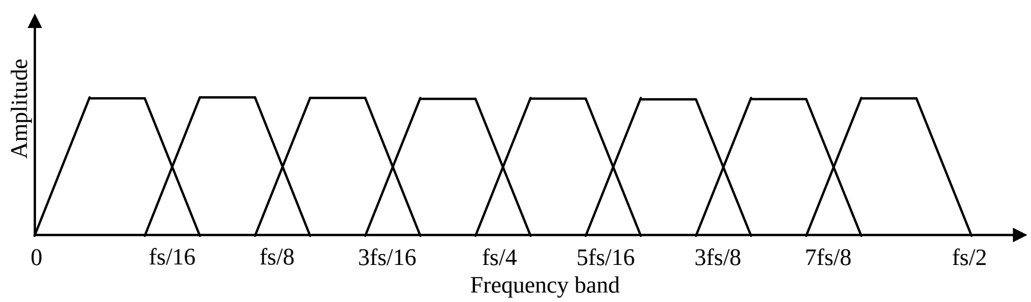

Figure 1.7: Frequency bandwidth for a DWPT

Hilbert-Huang Transform

Hilbert-Huang Transform (HHT) is an adaptive method to decompose the stationary as well as non-stationary signal. It consists of two distinct processes. The first process is known as Empirical Mode Decomposition (EMD), which will break down the signal into the Intrinsic Mode Functions (IMFs) using the sifting process [17], [18]. The main purpose of the sifting process is the subtraction of large-scale features of the signal consecutively until either the residue $r_n(t)$ is small, or residual $C_i(t)$ becomes a monotonic function. The signal is expressed in the form of IMFs as follows,

$$x(t) = \sum_{i=1}^{N} C_i(t) + r_n(t) \tag{1.9}$$

In the second step, the Hilbert transform is applied to each IMF to obtain the complex conjugate $D_i(t)$ corresponding to each IMF.

$$D_i(t) = H\left[C_i(t)\right] = \frac{1}{\pi} \int_{-\infty}^{+\infty} \frac{C_i(\tau)}{t-\tau} d\tau \tag{1.10}$$

The analytic signal corresponding to each IMF is expressed as follows,

$$Z_i(t) = C_i(t) + jD_i(t) = A(t)e^{j\theta(t)} \tag{1.11}$$

where $A(t)$ and $\Theta(t)$ are instantaneous amplitude and phase angle.

ESPRIT

Estimation of signal parameters via Rotational Invariance Technique (ESPRIT) is a high-resolution parametric technique and hence, a more accurate method for measurement of harmonics and interharmonics in the power system. The ESPRIT method can be summarised in following step [19], [20],

1. Create an autocorrelation matrix R_x from the samples of the signal $x(n)$.

$$R_x = \frac{1}{L-M} X^H X \tag{1.12}$$

here, X is the Hankel matrix of order M and L is the length of the signal under consideration. It is constructed from the signal $x(n)$ as shown below

$$\begin{pmatrix} x(0) & x(1)\cdots & x(M-1) \\ x(1) & x(2)\cdots & x(M) \\ \vdots & \vdots & \vdots \\ x(L-M) & x(L-M+1) & x(L-1) \end{pmatrix}$$

2. Decompose the autocorrelation matrix R_x into signal subspace matrix R_{xs} and noise subspace matrix R_{xn}.
3. Derive two shifted submatrices R_1 and R_2 from the signal subspace R_{xs} using the formula given below.

$$Ri = S_i R_{xs} \quad \forall i = 1 \, and \, 2 \tag{1.13}$$

   where, $S_1 = [I_{N_s} \; 0_{d_s}]$ and $S_2 = [0_{d_s} \; I_{N_s}]$. The I_{N_s} is an identity matrix of order $N_s \times N_s$, where $N_s = M - d_s$ and d_s is the distance between two submatrices, which is normally kept as 1.
4. The shifted submatrices R_1 and R_2 can be related through a matrix Ψ using shift-invariance property such that $R_2 = R_1\Psi$. The matrix Ψ is found out using the following least-squares estimate.

$$\Psi = \left(R_1^H R_1\right)^{-1} R_1^H R_2 \tag{1.14}$$

5. The frequency (f_k) and attenuation factor (AF_k) of the components of the signal is derived from the eigenvalues of the matrix Ψ.

$$f_k = f_s \times \frac{imag(\log(\lambda_{\Psi k}))}{(2\pi)} \quad \forall k = 1,2,3.....2n \tag{1.15}$$

$$AF_k = f_s \times real(\log(\lambda_{\Psi k})) \quad \forall k = 1,2,3.....2n \tag{1.16}$$

   here, f_s is the sampling frequency and $\lambda_{\Psi k}$ is the Eigenvalue of the matrix Ψ.

PRONY'S Method

In the Prony method, the signal is represented as a linear combination of exponential functions [21] . Each sinusoid or exponential signal are extracted by solving a set of linear equations. Let, data samples of $x(n)$ be estimated by a function $g(x)$ such that,

$$g(x) = Re^{rx} + Se^{sx} + ... + Ve^{vx}, \tag{1.17}$$

where, R, S, …, V and r, s, …, v are constants. The function $g(x)$ satisfies the following linear equation,

$$Ag_{n+u} + Bg_{n+u-1} + ... + Ug_n = 0, \tag{1.18}$$

where u is the order of the system. The roots of (1.18) give the exponent of (1.17), which are used to get the coefficients of (1.18). Coefficients part gives the corresponding amplitude and phase, while exponent terms provide frequency and damping factor.

1.4 Platform for Hardware Implementation

Fast progress in VLSI technology has made it possible to develop a compact digital circuit with very high operational speed for any specific application. Depending upon a system architecture and its computational requirement, different digital signal processing tools, such as general-purpose processor, Digital Signal Processor (DSP) and field-Programmable Gate Arrays (FPGA) are available for implementation of the algorithm. The main advantages of DSP over the FPGA are that it provides the easy implementation of hardware architecture using higher-level programming languages and the capability of floating-point calculations. But the drawback of DSP is that algorithms sequentially run on the DSP board, which reduces the processing speed of algorithm and optimization of various parameters such as timing constraint and resource utilization is not possible with DSP.

FPGAs are reconfigurable digital devices that allow the design of complex systems easily and efficiently. For better optimization of different application constraints (resource constraints, timing constraint and modularity constraint), FPGAs are a better option than DSP due to its ‘flexibility in design’ feature. Several building blocks are available on FPGAs, in which fundamental elements are programmable lookup table and storage registers. These blocks are interconnected by programmable interconnection. In addition to these basic elements, modern FPGAs are also comprising of computational and data storage blocks such as embedded memories, Phase-Locked-Loops (PLLs), Multiply-

Accumulate blocks (MACs), which increase the efficiency of the device. Also, there has been significant progress in computer-aided design software for developing FPGA designs. This software facilitates the design of complex systems easily and efficiently. Exploring these technologies, FPGAs are a better option for the implementation of the algorithm on dedicated hardware [22], [23].

1.5 Motivation and Objectives

A literature survey has been carried out to identify the present state of the art and research gaps relevant to this research work. A literature survey helps to gain some insight and knowledge of existing facts about power quality monitoring and its hardware implementation. The research articles [1], [13], [24]-[27] present an impressive review of the used method for measurement of harmonics, interharmonics and power quality indices. The well-known conventional method used to estimate the harmonics is the Fast Fourier Transform (FFT) due to its simplicity and fast computation [7]. However, FFT has its own limits and restrictions and produces inaccurate results in the case of the non-stationary signal. Most power quality events are usually non-stationary and exhibit time-varying characteristics such as voltage sag, voltage swell, switching transient, etc. Therefore, the accuracy of the FFT-based method is deteriorated in the presence of power quality disturbances typically found in electrical power systems due to spectral leakage and fundamental frequency deviation [1], [28]. In addition, FFT also does not provide any information about time since analysis is performed in the frequency domain. Several other approaches, such as windowed and interpolated DFT such as Blackman-Harris window [29], [30], [31] improved FFT based algorithm [32], [33], [34] Hanning window [35], [36], [37] multipoint interpolated DFT [38], [39] and adaptive window [40], [41], [42] can also be applied to resolve these problems of the FFT, but at the cost of additional computational complexity. The STFT based analysis for voltage disturbance is suggested in [43]. However, the drawback of STFT is that it has a fixed window width, hence, needs to compromise between time and frequency resolution. The STFT also suffers from typical FFT limitations such as spectral leakage and picket fencing. A new spectral envelop pre-processor based on sinusoid fitting and the DFT is described in [44] for accurately extracting the harmonic information.

Time-domain filtering methods have been proposed in [45], [46] for estimation of power quality indices according to IEEE Standard 1459-2010, without using any spectral-analysis technique. The computational complexity is reduced, but the inherent drawback of these methods is the use of higher-order low-pass filters with specific cut off frequencies for extraction of fundamental component [47]. Performance of the time-domain technique proposed in [45], [46] is improved by replacing low-pass filters with a recursive algorithm in [47] which estimates the average values. But similar to FFT, this method also suffers from the synchronization problem [48].

Stationary sinusoidal waveforms are used as a basis function in Fourier analysis; therefore, Fourier transform produces inaccurate result in power quality analysis due to the non-stationary nature of power signal. The wavelet transform is a multiresolution technique, which overcomes the problem of Fourier transform by using a short duration oscillating waveform called mother wavelet. The mother wavelet is dilated and shifted to vary the time-frequency resolution. The main advantage of the wavelet transform is that it preserves both time and frequency information simultaneously. Many methods based on DWT [27], [49]-[52] have been used for power quality monitoring. The formulation of power quality indices using the DWT has been proposed in [52]. The work [53] proposes a technique based on DWT for locating and analyzing the low-frequency oscillations in the power system. The DWT provides a non-uniform frequency band; hence, there is a possibility that the two or more frequency components are present in the same frequency band [54]. Therefore, an accurate analysis of all the frequency components is not possible.

The Discrete Wavelet Packet Transform (DWPT), a more general version of the DWT, has received considerable attention from researchers because of its capability to decompose the input signal into uniform frequency bandwidth [16], [55]-[58]. The DWPT has been successfully applied in the harmonics estimation [16], [57], [59]-[61] and power quality indices estimation [55], [58], [62] . Barros and Diego [16] proposed the use of “db20” and “Vaidyanathan 24” as the mother wavelet to improve the capability of the DWPT in harmonic estimation. But this increases computational complexity and requires more hardware resources. Eren et al. [57] and Bruna et al. [60] have used Infinite Impulse Response (IIR) filters to decompose the signal using the DWPT, due to its better frequency selectivity and less computational complexity. However, the significant drawbacks associated with the use of IIR filters are the possibility of instability due to quantization error, nonlinear phase response, etc. Polyphase decomposition-based wavelet filters have been proposed in [59] for implementation of DWPT, which reduces computational complexity and required resources, thereby improving the performance of DWPT for harmonics estimation. Even though the DWPT is quite popular for measurement of harmonics and power quality indices, the selection of suitable mother wavelet and choosing the adequate sampling frequency limits the application of DWPT for analyzing real-time non-stationary signals [51].

To address the drawbacks of the above-mentioned techniques, various adaptive techniques have been proposed, such as HHT, S-Transform (ST) and Empirical Wavelet Transform (EWT) for analysis of time-varying as well as stationary signals. In [63], an iterative frequency shifting algorithm based on wavelet transform and Hilbert transform is proposed for analyzing non-stationary power signal. Iterative HHT (Hilbert-Huang transform), in conjunction with the Symbolic Aggregate Approximation (SAX) algorithm, is employed in [64] for the analysis of power quality. However, the real-time performance of these methods is degraded due to the iterative nature of the algorithm. The other disadvantage of HHT is mode mixing, resulting in a combination of two or more frequency components and is highly sensitive to noise. Gaussian windowing is used in S-Transform and has also been applied in power quality analysis [65] because of its ability to provide both magnitude and phase spectrum with respect to time. However, it is computationally expensive, which has been overcome in [66] by using fast adaptive generalised S-Transform. An EWT based method is developed for the estimation of power quality indices in the power grid with better accuracy [67]. However, this method requires 20 cycle data and the nature of the algorithm is also complex, which would deteriorate its real-time processing capability. A modified EWT approach termed as generalised empirical wavelet transform has been proposed in [68] to overcome the drawback of EWT.

Parametric methods such as Prony [69], ESPRIT [19], [70] and other eigenvalue-based methods offer the reliable and accurate estimation of harmonics without any limitation on the number of data samples. Kalman filter (KF) [71], [72], [73] and adaptive linear combiner (ADALINE) [74] are robust recursive estimation methods and suitable for continuous tracking of time-varying harmonics and power quality indices. Although these techniques can estimate the power quality indices in one cycle, they are recursive, need prior information of the signal for accurate modeling and computationally complex. Artificial Neural Network (ANN) based techniques such as Back Propagation Neural Network (BPNN) [75], Radial Basis Function Neural Network (RBFNN) [76], [77] and Adaptive Wavelet Neural Network (AWNN) [78] require the only half cycle of a power signal for estimation of selected harmonic components and power quality indices. Still, a significant error may occur due to the unavailability of sufficient training data and the time-varying nature of the power signal.

Above mentioned works are simulated/implemented on Personal Computers (PCs) using numerical analysis software limiting their flexibility, portability and computational speed. Further, its practical implementation will increase the power consumption and per-unit cost of the device. Digital Signal Processors (DSPs) and Field-Programmable Gate Arrays (FPGAs) are two preferred options for the implementation of different algorithms in industrial applications on the real-time platform. DSPs are a software-based processor and became popular in power quality analysis due to ease of programming using C-language and less development time [79]-[82]. On the other hand, advances in FPGA technology have led to low-cost devices with high performance due to its various attractive features. It is flexible in design, which enables optimized use of available hardware resources for the specific application. Other features include adjustable word-length for filter coefficients and arithmetic computation to achieve the desired accuracy, portability and short time-to-market. Enough I/O (input/output) and memory capability of FPGA is also an important factor for the present application because of the need to monitor a large number of power quality indices. Reconfigurable properties of FPGA allow adding other processing tasks of different applications easily. The higher degree of parallelism and throughput decreases computational time in FPGA. If system design is appropriately planned, FPGAs have a better benefit-cost ratio in comparison to DSPs [83]. As a result, FPGA technology has become a preferred implementation platform for the measurement of power components [84]-[87].

The literature review reveals that the accurate and fast measurement of harmonics and power quality indices are a fundamental need for real-time monitoring and analysis of power quality in the modern power system. It can be concluded from the available literature on power quality monitoring that none of the techniques provide all the desirable features, viz. ability to deal with the time-varying signal with high measurement accuracy, low computational burden, high time and frequency resolution and robustness against fundamental frequency deviation and noise. Furthermore, the real advantages of any technique can be ascertained only after the hardware implementation of the algorithm. Although the reported methods claimed satisfactory performance, their hardware implementation confronts many issues, such as implementation complexity, response time, selection of suitable world-length to attain reasonable accuracy, choosing proper hardware architecture and hardware resource requirement. Therefore, a better option is to develop a hardware efficient algorithm for power quality monitoring in such a way that the above parameters are optimized. Thus, it requires the design and development of proper simulation models and suitable hardware architecture.

Considering the importance of real-time power quality monitoring and limitations of existing techniques, as explained above, the major objectives of this thesis are:

1. To propose a simple and efficient technique for measurement of harmonics and power quality indices with less computational complexity.
2. To develop a hardware efficient algorithm for monitoring of power quality, which optimizes the various parameters associated with it.
3. To design the digital hardware architecture of algorithm by utilizing parallelism and pipelining capability of FPGA in such a way that it meets the requirements of response time and resource utilization.
4. To analyze the time-varying power signals and estimate the instantaneous power quality indices accurately.

There is a requirement of the accurate, simple and efficient approach for real-time power quality monitoring with less implementation complexity. The Undecimated Wavelet Packet Transform (UWPT) [88], [89] is a multiresolution technique with additional features of redundancy and time invariance. Hence, it is more suitable for dealing with time-varying signals. The UWPT has some other good features like less implementation complexity (no additional complex operations are required, such as computation of exponential, sine and cosine function, matrix inversion, interpolation, etc.), easy implementation using filter banks and capability of parallel processing using filters. It is highly suitable for real-time applications with easy implementation on FPGA hardware. Hence, this work explores the potentials of this method and customizes it for the analysis of time-varying voltage and current signals.

1.6 Thesis Outline

The thesis is divided into six chapters. The current chapter discusses the background of power quality problems, possible causes and their effect on the power system. This chapter also presents the relevance of power quality monitoring, reviews the existing concepts and established the motivation behind this research work.

Chapter 2 proposes a fast algorithm based on Undecimated Wavelet Packet Transform (UWPT) to estimate the amplitude of fundamental and harmonic components of stationary as well as a time-varying power signal. The performance of the proposed scheme is compared with similar techniques, such as the DWPT and the FFT. The UWPT algorithm has also been implemented on the Xilinx Virtex-6 FPGA ML-605 Board, using XSG/ISE design suite 14.2. Its performance, in terms of hardware accuracy, resource utilization, as well as timing requirements, has been tested using the experimental test signal**.**

Chapter 3 reviews the traditional power quality indices defined by IEEE Standard 1459-2010 and reformulates the power quality indices using UWPT. This work also develops an FPGA-based measurement system for the estimation of power quality indices using modified UWPT. The effectiveness of the proposed measurement system has been demonstrated through simulation and experimental results. Simulation results show the accuracy and robustness of the proposed measurement system under different operating conditions. Further, experimental results validate its performance in terms of hardware accuracy, resource utilization and timing requirements.

In **chapter 4,** a method is presented for visualization of time-varying power quality disturbances in electrical power distribution system using an Undecimated Wavelet Packet Transform (UWPT). The proposed method decomposes the input signal in various frequency bands and provides clear visualization of fundamental and each harmonic component. Different types of stationary and time-varying waveforms have been used to show the effectiveness of the proposed scheme. The results confirm that the proposed technique based on UWPT efficiently decomposes the fundamental and harmonics component from the distorted signal, reflecting its suitability for power quality monitoring and analysis.

Chapter 5 presents a measurement technique based on the UWPT and Hilbert Transform (HT) to estimate power quality parameters at every sample. Thus, it results in improved time resolution and allowing us to track the variation of power quality parameters with respect to time. The proposed scheme has been successfully implemented on the Xilinx Virtex-6 FPGA ML-605 evaluation kit. The simulation as well as the experimental results demonstrate the effectiveness of the proposed method in terms of estimation accuracy, timing requirements and resource utilization.

Chapter 6 provides the concluding remarks by summarizing the contribution and conclusion of all the chapters and suggests a few possible works for future research.

Chapter 2

Fast Amplitude Estimation of Harmonics Using Undecimated Wavelet Packet Transform

2.1 Introduction

Accurate and fast estimation of harmonics is one of the primary requirements for online monitoring and control of power grid from power quality and safety point of view. It is essential for identification of harmonic sources [90], which helps in design and development of Active Power Filters (APFs) for harmonic compensation [91], [92], harmonic metering [93] and distortion-based tariff realization. If the operating conditions of power system change abruptly, it results in time-varying characteristics of both the voltage and current signals. For any time-varying phenomenon occurring in a very short time window, the estimation of harmonics with large window width may give inaccurate results. Also, the variations may increase with an increase in the length of the window. Moreover, the acquisition of more number of the fundamental cycles not only delays the estimation process but also increases the memory requirements. The well-known conventionally employed Fast Fourier transform (FFT) is computationally efficient but requires at least one cycle data. The one cycle estimation using the FFT gives incorrect results in the case of time-varying signals [76]. Therefore, the IEC 61000-4-7 [11] recommends the use of the FFT for estimation of harmonics and interharmonics considering ten cycles window for 50 Hz signal. Further, the increase in the time window length to ten cycles compromises the time resolution. Also, the FFT suffers from the problem of spectral leakage and is sensitive to fundamental frequency deviation. DWPT is a multiresolution technique and improves the performance of harmonic estimation for time-varying signal. However, a major limitation of the DWPT is that it is not a time-invariant transform, which results in its reduced capability to analyze a time-varying signal. Further, the downsampling at each increasing decomposition level reduces the length of wavelet coefficients by half. Hence, in order to have an accurate and precise harmonic estimation, wavelet coefficients of more than one fundamental cycle need to be calculated, which degrades the time resolution of DWPT.

Undecimated Wavelet Packet Transform (UWPT) [88], [89] is also a multiresolution technique with additional features of redundancy and time-invariance. In addition to this, it can be easily implemented using a set of filter banks. The UWPT does not perform downsampling on wavelet coefficients at each decomposition level thus, preserving time-invariant property, which is lost in the DWPT. This time-invariant property of the UWPT has been exploited in this chapter to estimate time-varying harmonics accurately in one cycle of the fundamental frequency enabling it to be suitable for online applications.

This chapter proposes a simple and efficient algorithm based on the UWPT for accurate amplitude estimation of time-varying harmonics, which has much faster estimation speed than other wavelet transform based methods. The main attribute of this work is that the proposed method uses only one fundamental cycle data for estimation of the fundamental and harmonics amplitude. This not only reduces the computational time but also improves the time-resolution and real-time processing capability. Further, the UWPT algorithm is more suitable for implementation on FPGA hardware platform due to less implementation complexity, the capability of parallel processing using UWPT wavelet filters and simple nature of the algorithm. Multiply- accumulate (MAC) based architecture is adopted for the implementation of UWPT wavelet filters, which is the best compromise between resource utilization and timing requirements for the proposed application. The proposed algorithm has been successfully implemented on Virtex-6 FPGA ML-605 board after proper analysis and synthesis in XSG/ISE design suite 14.2. The performance of the proposed method has been investigated on synthetic as well as experimental test signals. The results confirm the effectiveness of the proposed algorithm for estimation of stationary and time-varying harmonics in power system.

2.2 Undecimated Wavelet Packet Transform

To define the UWPT, a brief review of DWPT is required because UWPT is a modified version of DWPT. Let $\boldsymbol{X}$ be a measurement vector, which consists of N samples $\boldsymbol{X_0}, \boldsymbol{X_1}, \ldots$

., $\boldsymbol{X_{N-1}}$ from a distorted signal. The even length low-pass filter and high-pass filter are indicated by $\{h(l) : l = 0, 1, \ldots, L-1\}$ and $\{g(l) : l = 0, 1, \ldots, L-1\}$ respectively, where L is the length of the filter. Both the filters satisfy the following property for all non-zero integer n.

$$\sum_{l=0}^{L-1} z^2(l) = 1, \sum_{l=0}^{L-1} z(l)z(l+2n) = \sum_{l=-\infty}^{\infty} z(l)z(l+2n) = 0 \tag{2.1}$$
$$\text{where, } z(l) :\Leftrightarrow h(l) \text{ or } g(l)$$

In addition to this property, the high and low pass filters are also Quadrature Mirror Filters (QMFs) satisfying the following equation (2.2) and (2.3).

$$g(l) = (-1)^l h(L-l-1) \tag{2.2}$$

$$h(l) = (-1)^{l+1} g(L-l-1) \quad \forall l = 0, \ldots, L-1 \tag{2.3}$$

The wavelet coefficients at each decomposition level are extracted by convolution of the previous level wavelet coefficients with the impulse response of the wavelet filters, followed by downsampling by a factor of two. The wavelet coefficients of the input signal at the j^{th} decomposition level, n^{th} point and $2i^{th}$ node can be calculated as:

$$X_j^{2i}(n) = \sum_{l=0}^{L-1} h(l) X_{j-1}^{i}(2n-l) \tag{2.4}$$

$$X_j^{2i+1}(n) = \sum_{l=0}^{L-1} g(l) X_{j-1}^{i}(2n-l) \tag{2.5}$$

The problem associated with the DWPT is that it is not a time-invariant transform [94]. The relevance of time-invariant property is that any change in the behaviour of a signal is reflected by the same change in the transformed coefficients. It helps to identify and detect the time-varying characteristics of the signal, but this property is lost mainly due to downsampling. Since the wavelet coefficients are calculated only in alternate sampling, it is not possible to obtain wavelet coefficients at every time instant [88]. As a result, the number of wavelet coefficients gets reduced by two with an increase in decomposition levels, thus limiting its ability to carry out an accurate harmonic analysis of a time-varying signal.

The UWPT is a generalized form of the DWPT and decomposes the measured signal in the uniform frequency band. The UWPT holds all the advantage of the DWPT but overcomes the problem of insufficient wavelet coefficients. Its capability is utilized in many applications of electrical engineering [95], [96], [97]. In the UWPT, rescaling of the defined wavelet filters is required to conserve the energy of coefficients.

$$\tilde{h}(l) = h(l) \big/ \sqrt{2} \tag{2.6}$$

$$\tilde{g}(l) = g(l) \big/ \sqrt{2} \tag{2.7}$$

With incorporation of (2.6) and (2.7), (2.1) now becomes

$$\sum_{l=0}^{L-1} \tilde{z}^2(l) = 1/2, \sum_{l=0}^{L-1} \tilde{z}(l)\tilde{z}(l+2n) = \sum_{l=-\infty}^{\infty} \tilde{z}(l)\tilde{z}(l+2n) = 0 \tag{2.8}$$

where, $\tilde{z}(l) :\Leftrightarrow \tilde{h}(l)$ or $\tilde{g}(l)$

and the wavelet filters are still Quadrature Mirror Filters (QMF) satisfying the following property

$$\tilde{g}(l) = (-1)^l \tilde{h}(L-l-1) \tag{2.9}$$

$$\tilde{h}(l) = (-1)^{l+1} \tilde{g}(L-l-1) \tag{2.10}$$

In contrast to the DWPT, the UWPT does not carry out downsampling by a factor of two during decomposition process [88]. Thus, it creates appropriate new filters at each decomposition level, performing filter upsampling [94] by padding $2^{j-1}-1$ zeros between each coefficient of $\{\tilde{h}(l)\}$ and $\{\tilde{g}(l)\}$

$$\tilde{h}_j(l) = \left[\tilde{h}(0), \underbrace{0,\ldots,0}_{2^{j-1}-1}, \tilde{h}(1), \underbrace{0,\ldots,0}_{2^{j-1}-1}, \tilde{h}(2), \ldots\ldots\ldots, \tilde{h}(L-1), \underbrace{0,\ldots,0}_{2^{j-1}-1} \right] \tag{2.11}$$

$$\tilde{g}_j(l) = \left[\tilde{g}(0), \underbrace{0,\ldots,0}_{2^{j-1}-1}, \tilde{g}(1), \underbrace{0,\ldots,0}_{2^{j-1}-1}, \tilde{g}(2), \ldots\ldots\ldots, \tilde{g}(L-1), \underbrace{0,\ldots,0}_{2^{j-1}-1} \right] \tag{2.12}$$

At the first decomposition level, the UWPT applies the initial low pass filter and high pass filter to split the frequency spectrum of the input signal into low and high-frequency components (approximation coefficients and detail coefficients). This process repeats recursively, and the decomposition is performed on both the approximation as well as detail coefficients at each level. The structure of three level UWPT is shown in Figure 2.1. The wavelet coefficients of the input signal at the j^{th} decomposition level, n^{th} point and $2i^{th}$ node can be represented as:

$$X_j^{2i}(n) = \sum_{l=0}^{L-1} \tilde{h}_j(l) X_{j-1}^{i}(n-l) \tag{2.13}$$

$$X_j^{2i+1}(n) = \sum_{l=0}^{L-1} \tilde{g}_j(l) X_{j-1}^{i}(n-l) \tag{2.14}$$

2.3 Application of UWPT for Harmonics Estimation

In general, the distorted waveform of a power system voltage (or current) signal $x(t)$ can be modeled as the sum of sinusoids with additive white Gaussian noise,

$$x(t) = y(t) + \eta(t) \approx \sum_{h=1}^{H} A_h \sin(2\pi f_h t + \theta_h) + \eta(t) \tag{2.15}$$

where t is the time, $\eta(t)$ is the white Gaussian noise with zero mean, h is the harmonic order, and f_h, A_h and θ_h are the frequency, amplitude and phase angle of h^{th} harmonic component respectively. When time domain sampling is applied on the measured signal at a regular sampling interval of T_s, then (2.15) can be expressed in discrete form for the n^{th} sample as:

$$x[n] = x(nT_s) = y(nT_s) + \eta(nT_s) \approx \sum_{h=1}^{H} A_h \sin(2\pi f_h nT_s + \theta_h) + \eta(nT_s) \tag{2.16}$$

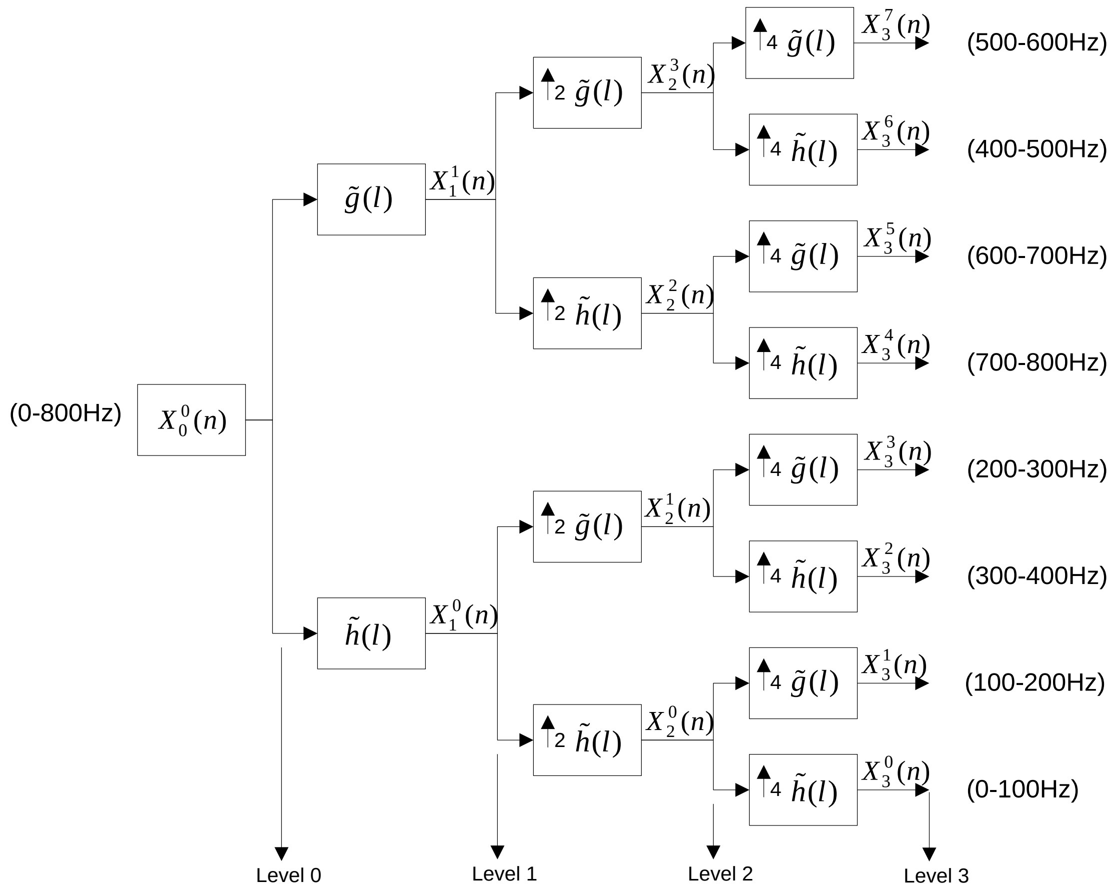

Figure 2.1: Three-level UWPT decomposition tree

The proposed UWPT based algorithm is redundant and translational invariant transform, which executes the same filtering step as in the DWPT and also depends on some parameter, such as sampling frequency f_s, the frequency response of the wavelet filters and the number of decomposition level. The major difference is that it does not perform downsampling on the output wavelet coefficients of any decomposition level. Figure 2.1 illustrates the implementation procedure for estimation of power system harmonics using the UWPT. The spectral partition of the input signal $x(\mathrm{n})$ is obtained at the first decomposition level using the quadrature mirror filters $\tilde{h}(l)$ and $\tilde{g}(l)$, which split the frequency spectrum into two equal parts from 0 to $(\pi/2)$ rad and from $(\pi/2)$ to (π) rad. To further divide the frequency spectrum of these subbands at the next level, the process of filter upsampling is first performed by inserting the zero in-between each pair of coefficients. Due to the upsampling process at the second decomposition level, the frequency response of initial wavelet filters is compressed in $|f/\pi| \le 1/2$, and its mirror image lies in the range of $1/2 < |f/\pi| \le 1$ as shown in Figure 2.2(b). Figure 2.2 shows the frequency response of wavelet filters at different decomposition level. At subsequent decomposition levels, the process of filter upsampling is performed in a similar manner. Hence at decomposition level *j*, the frequency response of wavelet filters is compressed in the spectrum by $|f/\pi| \le 1/2^{j-1}$ and the image of this graph (different lobes) is covered over the whole spectrum. For this work, the "db20" with 40 coefficients have been used as the mother wavelet. Thus, the wavelet coefficients at each decomposition level are calculated by the convolution of previous level wavelet coefficients with the impulse response of the modified wavelet filter of the current decomposition level in accordance with (2.13) and (2.14).

The proposed structure for harmonic estimation comprises of three level decomposition tree as shown in Figure 2.1. The flowchart shown in Figure 2.3 describes the implementation procedure of the proposed algorithm for amplitude estimation. With 1.6 kHz sampling frequency, output nodes at the last decomposition level are partitioned into eight bands with fixed interval of 100 Hz. The proposed structure is designed to extract only the fundamental component and the odd harmonics up to 15th component. However, the estimation of higher order harmonics can be achieved by increasing the number of levels in the UWPT decomposition tree and choosing the corresponding sampling frequency.

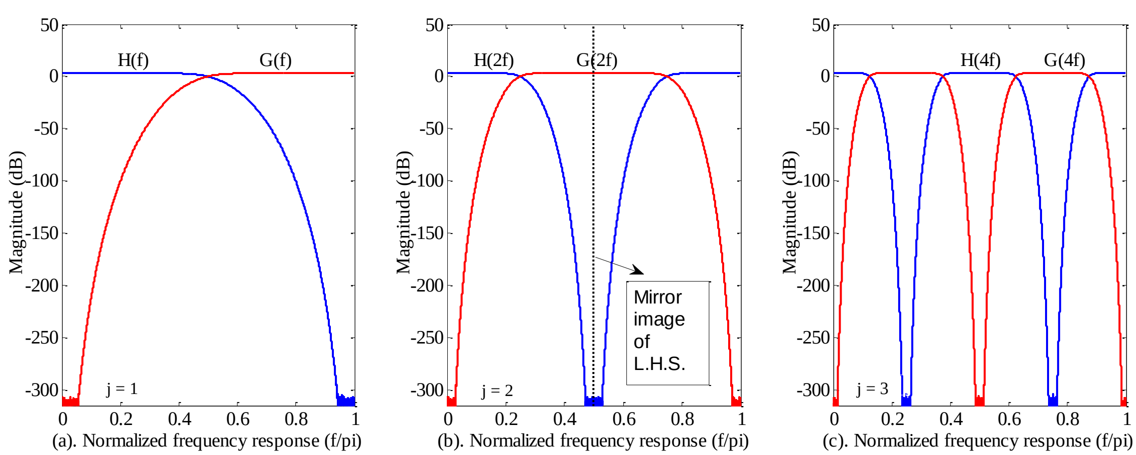

Figure 2.2. Frequency response of Daubechies-20 filters at decomposition level *j*=1, 2, and 3.

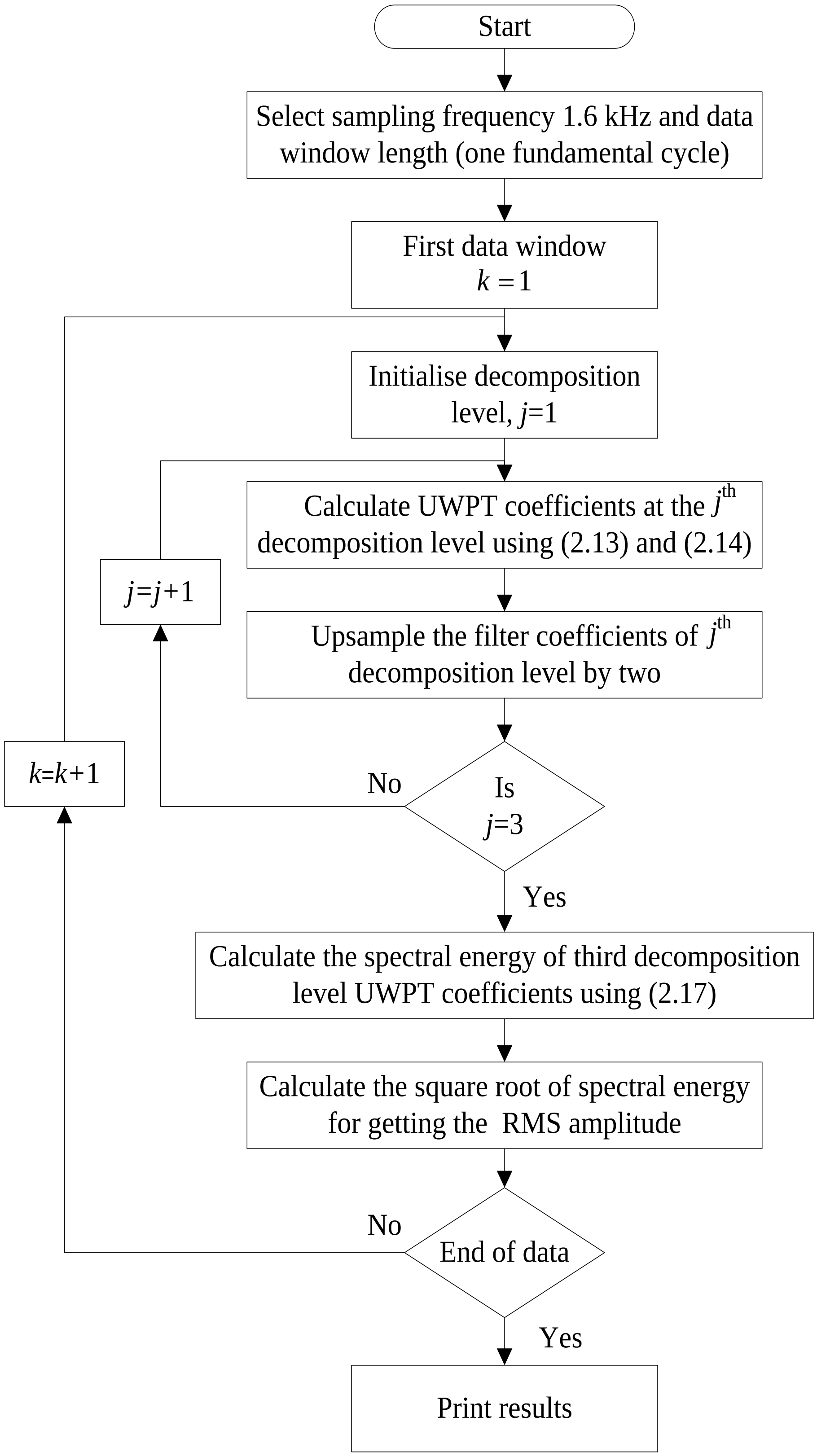

Figure 2.3. Flowchart of the proposed UWPT algorithm for three level decomposition tree

One of the major advantages of the UWPT, which is contrary to the decimated DWPT, is that the wavelet coefficients contain the same number of samples at each level as taken in the original signal. This enables it to estimate the power system harmonics in only one fundamental cycle i.e. 20 ms in a 50-Hz system. Information about the number of nodes at each decomposition level, samples per node and bandwidth of the nodes at each decomposition level is given in Table 2.1.

According to Parseval's theorem [98], the spectral energy of the distorted signal $x(n)$ can be decomposed in terms of the wavelet coefficients energy. Therefore, the spectral energy of an input signal in terms of wavelet coefficients energy at j^{th} decomposition level and $2i^{\text{th}}$ node can be represented as follows:

$$\sum_{-\infty}^{\infty}\left|x(n)\right|^{2} = \sum_{j=0}^{\infty}\sum_{i=0}^{j}\sum_{n=-\infty}^{\infty}\left|x_j^{2i}(n)\right|^{2} + \sum_{j=0}^{\infty}\sum_{i=0}^{j}\sum_{n=-\infty}^{\infty}\left|x_j^{2i+1}(n)\right|^{2} \tag{2.17}$$

Each output node of the last decomposition level contains the energy of the respective frequency components in terms of wavelet coefficients energy, which can be used to estimate the RMS amplitude of the fundamental and the odd harmonics.

Table 2.1: Details of three level UWPT decomposition tree

Decomposition level	Number of nodes	Samples per node	Bandwidth of node (in Hz)
1	2	32	400
2	4	32	200
3	8	32	100

2.4 Performance Evaluation

In this section, simulation results have been presented to investigate the performance of the proposed algorithm for power system harmonic estimation. One cycle of each test signal has been analyzed using the proposed method based on the UWPT. Since IEC 61000-4-7 [11] recommends the use of the DFT for harmonic estimation using ten cycles windowed signal, the performance of the DFT has been evaluated considering ten cycles of the signal. However, the performance comparison of the proposed method has been made with the

DWPT considering both one cycle and ten cycles of the signals. The absolute amplitude error of the estimated amplitude of each frequency component is calculated as defined in (2.18). The mean and maximum values of the absolute amplitude errors of all harmonics have been used to compare the performance of different methods.

$$Absolute\ amplitude\ error = |Estimated\ RMS\ value - Actual\ RMS\ value| \tag{2.18}$$

The sampling frequency for each test case is 1.6 kHz, i.e., 32 samples per fundamental cycle and $\omega=2\pi f$, where f is the fundamental frequency of 50 Hz. In the case of the DWPT and the UWPT methods, decomposition up to the third level has been done with "db20" mother wavelet. All the computations are carried out in MATLAB hosted on a laptop having an Intel Core i5 2.4 GHz processor, with 4 GB random access memory.

2.4.1 Test 1: Stationary Signal

The first test demonstrates the performance of the proposed algorithm to estimate the fundamental and harmonic components of a stationary signal. The synthesized signal is composed of odd integer harmonics along with the fundamental frequency component and is generated using (2.19) for 1 s duration. However, in order to show the signal variations clearly, only ten cycles are shown in Figure 2.4. In many practical situations, power supply waveforms are contaminated by noise. Hence, the signal is contaminated by the white Gaussian noise of 50 dB SNR.

$$v(t) = \sqrt{2}\begin{bmatrix} \sin(\omega t+\theta_1)+0.2\sin(3\omega t+\theta_2)+0.2\sin(5\omega t)+0.1\sin(7\omega t) \\ +0.1\sin(9\omega t)+0.1\sin(11\omega t)+0.1\sin(13\omega t)+0.1\sin(15\omega t) \end{bmatrix}+\eta(t) \tag{2.19}$$

Table 2.2 compares the mean and maximum values of absolute amplitude errors (Volt) obtained in the amplitude estimation of the individual harmonic components of the test signal-1 using the FFT, the DWPT, and the UWPT. As expected, the values of absolute amplitude errors obtained with the FFT are less than the wavelet-based algorithm. This is because the FFT performs better for stationary signals. The mean and maximum values of absolute amplitude errors obtained using the DWPT algorithm with one cycle window is quite high due to the downsampling of wavelet coefficients. However, the performance of the DWPT algorithm improves with an increase in the window length. Hence, ten cycles windowed signal has been considered for the performance comparison of the DWPT. It can be observed that the mean and maximum values of absolute amplitude errors obtained with the proposed algorithm are less in comparison to those obtained using the DWPT in both cases, viz. one cycle and ten cycles. The proposed algorithm can estimate the harmonic components within one cycle with better accuracy indicating the suitability of the proposed algorithm for real-time applications.

Table 2.2: Mean and maximum values of absolute amplitude error for the stationary test signal-1

Method		**Absolute Amplitude Error (Volt)**							
		1st	**3rd**	**5th**	**7th**	**9th**	**11th**	**13th**	**15th**
FFT	*Mean*	1.54E-04	9.20E-05	1.98E-04	8.70E-05	1.00E-04	2.31E-04	1.10E-04	1.19E-04
	Max	2.73E-04	1.39E-04	4.67E-04	1.75E-04	2.25E-04	3.17E-04	2.11E-04	2.41E-04
DWPT (10 cycles)	*Mean*	8.98E-03	2.16E-02	9.34E-04	5.11E-03	5.80E-03	4.15E-03	3.44E-03	2.91E-03
	Max	9.12E-03	2.18E-02	1.10E-03	5.33E-03	6.01E-03	4.46E-03	3.71E-03	3.20E-03
DWPT (1 cycle)	*Mean*	2.46E-02	6.79E-02	1.79E-02	2.32E-02	1.26E-02	1.79E-02	1.48E-02	5.19E-03
	Max	2.63E-02	6.89E-02	1.85E-02	2.45E-02	1.39E-02	1.88E-02	1.57E-02	6.51E-03
Proposed method	*Mean*	3.48E-04	4.46E-04	3.79E-04	3.32E-04	3.59E-04	4.74E-04	4.29E-04	4.27E-04
	Max	1.15E-03	1.24E-03	1.02E-03	1.48E-03	1.09E-03	1.51E-03	1.76E-03	1.51E-03

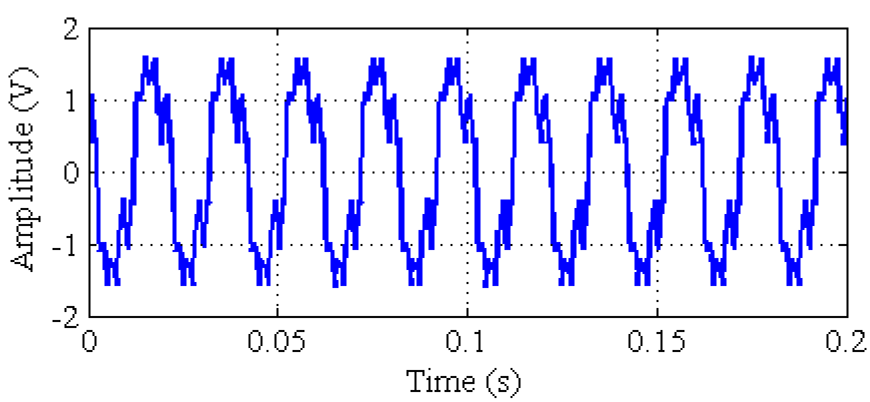

Figure 2.4. Test signal-1: Synthetic stationary signal

2.4.2 Test 2: Time-Varying Signal

1) Large Amplitude Fluctuation

The real power system is time-varying in nature, where the amplitude, phase and frequency of fundamental component and harmonics fluctuate with respect to time. For this purpose, test signal-2(a) of 1 s, shown in Figure 2.5 is generated by simulation of equation (2.16) with large variation in amplitude. The time-varying parameters of the signal are mentioned in Table 2.3. In the test signal-2(a), the fundamental frequency and amplitudes are varied at every 0.1 s within the range of ±0.5 % and ±20 %, respectively and white Gaussian noise of Signal-to-Noise Ratio (SNR) of 40 dB is added to the signal.

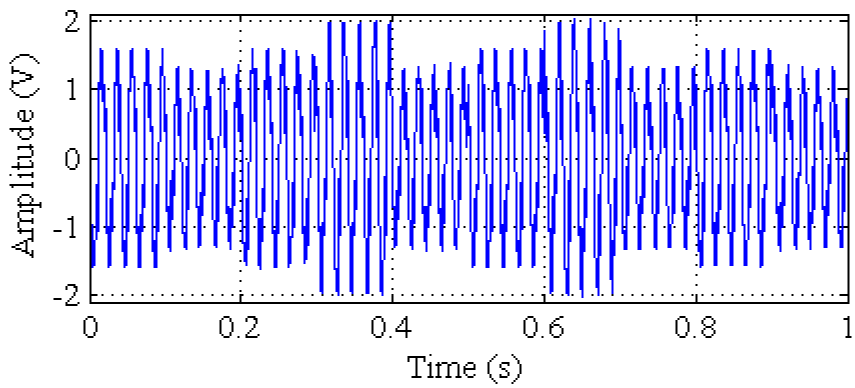

Figure 2.5. Test signal-2(a): Synthetic signal with large amplitude fluctuation, fundamental frequency deviation and noise

Table 2.3: Parameters of the test signal-2(a)

Time (s)	Amplitude ($A_h/\sqrt{2}$), Frequency components (f_h in Hz) and Phase angle (θ_h in degree)							
0.0-0.1	1, 50, 152	0.2, 150, 35	0.2, 250, 0	0.1. 350, 0	0.1, 450, 152	0.1, 550, 35	0.1, 650, 0	0.1, 750, 0
0.1-0.2	0.8, 50.25, 152	0.18, 150.75, 0	0.18, 251.25, 0	0.08, 351.75, 0	0.08, 452.25, 152	0.08, 552.75, 35	0.08, 653.25, 0	0.08, 753.75, 0
0.2-0.3	1, 50.25, 152	0.2, 150.75, 35	0.2, 251.25, 0	0.1, 351.75, 0	0.1, 452.25, 152	0.1, 552.75, 35	0.1, 653.25, 0	0.1, 753.75, 0
0.3-0.4	1.2, 50, 152	0.22, 150, 0	0.22, 250, 0	0.12. 350, 0	0.12, 450, 152	0.12, 550, 35	0.12, 650, 0	0.12, 750, 0
0.4-0.5	0.8, 50.25, 152	0.18, 150.75, 0	0.18, 251.25, 0	0.08, 351.75, 0	0.08, 452.25, 152	0.08, 552.75, 35	0.08, 653.25, 0	0.08, 753.75, 0
0.5-0.6	1, 50, 152	0.2, 150, 35	0.2, 250, 0	0.1. 350, 0	0.1, 450, 152	0.1, 550, 35	0.1, 650, 0	0.1, 750, 0
0.6-0.7	1.2, 49.75, 152	0.22, 149.25, 0	0.22, 248.75, 0	0.12. 348.25, 0	0.12, 447.75, 152	0.12, 547.25, 35	0.12, 646.75, 0	0.12, 746.25, 0
0.7-0.8	0.8, 50, 152	0.18, 150, 0	0.18, 250, 0	0.08, 350, 0	0.08, 450, 152	0.08, 550, 35	0.08, 650, 0	0.08, 750, 0
0.8-0.9	1, 50, 152	0.2, 150, 35	0.2, 250, 0	0.1. 350, 0	0.1, 450, 152	0.1, 550, 35	0.1, 650, 0	0.1, 750, 0
0.9-1.0	0.8, 49.75, 152	0.18, 149.25, 0	0.18, 248.75, 0	0.08. 348.25, 0	0.08, 447.75, 152	0.08, 547.25, 35	0.08, 646.75, 0	0.08, 746.25, 0

Table 2.4: Mean and maximum values of absolute amplitude error (Volt) for the time-varying test signal-2(a)

Method		**Absolute Amplitude Error (Volt)**							
		1st	**3rd**	**5th**	**7th**	**9th**	**11th**	**13th**	**15th**
FFT	*Mean*	9.74E-02	6.83E-02	7.03E-02	4.03E-02	4.58E-02	4.44E-02	3.91E-02	5.43E-02
	Max	2.44E-01	1.79E-01	1.53E-01	8.55E-02	8.87E-02	6.24E-02	7.43E-02	8.28E-02
	SD	9.62E-02	6.81E-02	5.27E-02	2.80E-02	3.95E-02	1.71E-02	3.16E-02	2.75E-02
DWPT (10 cycles)	*Mean*	4.47E-02	1.71E-02	5.98E-03	7.57E-03	6.03E-03	5.19E-03	1.61E-03	5.74E-03
	Max	7.80E-02	2.81E-02	8.93E-03	1.43E-02	9.71E-03	1.25E-02	2.68E-03	9.51E-03
	SD	2.60E-02	9.23E-03	1.97E-03	4.24E-03	3.00E-03	4.29E-03	1.12E-03	2.91E-03
DWPT (1 cycle)	*Mean*	3.11E-02	4.50E-02	1.81E-02	1.91E-02	1.66E-02	1.13E-02	1.12E-02	7.11E-03
	Max	8.25E-02	8.04E-02	4.11E-02	3.03E-02	4.37E-02	2.32E-02	2.00E-02	2.46E-02
	SD	1.67E-02	2.74E-02	8.70E-03	8.29E-03	8.89E-03	7.06E-03	5.45E-03	5.61E-03
Proposed method	*Mean*	2.34E-03	2.39E-03	1.84E-03	2.37E-03	2.18E-03	2.25E-03	2.07E-03	2.36E-03
	Max	6.69E-03	6.22E-03	6.61E-03	8.08E-03	8.39E-03	6.57E-03	6.32E-03	8.25E-03
	SD	1.70E-03	1.69E-03	1.45E-03	1.94E-03	1.61E-03	1.98E-03	1.41E-03	2.06E-03

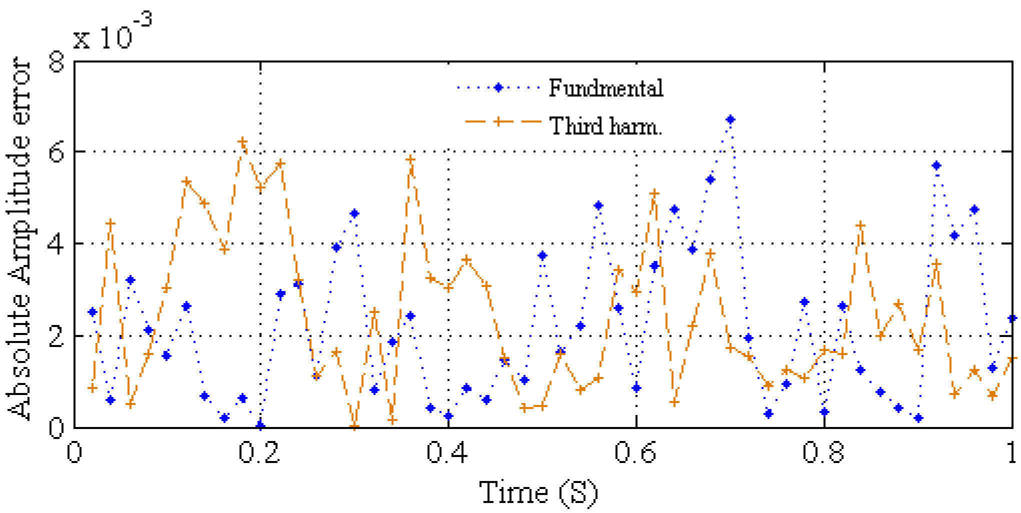

Figure 2.6. Absolute amplitude errors of the UWPT in amplitude estimation of the fundamental and third harmonic of test signal-2(a)

Figure 2.6 shows dynamic absolute amplitude errors obtained using the UWPT for the fundamental and third harmonic with reference to time. The mean, maximum and Standard Deviation (SD) of absolute amplitude errors (Volt) for the time-varying test signal-2(a) are presented in Table 2.4. It can be observed that due to the time-varying nature of the test signal-2(a), estimation accuracy of all the methods is reduced. The mean values of absolute amplitude errors reveal that the estimation accuracy of the FFT is most affected while the proposed technique is least affected. For the thirteenth harmonic, the mean and maximum of absolute amplitude errors of the proposed method is slightly higher than the DWPT algorithm with ten cycle window. But consistently low values of mean and maximum of absolute amplitude errors from first to eleventh and fifteenth harmonics confirm the suitability of the UWPT algorithm over the DWPT algorithm with ten cycle window. It is also observed from the standard deviation of the absolute amplitude errors that the UWPT has at most SD of 2.059E-03 whereas for the other approaches it ranges from 1.12E-03 to 9.62E-02. It is worth noticing that these results for the UWPT algorithm are obtained using only one cycle. The main objective of test signal-2(a) is to demonstrate the capability of the proposed method to examine the influence of large fluctuation in amplitude, noise contamination, and robustness against fundamental frequency deviation.

2) Small Amplitude Fluctuation

To demonstrate the effectiveness of the proposed method, a time-varying test signal-2(b) of 1 s duration is simulated with little variation in amplitude according to (2.16). In this test signal, variations in amplitudes and frequencies are at most 5 % and 0.5 %, respectively with the Gaussian white noise of 40 dB SNR. The time-varying parameters are specified in Table 2.5 and the signal is shown in Figure 2.7.

The mean, maximum and Standard Deviation (SD) of absolute amplitude errors (Volt) for the FFT, DWPT and the proposed method are presented in Table 2.6. It can be noticed from the Table 2.6 that the FFT performs poorly due to spectral leakage and the DWPT results are better relative to the FFT. Whereas the proposed method provides more reliable results and absolute amplitude errors are quite low as compared to that of the FFT and the DWPT. The estimated per-cycle RMS amplitudes for the fundamental component, third, fifth and eleventh harmonics using UWPT method are shown in Figure 2.8 (a). Figures 2.8 (b) and (c) show the zoomed view of Figure 2.8 (a) from t = 0.68 s to t = 0.75 s, where the amplitude of fundamental and harmonics components is changing significantly. It is clear from the results that the proposed technique based on the UWPT

Table 2.5: Parameters of the test signal-2(b)

Time (s)	Amplitude (Variation ±5%) ($A_h/\sqrt{2}$), Frequency components (f_h in Hz) and Phase angle (θ_h in degree)							
0.0-0.1	1, 50, 152	0.2, 150, 35	0.2, 250, 0	0.1, 350, 0	0.1, 450, 152	0.1, 550, 35	0.1, 650, 0	0.1, 750, 0
0.1-0.2	0.95, 50.25, 152	0.19, 150.75, 0	0.19, 251.25, 0	0.095, 351.75, 0	0.095, 452.25, 152	0.095, 552.75, 35	0.095, 653.25, 0	0.095, 753.75, 0
0.2-0.3	1.02, 50.25, 152	0.204, 150.75, 35	0.204, 251.25, 0	0.102, 351.75, 0	0.102, 452.25, 152	0.102, 552.75, 35	0.102, 653.25, 0	0.102, 753.75, 0
0.3-0.4	1.05, 50, 152	0.21, 150, 0	0.21, 250, 0	0.105. 350, 0	0.105, 450, 152	0.105, 550, 35	0.105, 650, 0	0.105, 750, 0
0.4-0.5	0.95, 50.25, 152	0.19, 150.75, 0	0.19, 251.25, 0	0.095, 351.75, 0	0.095, 452.25, 152	0.095, 552.75, 35	0.095, 653.25, 0	0.095, 753.75, 0
0.5-0.6	1, 50, 152	0.2, 150, 35	0.2, 250, 0	0.1, 350, 0	0.1, 450, 152	0.1, 550, 35	0.1, 650, 0	0.1, 750, 0
0.6-0.7	1.05, 50, 152	0.21, 150, 0	0.21, 250, 0	0.105, 350, 0	0.105, 450, 152	0.105, 550, 35	0.105, 650, 0	0.105, 750, 0
0.7-0.8	0.95, 50.25, 152	0.19, 150.75, 0	0.19, 251.25, 0	0.095, 351.75, 0	0.095, 452.25, 152	0.095, 552.75, 35	0.095, 653.25, 0	0.095, 753.75, 0
0.8-0.9	1, 50, 152	0.2, 150, 35	0.2, 250, 0	0.1, 350, 0	0.1, 450, 152	0.1, 550, 35	0.1, 650, 0	0.1, 750, 0
0.9-1.0	0.95, 50.25, 152	0.19, 150.75, 0	0.19, 251.25, 0	0.095, 351.75, 0	0.095, 452.25, 152	0.095, 552.75, 35	0.095, 653.25, 0	0.095, 753.75, 0

Table 2.6: Mean and maximum values of absolute amplitude error (Volt) for the time-varying test signal-2(b)

Method		**Absolute Amplitude Error (Volt)**							
		1st	**3rd**	**5th**	**7th**	**9th**	**11th**	**13th**	**15th**
FFT	*Mean*	1.04E-01	8.30E-02	6.54E-02	4.76E-02	3.85E-02	4.32E-02	5.66E-02	4.82E-02
	Max	2.59E-01	1.59E-01	1.58E-01	8.46E-02	8.51E-02	6.82E-02	8.74E-02	7.81E-02
	SD	1.08E-01	6.15E-02	6.10E-02	2.31E-02	3.36E-02	2.53E-02	3.67E-02	3.03E-02
DWPT (10 cycles)	*Mean*	1.75E-02	2.17E-02	8.03E-03	3.24E-03	7.12E-03	1.50E-03	2.29E-03	4.44E-03
	Max	2.90E-02	3.64E-02	1.31E-02	6.17E-03	1.28E-02	2.02E-03	4.30E-03	8.85E-03
	SD	9.74E-03	1.07E-02	4.38E-03	2.27E-03	4.61E-03	7.21E-04	1.36E-03	3.07E-03
DWPT (1 cycle)	*Mean*	3.50E-02	5.00E-02	2.31E-02	1.91E-02	1.60E-02	1.20E-02	1.16E-02	7.84E-03
	Max	7.87E-02	7.18E-02	6.16E-02	3.16E-02	4.36E-02	2.07E-02	2.16E-02	2.78E-02
	SD	1.50E-02	2.38E-02	1.50E-02	7.49E-03	9.63E-03	6.54E-03	5.57E-03	6.71E-03
Proposed method	*Mean*	1.91E-03	2.55E-03	1.84E-03	2.51E-03	2.11E-03	3.20E-03	1.68E-03	2.26E-03
	Max	5.22E-03	7.97E-03	4.57E-03	6.82E-03	6.82E-03	8.50E-03	7.11E-03	8.61E-03
	SD	1.42E-03	2.14E-03	1.20E-03	2.10E-03	1.78E-03	2.35E-03	1.51E-03	2.06E-03

can estimate the time-varying harmonics accurately and consistently in one fundamental cycle and is much robust against fundamental frequency deviation and noise.

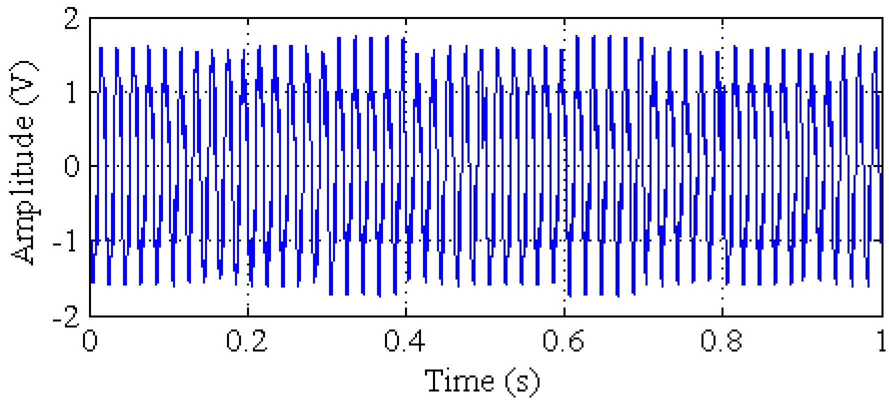

Figure 2.7. Test signal-2(b): Synthetic signal with small amplitude variation, fundamental frequency deviation and noise

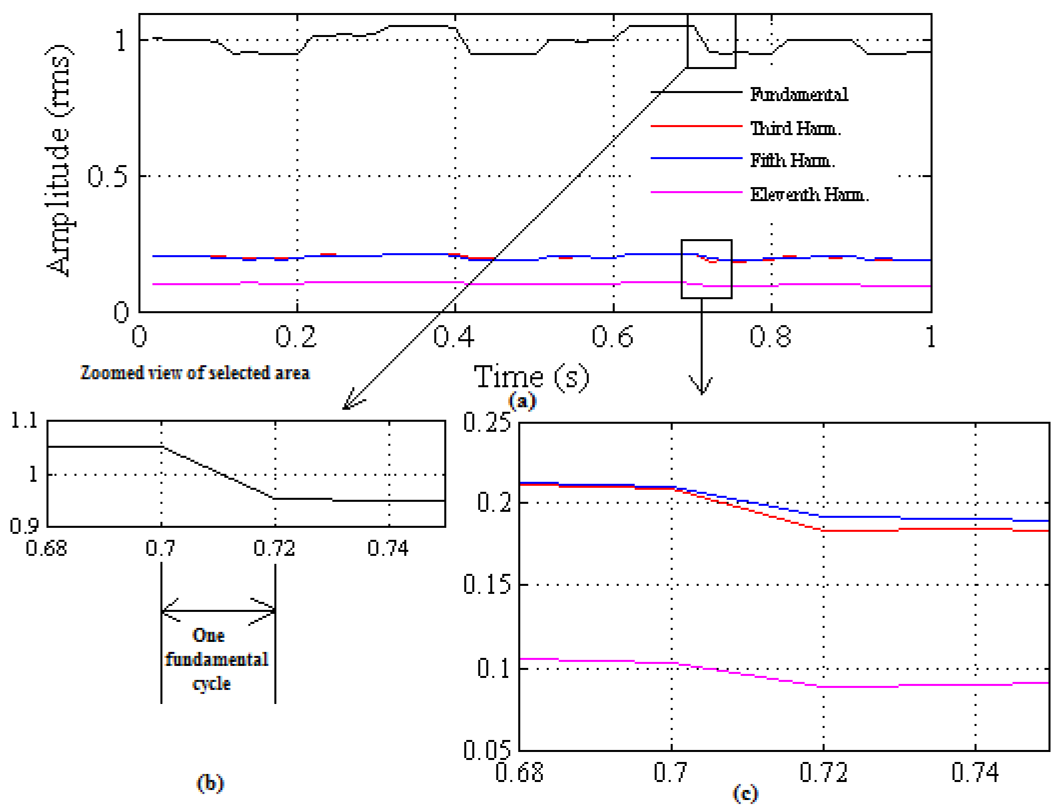

Figure 2.8. Estimated RMS amplitudes of the time-varying signal test signal-2(b)

2.4.3 Test 3: Time-Varying Measured Current Signal

It is a well-known fact that the non-linear loads introduce current harmonics into the system. Hence, an experimental setup is arranged in the laboratory to acquire a measured current signal using a current probe (A622). It consists of four different loads such as a Personal Computer (PC), a Laptop Charging (LC), a Mobile Charging (MC) and two Compact Fluorescent Lamps (CFLs). OROS-34 DAQ set up is interfaced to a laptop having the Nvgate software to acquire the measured current signal. The time-varying current signal is obtained by switching different loads. Initially, all the loads are connected to the supply and the current acquired is shown in segment-1 of Figure 2.9. Then the PC is switched off, leading to a reduction in current as can be seen from segment-2. The segment three is the current signal of PC and CFL loads. Four dominant harmonic components, namely 3rd, 5th 7th and 9th along with fundamental components are found in the measured current signal. In this signal, fundamental frequency also varies within the range of ±0.2 %.

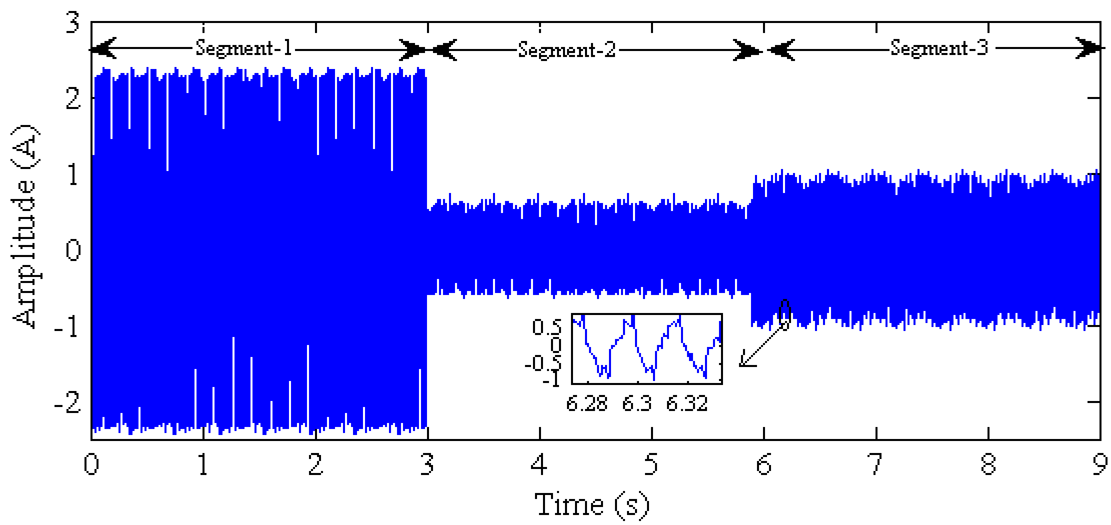

Figure 2.9. Test signal-3, measured time-varying signal

Test signal-3 of one cycle has been analyzed using the proposed method and the DWPT. Ten cycles of the signal with an overlap of nine cycles have also been used in the FFT, recommended by the IEC 61000-4-7 [11] for performance comparison. It is a known fact that the FFT-based estimation gives an accurate estimate of harmonics if the signal is stationary. The estimated RMS amplitude of the time-varying fundamental and third harmonic is shown in Figure 2.10. It can be noticed that when the signal amplitude is almost constant, both the UWPT and the FFT are able to estimate the RMS values of all the frequency components accurately. Since the UWPT uses one cycle data, it gives the estimated value just after a fundamental cycle while the FFT gives an average value of ten cycles. Because of this, the FFT-based estimate is constant and not varying with the cycle. When the signal changes abruptly from segment-1 to segment-2 and segment-2 to segment-

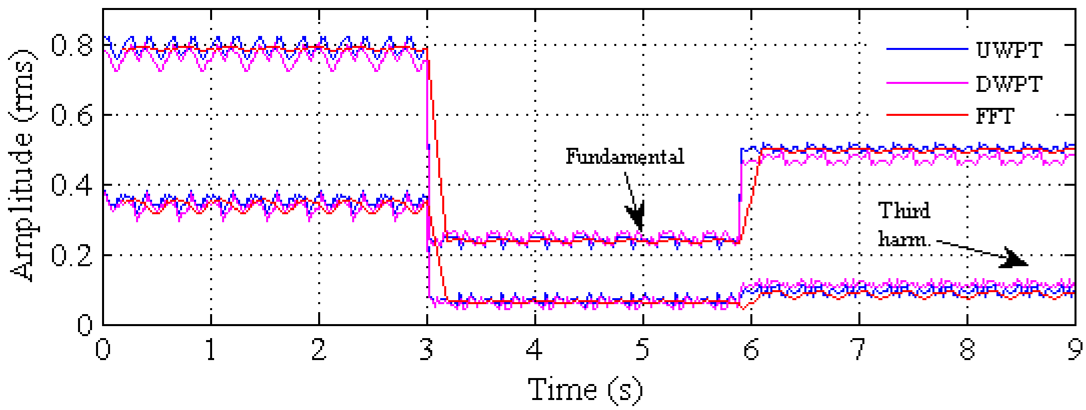

Figure 2.10. Estimated RMS amplitude of the fundamental and the third harmonic of test signal-3

3, the UWPT based amplitude estimation quickly reflects the change after one cycle while the FFT shows it after a delay of ten cycles. The DWPT for one cycle signal is also extracting the time-varying RMS, but the estimation accuracy is low in comparison to the UWPT and the FFT.

2.4.4 Noise Immunity

In real-time applications, measured voltage and current signal are corrupted by noise. Hence, it is important to investigate the accuracy of estimation in the presence of noise. The estimation accuracy of any technique in the presence of noise can be evaluated by comparing it with the Cramer-Rao Lower Bound (CRLB) [40], [99]. This provides a theoretical limit on the best possible estimation of parameters of the noisy signal. For this purpose, zero-mean white Gaussian noise of variance σ^2 is added to the test signal-1 and 1000 independent MATLAB simulations are performed. The CRLB for amplitude estimation [99] is calculated as

$$CRLB_A = \frac{2\sigma^2}{3N} \tag{2.20}$$

Where *N* is the number of samples in the adopted window. In the present case, the length of adopted window is one fundamental period and the sampling frequency is 1.6 kHz; hence the value of *N* is 32. Mean square error of the estimated amplitudes using the UWPT algorithm for the fundamental, third and fifth components are compared with the corresponding CRLBs as shown in Figure 2.11. It can be seen from the Figure 2.11 that the mean square error of the estimated amplitudes approaches the CRLB above 0 dB SNR, which demonstrates the robustness of the proposed method against noise.

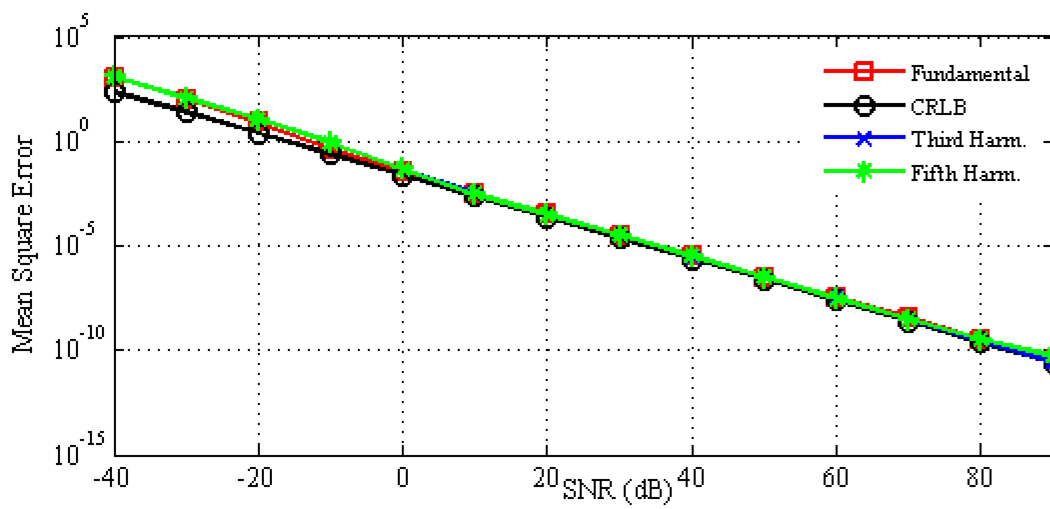

Figure 2.11. Mean square error versus SNR plot for the fundamental third and fifth harmonics component using test signal-1

2.5 FPGA-based Hardware Design of UWPT for Harmonic Estimation

For hardware implementation of the proposed UWPT based algorithm, an FPGA-based digital hardware has been developed for real-time harmonics estimation using the Xilinx Virtex-6 FPGA ML-605 Board, connected to a PC with MATLAB/Simulink, Xilinx System Generator, via JTAG interface.

XSG Implementation of the proposed architecture for harmonics estimation is shown in Figure 2.12. All the functional modules were implemented using Xilinx components [100]. The proposed UWPT based architecture comprises mainly of two functional modules. The first module is responsible for real-time calculations of wavelet coefficients, whereas the second module is implemented for the computation of RMS amplitudes of fundamental and harmonics using wavelet coefficients. Parallel computations are performed in each functional module utilizing the parallelism capability of FPGA. There are mainly two attributes in designing any architecture on FPGA platform. One is the timing requirement, and other is the resource utilization. Since the trade-off exists between these two attributes, they are usually decided on the basis of specific application requirement and the design criteria. The proposed digital architecture meets both the requirements for harmonic estimation.

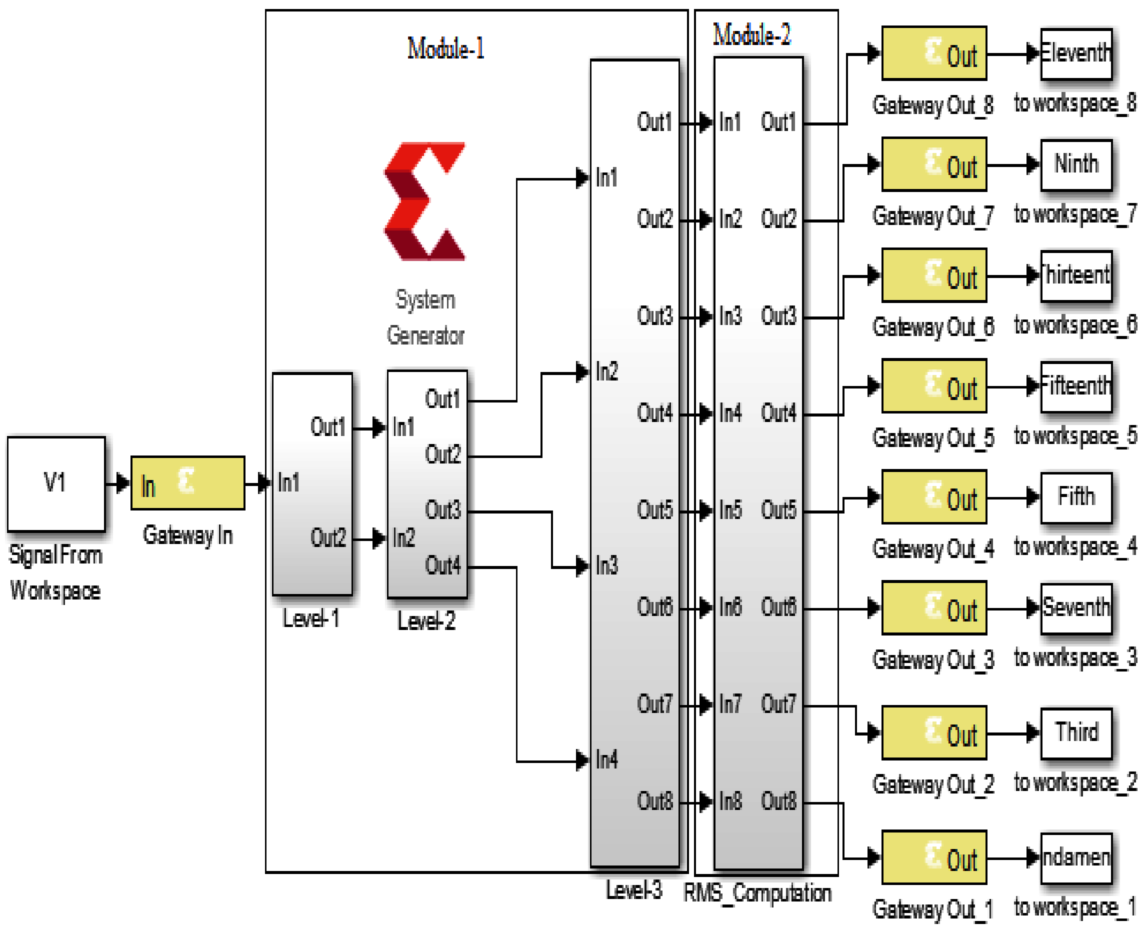

Figure 2.12. Digital design of three level UWPT decomposition tree on XSG

2.5.1 UWPT Wavelet Filter and RMS Calculation

Usually, the number of filter coefficients determine the cost of hardware for any filter. In UWPT, the number of filter coefficients increases by a factor of two at each increasing decomposition level because of the filter upsampling, thereby, increasing in memory requirements. Direct or transposed form based digital architecture requires more number of the embedded multiplier, which are limited on the FPGA board. Therefore, Multiply-Accumulate (MAC) based digital architecture is adopted rather than direct or transpose form. In MAC based architecture, all the filter coefficients may be stored in a single block RAM or distributed memory depending on the resources available for that FPGA board and a single embedded multiplier performs all the multiplications of that filter. However, its speed is slower than direct or transpose form but meet the timing requirements of the proposed application. Based on the requirements, this algorithm can be fit into a low-cost FPGA chip. Figure 2.13 shows the digital architecture of MAC-based FIR filter, in which filter coefficients are stored in a single port ROM in 18-bit fixed point format having 12 fractional bits. All the multiplications are accomplished in 18-bit fixed point format (within the width of the embedded multipliers).

In the second module, computation of RMS magnitude of the fundamental and each odd harmonics is carried out simultaneously by using eight parallel RMS processing units.

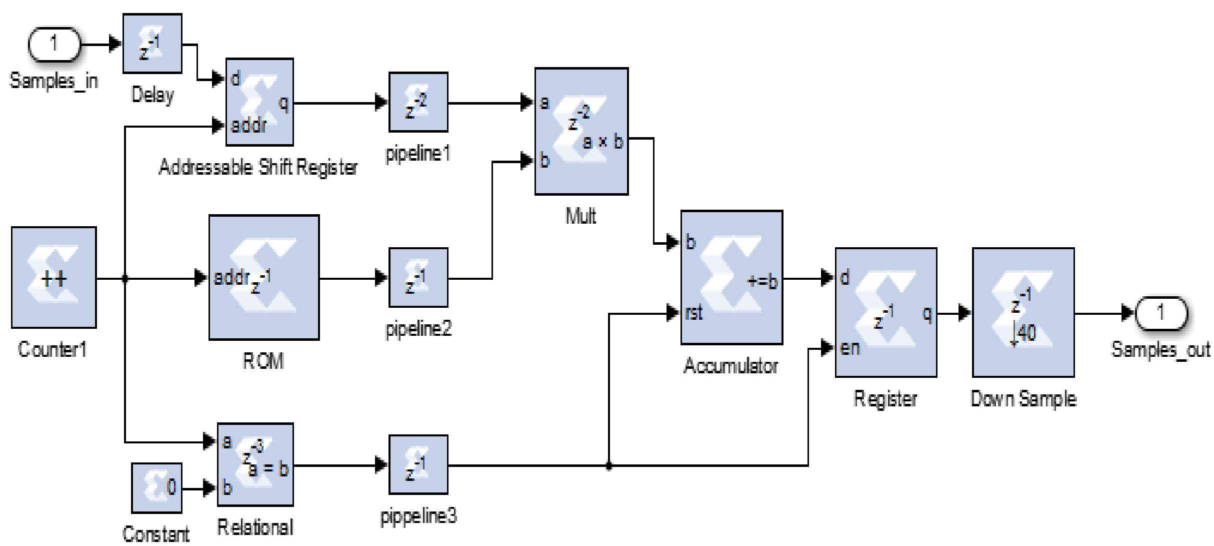

Figure 2.13. MAC based FIR filter on XSG

2.5.2 FPGA Implementation Result

Table 2.7 summarizes resource utilization and maximum operating frequency of the UWPT algorithm for estimation of harmonics in power system using Xilinx Virtex-6 FPGA ML-

605 Board. It can be observed that the resource utilization for MAC based digital architecture of the UWPT algorithm is very less and it can be easily implemented on a low-cost FPGA chip.

Table 2.7: Resource utilization summary after implementation for Xilinx Virtex-6 FPGA ML-605 board

Resource type	Used	Available
Number used as a FFs	6,629 (2 %)	301,440
Number of slice LUTs	16,298 (10 %)	150,720
Number of RAMB18E1s	14 (1 %)	832
Number of DSP184E1s	36 (4 %)	768
Max. operating frequency	58.51 MHz	

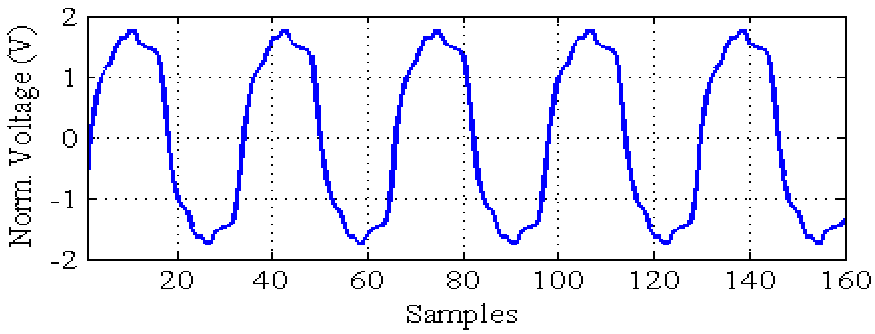

Figure 2.14. Measured voltage signal

Table 2.8: Amplitude estimation results for measured voltage signal

Harmonic component	True values	UWPT MATLAB results		UWPT hardware results (FPGA)	
		Mean	*Absolute amplitude error*	*Mean*	*Absolute amplitude error*
1st	1.3232	1.3233	1.00E-04	1.3194	0.0038
3rd	0.1907	0.1904	3.00E-04	0.1965	0.0058
5th	0.1363	0.1367	4.00E-04	0.1432	0.0069
7th	0.0521	0.0492	2.90E-03	0.0655	0.0134
11th	0.0353	0.0352	1.00E-04	0.0462	0.0109

The timing performance and the hardware accuracy of the proposed digital hardware have been investigated on a measured voltage signal [59] of duration 1 s. A few cycles of this signal is shown in Figure 2.14. As reported in [59], the measured voltage signal is having five dominant harmonic components, namely, fundamental, 3rd, 5th 7th and 11th harmonics. Since the fundamental and harmonic components of the voltage signal are unknown, results calculated from a high-resolution parametric technique [19] are considered as true values. Table 2.8 shows the mean value of the estimated amplitude and absolute amplitude errors of the fundamental and each harmonic. Results are obtained on Xilinx Virtex-6 FPGA ML-605 Board and MATLAB tool using the proposed algorithm. It can be observed from Table 2.8 that the accuracy in harmonic estimation is slightly reduced on hardware (FPGA) platform in comparison to the MATLAB based computation. This is because the quantization effect arises due to finite word-length of UWPT wavelet filters and the ADC resolution. The average and maximum absolute amplitude errors in harmonics estimation is 8.16E-03 and 0.0134 respectively, on hardware (FPGA) platform.

Table 2.9: Effect of finite word length of filter coefficients and ADC resolution for measured voltage signal

Harmonic components	**True values**	**F_fixed_18_12**		**F_fixed_12_8**	
		A_fixed_ 18_12	**A_fixed_ 12_8**	**A_fixed_ 18_12**	**A_fixed_ 12_8**
1st	1.3232	1.319483	1.319426	1.327332	1.327411
3rd	0.1907	0.196502	0.196493	0.199045	0.199050
5th	0.1363	0.143262	0.143271	0.143835	0.143853
7th	0.0521	0.065590	0.065595	0.066038	0.066030
11th	0.0353	0.04625	0.046481	0.046462	0.046493

In order to better explain the quantization effect, four experimental tests have been performed using the measured voltage signal with a different combination of wavelet filter coefficients word length and ADC resolution. Mean value of estimated amplitudes are shown in Table 2.9, where notation F_fixed_18_12 denotes word length of UWPT filter coefficients on FPGA in fixed point format having 12 fractional bits, 1 sign bit and 5 integer bits whereas A_fixed_18_12 indicates the resolution of the ADC in a similar manner. It can be observed from Table 2.9 that the estimation accuracy is more affected when the word length of filter coefficients is reduced as compared to change in the ADC resolution. This is due to accumulation of numerical errors because of the finite word length precision of the filter coefficients.

Table 2.10 shows the number of clock cycle required and the time taken by the fundamental and each harmonic on the Xilinx Virtex-6 FPGA ML-605 Board. The proposed algorithm on FPGA takes maximum 64,160 clock cycles for estimation of fundamental component, which is equivalent to 1.283 ms on a Virtex-6 FPGA ML-605 Board with the system clock frequency of 50 MHz. This is much less than the sampling window width of 20 ms (one fundamental cycle), thereby, confirming the utility of the proposed algorithm for online applications.

Table 2.10: Clock cycles required for estimation of power system harmonics of a measured voltage signal

Harmonic order	Clock cycles	FPGA (ms)
1st	64,160	1.283
3rd	45,120	.0902
5th	37,280	.0745
7th	53,760	1.075
11th	35,840	.0716

Table 2.11: Number of multiplications and additions

Method	Number of Multiplications	Number of additions
DWPT [16]	76800	74880
Proposed algorithm	53760	53312

2.5.3 Computational Complexity

The number of multiplications and additions per input sample define the computational cost of any algorithm, which in turn are also responsible for the time taken by the algorithm. The digital architecture of the algorithm as well as the hardware platform (FPGA and digital signal processors), both affect the computational time. The number of multiplications and additions of the proposed UWPT based algorithm and the three level DWPT [16] are listed in Table 2.11. It can be observed that the computational complexity is reduced significantly with the proposed algorithm.

2.6 Conclusion

In this chapter, a UWPT based technique has been presented for the estimation of stationary and time-varying harmonics. The proposed UWPT based method has the capability to estimate the amplitude of fundamental and each harmonic in one cycle of fundamental frequency with better accuracy. The performance of the proposed scheme is compared with similar techniques such as the DWPT and the FFT. Simulated and experimental results show that the UWPT algorithm has better estimation accuracy for different types of signals. Parallel processing using filters allows implementation of the UWPT algorithm on Xilinx Virtex-6 FPGA ML-605 Board. Resource utilization of the proposed digital architecture shows that the proposed scheme could be easily implemented on a low-cost FPGA-based chip. Performance with respect to accuracy, robustness, resource utilization and timing requirements confirm that the proposed scheme fulfills the requirement as provided by IEC Std. 61000-4-7.

Chapter 3

Measurement of Power Quality Indices Using Undecimated Wavelet Packet Transform

3.1 Introduction

The massive use of non-linear devices such as high-power semiconductor devices and power electronics converters has led to the deterioration of the quality of power supply from transmission level to distribution level. Many of the end-user devices are sensitive to power disturbances, therefore, the proper and continuous monitoring of power quality has become a significant concern for both power utilities as well as consumers. There is a need of common and concise techniques that can be easily understood by the utility provider, consumer and equipment manufacturer. The easiest method is to quickly quantify the quality of power supply in terms of power quality indices [7]. In this context, IEEE Standard 1459-2010 [12] suggests a common terminology that can be used for evaluation of power quality.

The conventional power quality indices suggested in the standards [2], [11], [12] are based on either Fourier series or FFT, which poses limitations in analysis of time-varying signals due to spectral leakage and does not provide any information about time. The DWT [52], the DWPT [55], [58], [62] and the EWT [67] have also been used for estimation of power quality indices. The literature survey presented in chapter one reveals that each of these has their own pros and cons. Harmonics amplitude estimation method based on the UWPT is proposed in chapter two and has been implemented on hardware also. It has been observed that UWPT is more suitable for real-time applications because of its inherent capability of parallel processing. Further, it requires only one fundamental cycle data resulting in a very fast estimation of harmonics amplitude and reduction in storage requirement for input samples. Moreover, it does not require any conditional and branching operations but involves simple algebraic operations, which makes it feasible to implement on dedicated hardware. However, the method proposed in chapter two is limited to only amplitude estimation of harmonics. In current scenario of smart grid, there is a need of measurement system capable of measuring power quality indices to provide information regarding energy consumption, quality of power supply and can be used for billing and revenue purposes. Therefore, utilizing the benefits of UWPT, this chapter develops a measurement system based on it for real-time measurement of power quality indices.

The hardware implementation of the proposed measurement scheme is quite challenging in comparison to chapter two. In case of power quality indices estimation, two parallel modules of signal processing technique are required: one for voltage signal and another for current signal. Moreover, the number of parameters (active, reactive and apparent powers, power factor etc.) to be monitored are large which increase the complexity of measurement system in terms of computational time, resource utilization and accuracy. In order to achieve the cost-effective measurement system as well as accurate and fast monitoring of the power quality indices, proper optimization between computational time, resource utilization and accuracy is required. This is because an improvement in any one of the specifications either computational time or resource utilization or accuracy becomes the reason for the deterioration of other specifications (either computational time or resource utilization or accuracy). Therefore, selection of suitable mother wavelet, choosing proper hardware architecture for measurement system and adequate selection of word-length for filter coefficients and algebraic operations are required.

Generally, for implementation of FIR filters on FPGA, direct or transpose form is used. Direct or transposed form-based hardware structure provides fast processing but at the cost of more hardware resources (specifically multipliers), which are available in limited amount on FPGA Board. These hardware structures are more suitable for signal processing applications such as communication system. In order to obtain better compromise between resource utilization and execution time, RAM based MAC FIR filter is used for implementation of wavelet filter. RAM based MAC FIR filter will consume only one multiplier and a dual port block RAM for implementation of single wavelet filter thereby significantly reducing the resource utilization in comparison to direct or transposed form-based hardware structure. The development of measurement system is described in next sections of this chapter. A set of tests have been carried out for performance verification of the proposed measurement system and the results show the capability of the proposed scheme in fulfilling the requirements as stated by IEEE Standard 1459-2010.

3.2 Review of Power Quality Indices

The definitions provided by the standard [12] are used to quantify the flow of electrical energy under the sinusoidal, nonsinusoidal, balanced or unbalanced conditions. This section provides a brief review of power quality indices for the single-phase system. In single phase system, a voltage and a current signal containing the fundamental and harmonic components can be represented by following mathematical equations:

$$v(n) = \sqrt{2}\sum_{h=1}^{H} V_h \sin(2\pi f_h nT_s + \theta_h) + \xi(nT_s) \tag{3.1}$$

$$i(n) = \sqrt{2}\sum_{h=1}^{H} I_h \sin(2\pi f_h nT_s + \phi_h) + \xi(nT_s) \tag{3.2}$$

where V_h, I_h, θ_h and ϕ_h are RMS amplitudes and phase angles of the voltage and current harmonics respectively, f_h is frequency, h is the harmonic order and ξ is the white Gaussian noise with zero mean. T_s is the sampling interval.

RMS Value of Voltage and Current

The RMS value of voltage and current signal can be calculated as:

$$V_{RMS} = \sqrt{V_1^2 + V_H^{\ 2}} = \sqrt{V_1^2 + \sum_{h>1} V_h^{\ 2}} \tag{3.3}$$

$$I_{RMS} = \sqrt{I_1^2 + I_H^{\ 2}} = \sqrt{I_1^2 + \sum_{h>1} I_h^{\ 2}} \tag{3.4}$$

where V_1 and I_1 are the RMS value of fundamental frequency components of voltage and current, respectively. H denote the non-fundamental component, and V_H and I_H are the total harmonic components.

Total Harmonic Distortion

Total harmonic distortion is defined as the deviation of distorted voltage or current waveform from its fundamental waveform and can be calculated as:

$$THD_v = \frac{V_H}{V_1} \quad and \quad THD_i = \frac{I_H}{I_1} \tag{3.5}$$

Active Power

The active power (P) is defined as the sum of the fundamental active power (P_1) and the harmonic active power (P_H)

$$P = P_1 + P_H \tag{3.6}$$

The fundamental active power is defined as:

$$P_1 = V_1 I_1 \cos\theta_1 \tag{3.7}$$

here θ_1 is the phase difference between fundamental voltage and current component.

The harmonic active power, also known as non-fundamental active power, is defined as:

$$P_H = \sum_{h>1} V_h I_h \cos\theta_h \tag{3.8}$$

here θ_h is the phase difference between harmonic voltage and current components.

Apparent Power

The apparent power (S) is the amount of active power that can be supplied to a load, under ideal condition. The fundamental apparent power is defined as

$$S_1 = V_1 I_1 = \sqrt{P_1^2 + Q_1^2} \tag{3.9}$$

The current and voltage distortion power (VAR) are

$$D_I = V_1 I_H \quad and \quad D_V = V_H I_1 \tag{3.10}$$

The harmonic apparent power (VA) and harmonic distortion power (VAR) are defined as

$$S_H = V_H I_H \quad and \quad D_H = \sqrt{S_H^2 - P_H^2} \tag{3.11}$$

The total apparent power is

$$S_H = V_{RMS} I_{RMS} = \sqrt{S_1^2 + D_I^2 + D_V^2 + S_H^2} \tag{3.12}$$

The nonactive power can be defined as

$$N = \sqrt{S^2 - P^2} \tag{3.13}$$

The non-fundamental apparent power can be defined as

$$S_N = \sqrt{D_I^2 + D_V^2 + S_H^2} \tag{3.14}$$

Reactive Power

The fundamental reactive power can be defined as

$$Q_1 = \sqrt{S_1^2 - P_1^2} = V_1 I_1 \sin\theta_1 \tag{3.15}$$

The reactive power of h^{th} harmonic component can be calculated from the corresponding active and apparent power

$$Q_h = \sqrt{S_h^2 - P_h^2} \tag{3.16}$$

Total harmonic reactive power is

$$Q_H = \sum_{h>1} Q_h \tag{3.17}$$

The total reactive power according to Budeanu's definition can be defined as

$$Q_B = Q_1 + Q_H \tag{3.18}$$

Power Factors

Displacement power factor and power factor can be defined as

$$dPF = \frac{P_1}{S_1}, \quad PF = \frac{P}{S} \tag{3.19}$$

3.3 UWPT-based Power Quality Indices

Details about three-level decomposition tree based on UWPT and frequency response of UWPT wavelet filters have been already discussed in chapter two. This section presents definitions of power quality indices based on UWPT.

According to IEEE Standard 1459-2010, first the fundamental and harmonic components are separated from each other using suitable spectral analysis technique and then power quality indices can be calculated. For this purpose, the wavelet coefficients of voltage and current signals at the j^{th} decomposition level, n^{th} point and $2i^{th}$ node are calculated using UWPT based spectral analysis method according to equations (3.20) and (3.21). Further, power quality indices are calculated using wavelet coefficients.

$$X_j^{2i}(n) = \sum_{l=0}^{L-1} \tilde{h}_j(l) X_{j-1}^{i}(n-l) \tag{3.20}$$

$$X_j^{2i+1}(n) = \sum_{l=0}^{L-1} \tilde{g}_j(l) X_{j-1}^{i}(n-l) \tag{3.21}$$

Here, $\tilde{h}(l)$ and $\tilde{g}(l)$ are UWPT low-pass filter and high-pass filter, respectively.

The RMS value of voltage signal of length N can be calculated using UWPT wavelet coefficients as:

$$\begin{aligned} V_{RMS} &= \sqrt{\frac{1}{N}\sum_{n=0}^{N-1}\left(X_j^0(n)\right)^2 + \frac{1}{N}\sum_{n=0}^{N-1}\sum_{i=1}^{2^j-1}\left(X_j^i(n)\right)^2} \\ &= \sqrt{(V_j^0)^2 + \sum_{i=1}^{2^j-1}(V_j^i)^2} \end{aligned} \tag{3.22}$$

here, V_j^0 is the RMS value of voltage component at node zero (i.e., RMS value of fundamental voltage component) and V_j^i is RMS value of harmonics voltage component at node i and level j. The RMS value of the current signal can be obtained similarly.

$$I_{RMS} = \sqrt{\frac{1}{N}\sum_{n=0}^{N-1}\left(X_j^{*0}(n)\right)^2 + \frac{1}{N}\sum_{n=0}^{N-1}\sum_{i=1}^{2^j-1}\left(X_j^{*i}(n)\right)^2}$$
$$= \sqrt{(I_j^0)^2 + \sum_{i=1}^{2^j-1}(I_j^i)^2} \tag{3.23}$$

here, X_j^i and X_j^{*i} represents UWPT wavelet coefficients of voltage and current signal at node i and level j, respectively.

The total harmonic distortion for voltage and the current signal can be calculated as:

$$THD_v = \frac{\sqrt{\sum_{i=1}^{2^j-1}(V_j^i)^2}}{V_j^0}, THD_i = \frac{\sqrt{\sum_{i=1}^{2^j-1}(I_j^i)^2}}{I_j^0} \tag{3.24}$$

For computation of THD and RMS Value of voltage and current parameters, UWPT wavelet coefficients of individual signal (voltage or current only) are required while concurrent UWPT wavelet coefficients of voltage and current signal are needed for calculation of active power. The total active power is calculated as the sum of fundamental active power (P_1) and harmonic active power (P_H),

$$P = P_1 + P_H \tag{3.25}$$

where fundamental active power is defined as,

$$P_1 = \frac{1}{N}\sum_{n=0}^{N-1} X_j^0(n) X_j^{*0}(n) \tag{3.26}$$

and harmonic active power is calculated as

$$P_H = \frac{1}{N}\sum_{n=0}^{N-1}\sum_{i=1}^{2^j-1} X_j^i(n) X_j^{*i}(n) \tag{3.27}$$

Apparent power can be defined as the product of RMS value of voltage component and current component,

$$S = V_{RMS} I_{RMS} = \sqrt{S_1^2 + S_N^2} \tag{3.28}$$

where S_1 and S_N are fundamental apparent power and nonfundamental apparent power, respectively, and calculated by following mathematical equations,

$$S_1 = V_j^0 I_j^0 \tag{3.29}$$

$$S_N = \sqrt{D_I^2 + D_V^2 + S_H^2} \tag{3.30}$$

D_I is the current distortion power defined as,

$$D_I = V_j^0 \left(\sqrt{\sum_{i=1}^{2^j-1} (I_j^i)^2} \right) \tag{3.31}$$

D_V is the voltage distortion power defined as,

$$D_V = I_j^0 \left(\sqrt{\sum_{i=1}^{2^j-1} (V_j^i)^2} \right) \tag{3.32}$$

S_H is the harmonic apparent power defined as the cross product of harmonic voltages and harmonic currents.

$$S_H = \left(\sqrt{\sum_{i=1}^{2^j-1} (V_j^i)^2} \right) \left(\sqrt{\sum_{i=1}^{2^j-1} (I_j^i)^2} \right) \tag{3.33}$$

The nonactive power can be defined as

$$N = \sqrt{S^2 - P^2} \tag{3.34}$$

The reactive power at each node can be calculated using corresponding active power and apparent power. The fundamental reactive power can be calculated as,

$$Q_1 = \sqrt{S_1^2 - P_1^2} \tag{3.35}$$

and the harmonic reactive power can be defined as

$$Q_H = \sum_{i=1}^{2^j-1} Q_j^i, \quad Q_j^i = \sqrt{(S_j^i)^2 - (P_j^i)^2} \tag{3.36}$$

The total reactive power according to Budeanu's definition can be computed by following mathematical equation

$$Q_B = Q_1 + Q_H \tag{3.37}$$

Displacement power factor and power factor can be expressed as follows

$$dPF = \frac{P_1}{S_1}, \quad PF = \frac{P}{S} \tag{3.38}$$

3.4 Proposed Measurement System

The block diagram of the proposed measurement system for power quality indices measurement is shown in Figure 3.1. Here, it is mandatory to select some parameters such as number of decomposition level, sampling frequency and mother wavelet of the proposed approach in advance. Once selected, it is possible to develop measurement system for power quality indices estimation. Here, the number of decomposition level and sampling frequency are chosen three and 1.6 kHz respectively, to achieve desired bandwidth at the output node of UWPT decomposition tree. The output nodes of three-level UWPT decomposition tree are divided into eight bands with the fixed interval of 100 Hz and harmonic components are present at the center of these bandwidths. Three level decomposition tree has eight output nodes which enable us to estimate the power quality indices of odd order harmonics component up to 15th order. Since odd order harmonics up to 15th order are usually significant harmonics in the distribution system, therefore, the measurement system is designed in such a way that it can perform the analysis of odd order frequency component up to 15th order. However, this is not the limitation of the proposed approach and the proposed approach can be extended for measurement of higher order frequency component but at the cost of increased implementation complexity, more resource utilization (on real-time hardware platform) and additional computational burden.

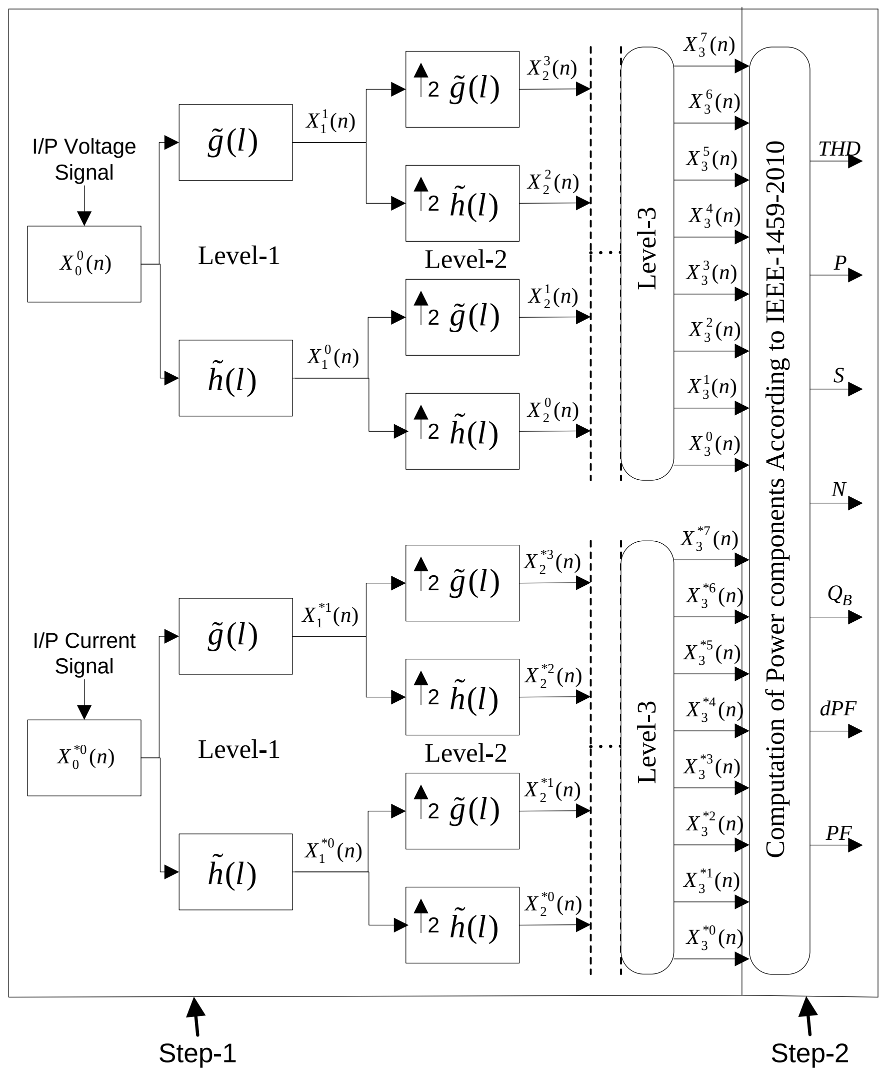

Figure 3.1. Proposed measurement system for measurement of power quality indices

The selection of suitable mother wavelet, which determines the accuracy, computational burden and resource utilization of the measuring system, is crucial in the measurement of power quality indices using UWPT. Usually, mother wavelet with more number of filter coefficients such as "db43" [62], [101] provides more accurate measurement due to low spectral leakage, but at the same time, it increases the considerable amount of resources on the hardware platform as well as computational complexity. Therefore, it is not suitable for real-time implementation. On the other hand, mother wavelet such as “db4” with less number of filter coefficients reduces the accuracy of measurement [102]. Therefore, in this work, “db20” is selected as mother wavelet, which gives the optimized response regarding accuracy, computational complexity and resource utilization. Measurement of power quality indices has been completed in two steps. Since concurrent UWPT wavelet coefficients of voltage and current signal are required for the analysis of power quality indices, therefore, in first step, voltage and current signals are fed into three-level decomposition tree for parallel computation of UWPT wavelet coefficients. Then, in the second step, power quality indices have been calculated using equations (3.22)-(3.38) according to IEEE Standard 1459-2010 as shown in Figure. 3.1.

3.5 FPGA Implementation of the Proposed Measurement System

In this section, a digital hardware is developed for measurement of power quality indices in real time. Hardware resources and timing constraint are two critical aspects for designing any algorithm on FPGA. These constraints are decided according to our application and requirements and the trade-off exist between these two constraints. Therefore, it is always better to optimize these two constraints according to design requirements. In order to cope with timing constraints, two strategies viz. pipelining and parallelization have been used in the hardware architecture. Pipelining is a process in which delay element is placed between two functional blocks in order to cut the maximum delay path. It is used to achieve higher operating frequency. Parallelization performs algebraic operation in parallel to save the time. Second constraint is optimization of hardware resources. Multiplier and Random-Access Memory (RAM) are scarce resources on any FPGA board and available in limited amount only. In the second step, more number of mathematical operations are involved for calculation of power quality indices. These operations will consume considerable number of multipliers (DSP184E1s slices) on FPGA board. Therefore, implementation of FIR wavelet filter in direct form or in transpose form is not a better option due to more consumption of multipliers (DSP184E1s slices). In order to save DSP184E1s slices, RAM based MAC FIR filter is used for implementation of wavelet filter. RAM based MAC FIR filter will consume only one multiplier and a dual port block RAM for implementation of single wavelet filter. However, RAM based MAC FIR filter will take more number of clock cycles in comparison to direct form or transpose form for producing wavelet coefficients but meet the timing requirements of current application.

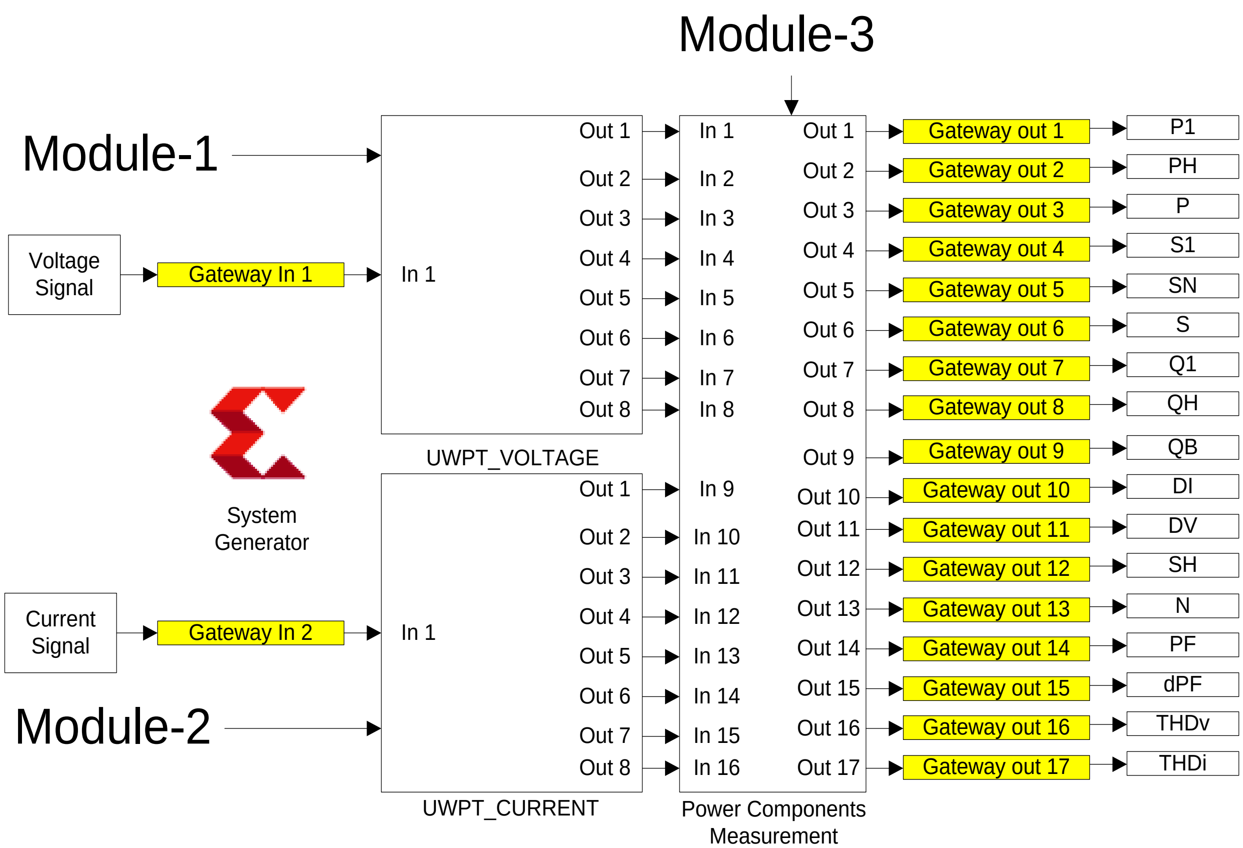

Figure 3.2. Digital design of the proposed measurement system

In order to implement the proposed measurement technique on FPGA, the complete hardware architecture is divided into mainly three modules for easier implementation as shown in Figure 3.2. The first and second module is responsible for computation of UWPT wavelet coefficients of voltage and current signals, whereas the third module is implemented for calculation of power quality indices according to IEEE Standard 1459-2010. Hardware architecture of the first and second module is similar and processes input voltage and current signal in parallel for producing their concurrent UWPT wavelet coefficients. These modules are implemented using FIR filter bank architecture in which main component is low-pass and high-pass wavelet filters. These filters are implemented on FPGA using dual port RAM based MAC FIR filter as shown in Figure 3.3. Wavelet filter coefficients are stored in dual port block RAM and can be read from port B whereas the incoming input sample is written and read from port A. Read address port of B operates *L* (*L* is the number of wavelet filter coefficients) times faster than the incoming input samples that are written into Port A. Two counters are employed in the architecture for creating FIR filter delay line. Counter 1 is used to address wavelet filter coefficients, while counter 2 drives the address port A for controlling the stored data sample. Relational block is used as a comparator, which provides write enable signal at port A for writing a new sample after every L clock cycle and also produces enable or disable signal for counter 2 for addressing the port A. When the last wavelet filter coefficient (*L*-1) is read out by port B, a new sample is inserted at port A after the reading of old sample. New data sample is repeatedly multiplied by *L* wavelet filter coefficients and then accumulated by accumulator and this process is repeated for all data samples. The wavelet coefficients are stored in dual port block RAM in signed fixed point data format with 12 bits and binary precision of 11 bits while data input bit width is 18 bits with binary precision of 12 bits.

The hardware architecture of the third module is implemented using equations (3.22)-(3.38) according to IEEE Standard 1459-2010. It can be seen from equations (3.22)-(3.38) that it solely involves simple algebraic operations such as summation, multiplication, subtraction, division and square root. The hardware architecture of four parameters namely apparent power (S), nonfundamental apparent power (S_N), nonactive power (N) and power factor (PF) is shown in Figure 3.4. It can be seen from Figure 3.4 that hardware architecture is designed using arithmetic blocks and corresponding equations. It is necessary to use cast block before division and square root operations for converting fixed-point format into single precision floating point format. This is because these blocks support calculation only in single and double precision floating point format.

The hardware resource utilization summary in terms of logic resources, maximum operating frequency and occupied percentage are represented in Table 3.1 using Xilinx Virtex-6 FPGA ML-605 Board.

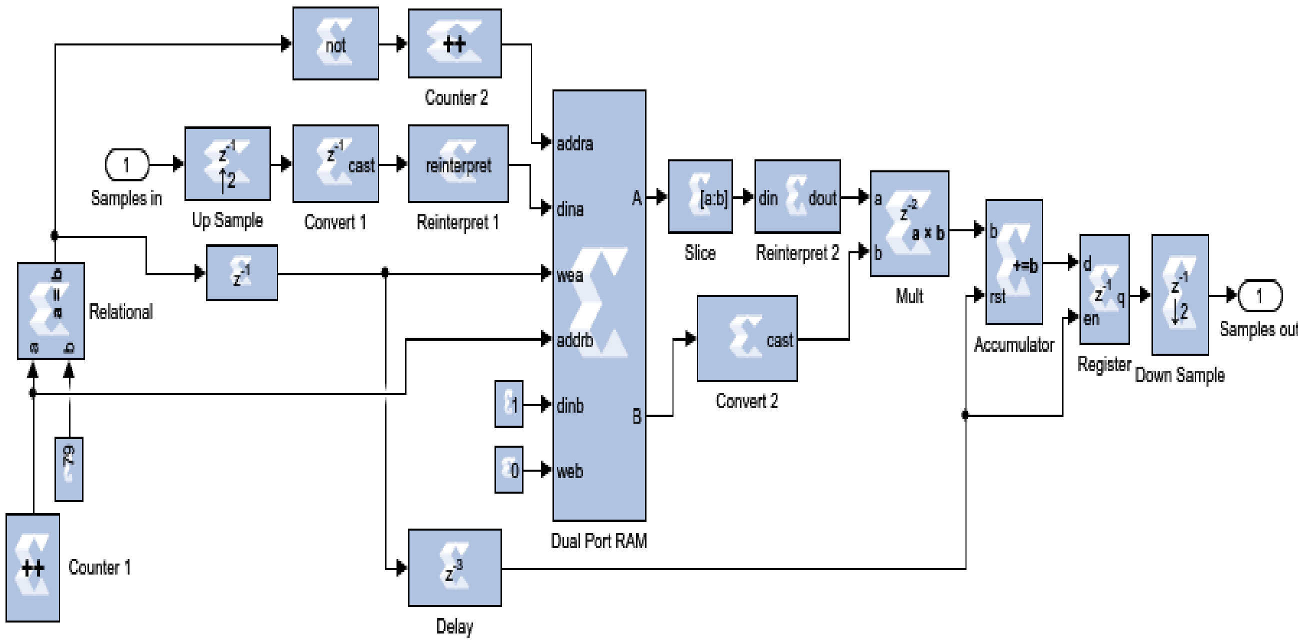

Figure 3.3. Dual port RAM based MAC FIR filter on XSG

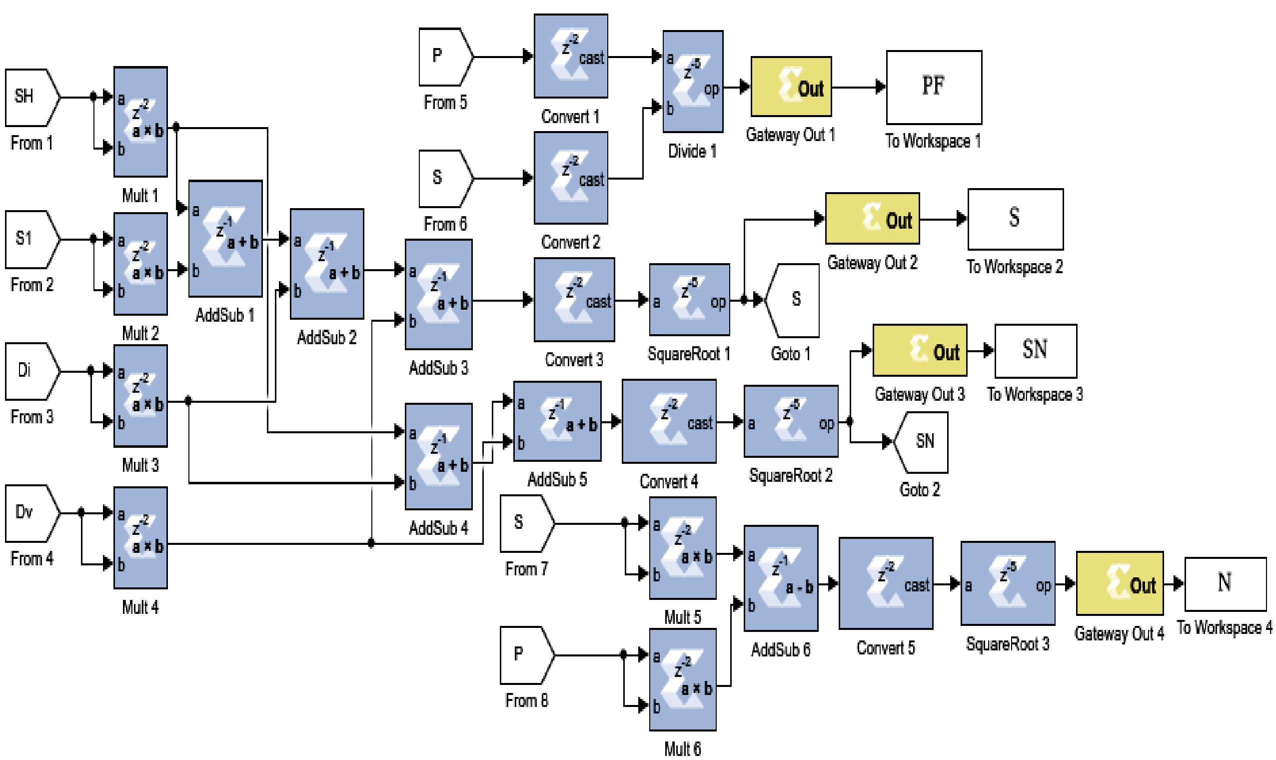

Figure 3.4. Computation of Power quality indices on XSG

Table 3.1: Resource utilization summary

Resource type	Used	Available
Number of slice registers	26,789 (8%)	301,440
Number of slice LUTs	73,234 (48 %)	150,720
Number of RAMB18E1s	28(3%)	832
Number of DSP184E1s	232 (30%)	768
Max. operating frequency	106.280 MHz	

3.6 Performance Evaluation

3.6.1 Simulation Study

The proposed technique has been tested on synthetic stationary as well as non-stationary signals. Simulations have been carried out in MATLAB hosted on a laptop having an Intel Core i5 2.4-GHz processor and 4-GB RAM. Synthetic voltage and current signals are sampled at a regular sampling interval of 1.6 kHz sampling frequency for each case. First, the power quality indices are calculated using IEEE Standard 1459-2010 for getting true values. Windowed signal of one fundamental cycle has been used for the computation of power quality indices using the proposed approach. Performance of the proposed technique has been compared with DWPT and FFT. In case of DWPT and FFT, the length of window width is ten cycles of the fundamental frequency.

The absolute error of estimated power quality indices has been calculated to show the effectiveness of the proposed approach in comparison to FFT and DWPT. The absolute error is defined in (3.39) by considering actual value as a reference. In case of DWPT, analysis has been performed using three-level decomposition tree and "db20" mother wavelet.

$$Absolute\ error = \left| Estimated\ value - Actual\ value \right| \tag{3.39}$$

1) Case-1: Stationary Signal

In order to evaluate the performance of the proposed approach, the first test considers synthetic stationary voltage and current signals. The synthesized voltage and current signals are composed of five frequency components whose amplitude, frequency and phase angle are given in Table 3.2 and 3.3, respectively and the signals are generated for 1-s duration using MATLAB software tool.

Table 3.2: Parameters of voltage signal for case-1

Time (s)	Amplitude ($V_h \times \sqrt{2}$), Frequency components (f_h in Hz) and Phase angle (θ_h in degree)				
0.0-1.0	5, 50, 0^0	1, 150, 70^0	0.5, 250, 0^0	0.3, 450, 0^0	0.2, 650, 20^0

Table 3.3: Parameters of current signal for case-1

Time (s)	Amplitude ($I_h \times \sqrt{2}$), Frequency components (f_h in Hz) and Phase angle (θ_h in degree)				
0.0-1.0	0.5, 50, 30^0	0.1, 150, 60^0	0.05, 250, 0^0	0.03, 450, 0^0	0.02, 650, 30^0

Table 3.4 (a) and (b) compares the estimated power quality indices using the proposed approach with three different mother wavelets “db4”, “db20”, “db43” to the true values obtained by IEEE Standard 1459-2010. The accuracy of measurement for the mother wavelet “db4” is very less in comparison to “db20” and “db43”. Mother wavelet “db43” provided more accurate measurement in comparison to “db20” due to low spectral leakage. However, mother wavelet “db43” contains 86 filter coefficients, whereas “db20” has only 40 filter coefficients. Due to more number of filter coefficients in “db43”, storage requirement and computational complexity are very high in comparison to “db20”. The number of multiplications and additions required for the one fundamental cycle at 1.6 kHz sampling frequency with three level UWPT decomposition tree for different mother wavelets are shown in Table 3.5. Therefore, “db20” is selected as a mother wavelet for present application.

True values of absolute errors obtained in measurement of power quality indices using the proposed method, FFT and DWPT are listed in Table 3.6. It can be noted that the performance of FFT method is better than the other techniques. This is because the FFT method provides accurate measurement in case of the stationary signal when there is no fluctuation in amplitude, phase and frequency. However, the absolute errors obtained using the proposed technique are also quite small and can be considered as negligible. The main advantage of the proposed technique in comparison to DWPT and FFT is its better time resolution of one fundamental cycle.

Table 3.4 (a): Power quality indices for stationary signal

Parameters	**IEEE-1459-2010**	**Proposed Method**		
		("db20")	**("db4")**	**("db43")**
Active Power				
P_1	1.0825318	1.0825318	1.0709307	1.0827987
P_3	0.0492404	0.0490131	0.0555751	0.0492457
P_5	0.0125	0.0127265	0.0168559	0.0125067
P_9	0.0045	0.0040147	0.0031478	0.0043468
P_{13}	0.0019696	0.0019574	0.0018187	0.0019697
P_H	0.06821	0.0682101	0.0798111	0.0682235
P	1.1507418	1.1507419	1.1507418	1.1510222
Apparent Power				
S_1	1.25	1.25	1.2365359	1.25
S_3	0.05	0.0497681	0.0580812	0.05
S_5	0.0125	0.0127312	0.0169591	0.0125068
S_9	0.0045	0.0040147	0.0031479	0.0043468
S_{13}	0.002	0.0019876	0.0018455	0.0020001
S_N	0.4210238	0.4210241	0.4590645	0.4211173
S	1.319	1.3190001	1.3190001	1.3193219
Reactive Power				
Q_1	0.625	0.625	0.6181653	0.6251541
Q_3	0.0086824	0.0086355	0.0168769	0.0086832
Q_5	0	0.0003459	0.0018689	4.71E-05
Q_9	0	1.12E-08	1.74E-05	0.00E+00
Q_{13}	0.0003473	0.0003451	0.0003134	0.0003473
Q_H	0.0090297	0.0093289	0.0193609	0.0090777
Q_B	0.6340297	0.6343289	0.6375263	0.6342318

Table 3.4 (b): Power quality indices for stationary signal

Parameters	IEEE-1459-2010	Proposed Method		
		(“db20”)	**(“db4”)**	**(“db43”)**
Distortion Power				
D_I	0.2936835	0.2936837	0.319327	0.2937489
D_V	0.2936835	0.2936837	0.319327	0.2937489
S_H	0.069	0.0690001	0.082464	0.0690137
N	0.6446351	0.6446352	0.644635	0.6447931
Power Factor				
dPF	0.8660254	0.8660254	0.866073	0.8660254
PF	0.872435	0.872435	0.872434	0.8724347
THD				
THDv	0.2349468	0.234947	0.2582434	0.2349412
THDi	0.2349468	0.234947	0.2582434	0.2349412

Table 3.5: Number of multiplications and additions

Proposed algorithm	Number of Multiplications	Number of additions
(“db4”)	10752	9856
(“db20”)	53760	53312
(“db43”)	115584	115136

2) Case-2: Non-Stationary Signal

The actual power system is dynamic in nature, where the operating conditions are continuously changing and exhibiting new phenomenon. In order to analyse the performance of the proposed technique under the dynamic condition, the non-stationary synthetic voltage and current signals are generated through MATLAB simulation for 1-s duration as shown in Figure 3.5. The main aim of this test is to observe the effectiveness of the proposed method when there is a sudden change in amplitude, in the presence of fundamental frequency deviation and noisy condition. For this purpose, voltage and current signals containing at most five harmonic components, whose amplitude and fundamental frequency are varying at every 0.1-s, are considered and Gaussian white noise with SNR of 40 dB is added to the signal. The time-varying parameters of voltage and current signals are shown in Tables 3.7 and 3.8, respectively.

Table 3.6: Absolute errors for the stationary signal case-1

PM: Proposed Method

Method	Absolute Error								
	P_1	P_H	P	S_1	S_N	S	Q_1	Q_H	Q_B
FFT	6.66E-16	1.39E-17	6.66E-16	4.44E-16	0.00E+00	4.44E-16	2.22E-15	8.23E-11	8.23E-11
DWPT	9.01E-02	2.94E-04	8.98E-02	8.08E-02	1.21E-02	8.04E-02	6.89E-03	1.79E-03	5.09E-03
PM	1.01E-08	9.14E-08	1.02E-07	1.11E-08	3.32E-07	1.16E-07	4.68E-09	2.99E-04	2.99E-04
Method	**Absolute Error**								
	D_I	D_V	S_H	N	PF	dPF	$THDv$	$THDi$	
FFT	0.00E+00	0.00E+00	1.39E-17	2.22E-15	7.77E-16	8.88E-16	8.33E-17	8.33E-17	
DWPT	8.69E-03	8.73E-03	4.60E-04	5.38E-03	1.59E-02	1.72E-02	8.78E-03	8.81E-03	
PM	2.25E-07	2.25E-07	1.05E-07	5.69E-08	2.25E-07	3.91E-10	1.78E-07	1.78E-07	

Table 3.7: Parameters of voltage signal for case-2

Time (s)	Amplitude ($V_h \times \sqrt{2}$), Frequency components (f_h in Hz) and Phase angle (θ_h in degree)				
0.0-0.1	5, 50, 0	1, 150, 70	0.5, 250, 0	0.3, 450, 0	0.2, 550, 20
0.1-0.2	4, 50.25, 0	0.8, 150.75, 70	0.4, 251.25, 0	0.24, 452.25, 0	0.16, 552.75, 20
0.2-0.3	5, 50.25, 0	1, 150.75, 70	0.5, 251.25, 0	0.3, 452.25, 0	0.2, 552.75, 20
0.3-0.4	6, 50, 0	1.2, 150, 70	0.6, 250, 0	0.36, 450, 0	0.24, 550, 20
0.4-0.5	4, 50.25, 0	0.8, 150.75, 70	0.4, 251.25, 0	0.24, 452.25, 0	0.16, 552.75, 20
0.5-0.6	5, 50, 0	1, 150, 70	0.5, 250, 0	0.3, 450, 0	0.2, 550, 20
0.6-0.7	6, 49.75, 0	1.2, 149.25, 70	0.6, 248.75, 0	0.36, 447.75, 0	0.24, 547.25, 20
0.7-0.8	4, 50, 0	0.8, 150, 70	0.4, 250, 0	0.24, 450, 0	0.16, 550, 20
0.8-0.9	5, 50, 0	1, 150, 70	0.5, 250, 0	0.3, 450, 0	0.2, 550, 20
0.9-1.0	4, 49.75, 0	0.8, 149.25, 70	0.4, 248.75, 0	0.24, 447.75, 0	0.16, 547.25, 20

Table 3.8: Parameters of current signal for case-2

Time (s)	Amplitude ($V_h \times \sqrt{2}$), Frequency components (f_h in Hz) and Phase angle (θ_h in degree)				
0.0-0.1	0.5, 50, 30	0.1, 150, 60	0.05, 250, 0	0.03, 450, 0	0.02, 550, 30
0.1-0.2	0.4, 50.25, 30	0.08, 150.75, 60	0.04, 251.25, 0	0.024, 452.25, 0	0.016, 552.75, 30
0.2-0.3	0.5, 50.25, 30	0.1, 150.75, 60	0.05, 251.25, 0	0.03, 452.25, 0	0.02, 552.75, 30
0.3-0.4	0.6, 50, 30	0.12, 150, 60	0.06, 250, 0	0.036, 450, 0	0.024, 550, 30
0.4-0.5	0.4, 50.25, 30	0.08, 150.75, 60	0.04, 251.25, 0	0.024, 452.25, 0	0.016, 552.75, 30
0.5-0.6	0.5, 50, 30	0.1, 150, 60	0.05, 250, 0	0.03, 450, 0	0.02, 550, 30
0.6-0.7	0.6, 49.75, 30	0.12, 149.25, 60	0.06, 248.75, 0	0.036, 447.75, 0	0.024, 547.25, 30
0.7-0.8	0.4, 50, 30	0.08, 150, 60	0.04, 250, 0	0.024, 450, 0	0.016, 550, 30
0.8-0.9	0.5, 50, 30	0.1, 150, 60	0.05, 250, 0	0.03, 450, 0	0.02, 550, 30
0.9-1.0	0.4, 49.75, 30	0.08, 149.25, 60	0.04, 248.75, 0	0.024, 447.75, 0	0.016, 547.25, 30

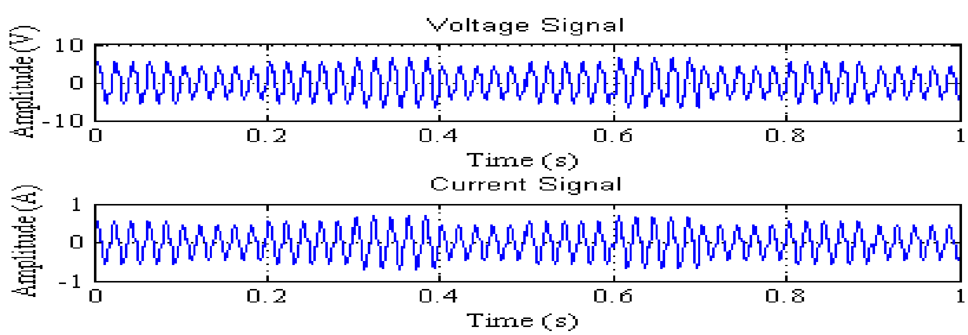

Figure 3.5. Synthetic non-stationary signal for case-2

Absolute errors are calculated according to equation (3.39). Mean and variance of absolute error obtained in the estimation of power quality indices for non-stationary signal are presented in Table 3.9. One cycle of non-stationary signal has been analysed using the proposed scheme. In case of FFT, ten cycles of windowed signal are used as recommended by IEEE 1459-2010 [12] and IEC 61000-4-7 [11]. However, performance of the proposed technique has been compared with DWPT considering both one cycle and ten cycles of the signal.

It can be observed that measurement accuracy of all the methods is reduced in the presence of non-stationary power quality disturbances. Performance of FFT method is severely affected due to spectral leakage and DWPT provides better results in comparison to FFT. This is because DWPT is also wavelet-based technique and more suitable for analysis of the non-stationary signal. The accuracy of measurement in case of DWPT with one cycle is less in comparison to DWPT with ten cycles. This is because, less number of wavelet coefficients are available at output in case of DWPT with one cycle. However, the measurements obtained using the proposed technique are more accurate as compared to FFT and DWPT in both cases, viz., one cycle and ten cycles.

Table 3.9: Mean and variance of absolute errors for case-2

PM: Proposed Method

Method		**Absolute Error**							
		P_1	P_H	P	$S1$	S_N	S	$Q1$	Q_H
FFT	*Mean*	1.81E-01	3.65E-02	2.17E-01	2.08E-01	1.68E-01	2.45E-01	1.04E-01	6.20E-03
	Variance	2.69E-02	2.74E-04	2.93E-02	3.59E-02	7.30E-03	3.87E-02	9.02E-03	1.22E-05
DWPT (10 Cycles)	*Mean*	8.67E-02	3.52E-03	8.84E-02	9.43E-02	2.70E-02	9.80E-02	4.76E-02	2.68E-03
	Variance	2.96E-03	7.83E-06	3.23E-03	3.43E-03	1.41E-04	3.36E-03	2.35E-04	3.03E-06
DWPT (1 Cycle)	*Mean*	1.55E-01	6.69E-03	1.49E-01	1.36E-01	9.82E-03	1.31E-01	5.86E-02	6.09E-03
	Variance	3.28E-03	1.18E-05	2.09E-03	3.79E-03	1.93E-04	1.64E-03	4.09E-04	2.08E-05
PM	*Mean*	2.34E-03	8.48E-04	2.26E-03	2.30E-03	2.57E-03	2.11E-03	1.54E-03	7.10E-04
	Variance	3.92E-06	7.02E-07	2.81E-06	4.11E-06	6.02E-06	2.74E-06	1.90E-06	2.49E-07

Method		**Absolute Error**						
		Q_B	D_I	D_V	S_H	N	PF	dPF
FFT	*Mean*	1.10E-01	1.16E-01	1.17E-01	3.70E-02	1.14E-01	3.11E-03	3.52E-04
	Variance	9.39E-03	3.54E-03	3.53E-03	2.85E-04	9.44E-03	2.33E-06	1.27E-07
DWPT (10 Cycles)	*Mean*	4.83E-02	1.92E-02	1.86E-02	3.64E-03	4.88E-02	8.91E-03	9.83E-03
	Variance	2.57E-04	1.67E-04	1.92E-05	8.49E-06	2.58E-04	3.70E-05	3.92E-05
DWPT (1Cycle)	*Mean*	6.92E-02	1.36E-02	7.72E-03	7.08E-03	6.25E-03	3.06E-02	3.40E-02
	Variance	1.72E-04	2.30E-04	1.32E-05	1.27E-05	1.22E-05	4.02E-05	4.49E-05
PM	*Mean*	1.73E-03	2.57E-03	1.32E-03	8.66E-04	1.53E-03	7.29E-04	7.41E-04
	Variance	2.06E-06	4.37E-06	2.14E-06	6.87E-07	1.60E-06	4.96E-07	5.51E-07

The power quality indices are retrieved from the proposed technique for non-stationary signal and the maximum values of mean and variance of absolute error are found to be 2.57E-03 and 6.02E-06, respectively. These values are associated with nonfundamental apparent power (S_N). These values are quite low and within acceptable limits. These results show the effectiveness of the proposed technique in analysing the non-stationary signal. Moreover, the proposed technique uses only one fundamental cycle, therefore it can capture the dynamic nature of disturbances.

The number of computations in terms of multiplications and additions and hardware platform decide the processing speed of any algorithm. The number of multiplications and additions required for the ten cycles at the sampling frequency 1.6 kHz for FFT, three-level DWPT with the mother wavelet "db20" and for the proposed technique are presented in Table 3.10. It can be noticed that number of computations in FFT is considerably small in comparison to wavelet-based method, but its measurement accuracy is also less for non-stationary signal due to spectral leakage. Among wavelet-based methods, the proposed technique provided more accurate results with less computations in comparison to DWPT. The comparison of important features between the proposed algorithm with its competitive algorithms is presented in Table 3.11.

Table 3.10: Number of multiplications and additions

Method	Number of Multiplications	Number of additions
FFT (Radix-2)	4608	9216
DWPT	76800	74880
Proposed Technique	53760	53312

3.6.2 Hardware Implementation Results and Timing Analysis

Hardware accuracy of the proposed scheme is investigated using measured real-time voltage and current signals. For this purpose, an experimental set-up is used to acquire the voltage and current signals. It consists of single-phase power supply, voltage probe, current probe and four non-linear loads such as a PC, a laptop charging, a mobile charging and two CFLs. OROS-34 DAQ set up is interfaced to a laptop having the Nvgate software to acquire the measured voltage and current signal with the resolution of 24 bits. The real-time voltage and current signals for 0.2-s are shown in Figure 3.6. The voltage signal is attenuated by a factor of 50, in order to fit the voltage signal within the dynamic range of the proposed hardware.

Table 3.11: Comparison between important features

Feature	FFT	DWPT	Proposed method
Processing speed	✓	×	✓
Time resolution	×	×	✓
Accuracy with non-stationary signal	×	✓	✓
Accuracy with frequency deviation	×	✓	✓

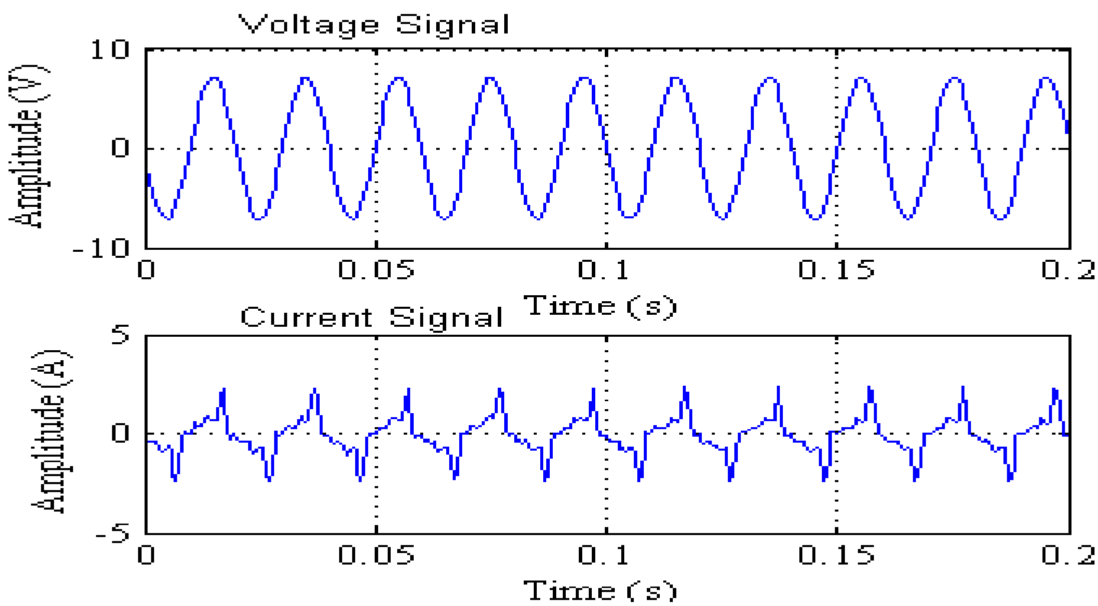

Figure 3.6. Measured real-time voltage and current signals

Real-time testing of the proposed scheme has been completed with the help of hardware co-simulation approach on the experimental set-up consisting of Xilinx Virtex-6 FPGA ML-605 Board as hardware platform. This is connected to a Personal Computer with, XSG/ISE design suite 14.2, MATLAB/Simulink via JTAG interface. Hardware co-simulation process is initiated through Gateway In and Gateway Out blocks that convert the input and output signal into the desired data types (fixed point or floating point). These blocks act as virtual analog-to-digital and digital-to-analog converters respectively, during hardware co-simulation. The input signal is quantized by Gateway In block in 18-bit fixed point format to feed it into the implemented architecture on Xilinx Virtex-6 FPGA ML-605 Board with the help of co-simulation process.

Table 3.12: Comparison between MATLAB and FPGA results

Results	***P***	***S***	Q_B	D_I	D_V	S_H	***N***	***PF***
MATLAB results	3.9274676	4.8965697	0.7820951	2.7950064	0.0709884	0.0494575	2.922682	0.802046
FPGA results	3.9353596	4.906711	0.894197	2.8054805	0.2196378	0.1533956	2.92906	0.801996
Absolute error	7.89E-03	1.01E-02	1.12E-01	1.05E-02	1.49E-01	1.04E-01	6.38E-03	4.93E-05

Table 3.13: Clock cycles required for estimation of power quality indices

Power quality indices	**Clock cycles**	**FPGA (ms)**
P	69,280	1.3856
S	71,520	1.4304
Q_B	71,360	1.4272
D_I	70,240	1.4048
D_V	70,080	1.4016
S_H	67,840	1.3568
N	72,800	1.456
PF	72,160	1.4432

Table 3.12 shows the results of power quality indices for the measured real-time voltage and current signals on MATLAB tool and Xilinx Virtex-6 FPGA ML-605 Board. It can be seen that the results of FPGA prototype and MATLAB are in good agreement. The minor deviations occurred in results due to finite word length in wavelet filter coefficients, algebraic blocks (summation, multiplication, subtraction and division) and ADC resolution. It can also be noticed that the minimum and maximum value of absolute

error between the FPGA and MATLAB (MATLAB as a reference benchmark) are 4.93E-05 and 1.49E-01, respectively.

Table 3.13 shows the number of clock cycle required and the time taken in the measurement of power quality indices using Xilinx Virtex-6 FPGA ML-605 Board with the clock frequency of 50 MHz. The maximum time required for measurement is 1.456 ms, which is associated with nonactive power (*N)* and much shorter than incoming data duration of 20 ms. It is, therefore, demonstrated that the proposed measurement system is suitable for practical and online applications.

3.7 Conclusion

The design and implementation of a measurement system based on UWPT has been proposed for measurement of power quality indices as defined in IEEE Standard 1459-2010. It has been shown that the proposed scheme is capable of estimating power quality indices in only one fundamental cycle data and it involves only simple algebraic operations. The results of the proposed technique demonstrate its superiority in comparison to FFT and DWPT under different operating conditions. In order to achieve higher operating frequency and save time, pipelined and parallel hardware architecture is used for implementation of the proposed technique on FPGA. Reported results in terms of accuracy, robustness, resource utilization and timing requirements prove that the proposed measurement system is capable of estimation of power quality indices in accordance with IEEE Standard 1459-2010.

Chapter 4

Visualization of Time-Varying Power Quality Disturbances Using Undecimated Wavelet Packet Transform

4.1 Introduction

Maintaining the quality of electricity is one of the major objectives in the development of smart grid. The estimation of signal parameters such as amplitude, frequency and phase angle of each mono-frequency component is the easiest way to specify the quality of power supply. Estimation of signal parameters is achieved in chapter two and three by windowed signal and does not indicate exact time localization of electrical disturbances. Hence, instead of estimation, it is better to decompose the signal into various frequency components for clear visualization of time-varying power quality disturbances. Visualization of power quality disturbances is very essential for better characterization of the time-varying voltage and current signals. This necessitates a technique to decompose the power system signal into fundamental and harmonics components for visualization of disturbances.

The parametric methods described in chapter one estimate amplitude, phase and frequency by assuming the signal within the window is stationary. Therefore, these methods are not suitable for exact time localization of power quality disturbances. The non-parametric techniques namely the DWT, the DWPT and the EWT can be utilized for detection of power quality disturbances. However, the major drawbacks associated with the DWT and the DWPT are that they are computationally expensive [59] and a time-variant transform [103], resulting in the inaccurate investigation of non-stationary power quality disturbances. The EWT is not suitable in case of fundamental frequency deviation due to the spectral leakage and nature of this algorithm is also complex.

In this chapter, an application of the UWPT is proposed for the decomposition of the individual frequency component and thereby visualizing time-varying electrical disturbances. The UWPT is also a wavelet-based method with extra features of redundancy and time-invariance. In the UWPT, down sampling process on the wavelet coefficients is not involved, therefore, this technique does not lose time-invariance property. The UWPT decomposes the input signal in various sub band and produces an exact replica of fundamental and each harmonic component. Hence, accurate detection of power quality disturbances is possible with UWPT.

4.2 Application of UWPT for Visualization of Power Quality Disturbances

The concepts of UWPT, details of three-level decomposition tree and frequency response of wavelet filters are explained in chapter two. For the sake of clarity and completeness, the elementary details and relevant equations are repeated here.

The UWPT is linear, time-invariant filtering operation and decomposes a signal into uniform frequency band. The UWPT is very similar to DWPT, except it does not involve downsampling, hence preserves time-invariant property and overcomes the problem of insufficient wavelet coefficients. The UWPT low-pass filter $\tilde{h}(l)$ and high-pass filter $\tilde{g}(l)$ are related to the DWPT low-pass filter *h(l)* and high-pass filter *g(l)* through (4.1) and (4.2).

$$\tilde{h}(l) = h(l)\big/\sqrt{2} \tag{4.1}$$

$$\tilde{g}(l) = g(l)\big/\sqrt{2} \tag{4.2}$$

Like the DWPT, the UWPT filters are also Quadrature Mirror Filters (QMF) and satisfy the following property.

$$\tilde{g}(l) = (-1)^l \tilde{h}(L - l - 1) \tag{4.3}$$

and

$$\tilde{h}(l) = (-1)^{l+1}\tilde{g}(L-l-1) \tag{4.4}$$

In comparison to DWPT, UWPT does not perform downsampling by a factor of two on the output wavelet coefficients of any decomposition level. Therefore, it is necessary to modify both filters at each decomposition level, by performing filter upsampling. Filters are modified at the j^{th} decomposition level by inserting 2^{j-1} zeros between each pair of coefficients of $\tilde{h}(l)$ and $\tilde{g}(l)$ according to following equations.

$$\tilde{h}_j(l) = \left[\tilde{h}(0), \underbrace{0,...,0}_{2^{j-1}-1}, \tilde{h}(1), \underbrace{0,...,0}_{2^{j-1}-1}, \tilde{h}(2), ..., \tilde{h}(L-1), \underbrace{0,...,0}_{2^{j-1}-1} \right] \tag{4.5}$$

$$\tilde{g}_j(l) = \left[\tilde{g}(0), \underbrace{0,...,0}_{2^{j-1}-1}, \tilde{g}(1), \underbrace{0,...,0}_{2^{j-1}-1}, \tilde{g}(2), ..., \tilde{g}(L-1), \underbrace{0,...,0}_{2^{j-1}-1} \right] \tag{4.6}$$

The UWPT wavelet coefficients of the incoming signal at the j^{th} decomposition level, n^{th} point and $2i^{\text{th}}$ node can be represented as:

$$X_j^{2i}(n) = \sum_{l=0}^{L-1} \tilde{h}_j(l) X_{j-1}^{i}(n-l) \tag{4.7}$$

$$X_j^{2i+1}(n) = \sum_{l=0}^{L-1} \tilde{g}_j(l) X_{j-1}^{i}(n-l) \tag{4.8}$$

4.3 Performance Evaluation

The numerical results are given to show the efficacy of the UWPT. Four test cases have been taken into consideration for visualization of power quality disturbances. The sampling frequency is set to 1.6 kHz, to achieve desired bandwidth at the output node of UWPT decomposition tree. In each case, three level decomposition has been used using “db20” mother wavelet. All the test simulations have been accomplished in the MATLAB using a personal computer. The configuration of personal computer is i5 Intel Core 6th generation 2.30 GHz processor with 8 GB RAM.

4.3.1 Case 1: Stationary Signal

This case investigates the effectiveness of the UWPT technique on stationary signal. The analyzed waveform is composed of 3rd, 5th and 11th harmonic components along with the fundamental component for 0.2-s, as depicted in Figure 4.1 (a) and is simulated using (4.9) on the MATLAB platform.

$$v(t) = \left[100\sin(\omega t) + 50\sin(3\omega t) + 30\sin(5\omega t) + 20\sin(11\omega t)\right] \tag{4.9}$$

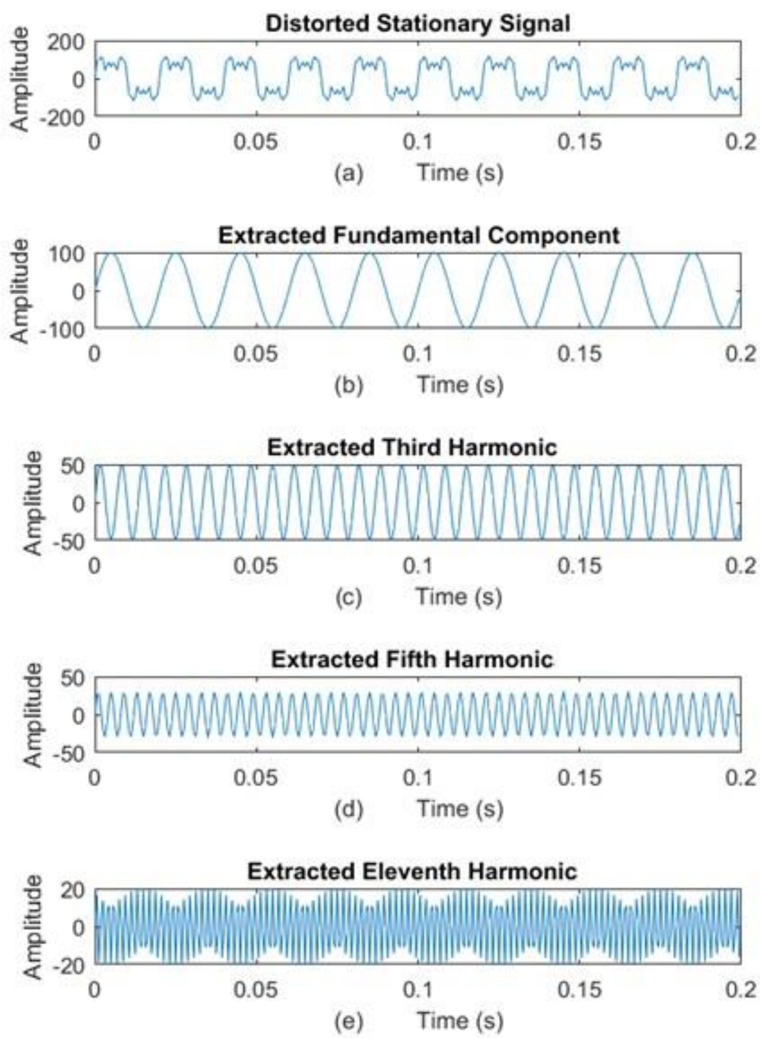

Figure 4.1. (a) Test signal-1: Synthetic distorted stationary signal. (b) Extracted fundamental component. (c) Extracted third harmonic. (d) Extracted fifth harmonic. (e) Extracted eleventh harmonic

It can be observed from the Figure 4.1 that the proposed scheme based on UWPT efficiently decompose the harmonics and fundamental component from the distorted signal and clearly shows the behavior of each component in time domain.

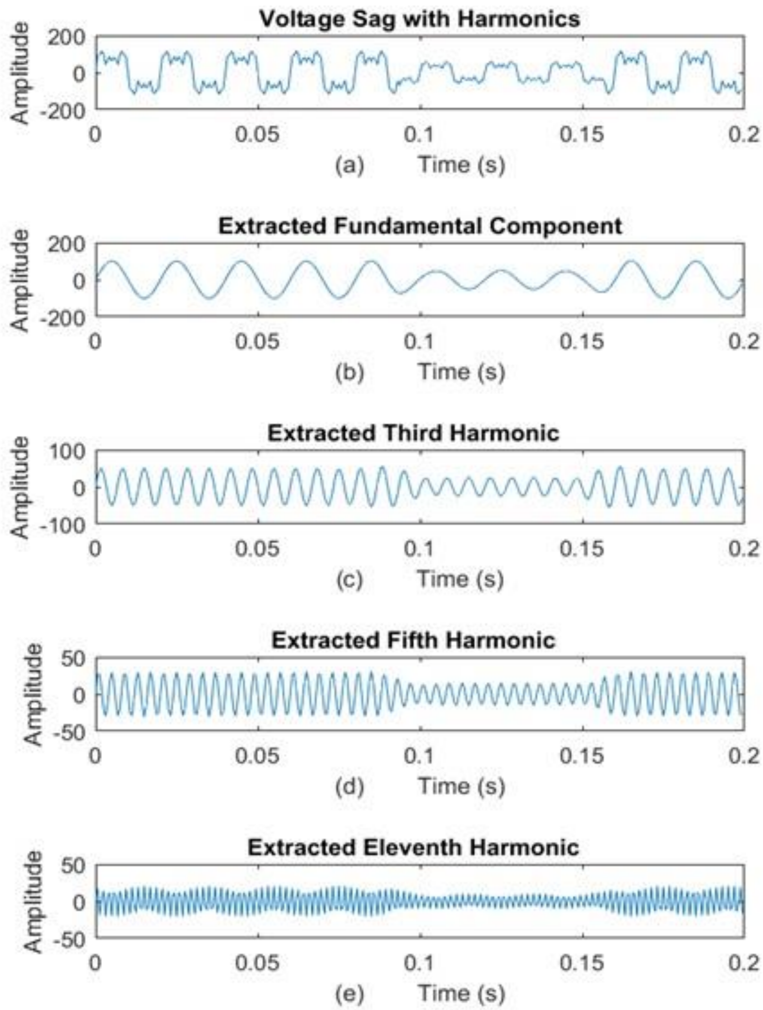

Figure 4.2. (a) Test signal-2: Synthetic signal with voltage sag and harmonics. (b) Extracted fundamental component. (c) Extracted third harmonic. (d) Extracted fifth harmonic. (e) Extracted eleventh harmonic

4.3.2 Case 2: Voltage Sag with Harmonics

Voltage sags are mainly caused by starting of large motors and short circuits. In voltage sag, the RMS value of the voltage drops from 10 % to 90 % of the original value. A synthetic voltage signal is generated in MATLAB for 0.2-s according to (4.10) to show the performance of the UWPT technique under sag condition. In this example, reduction in rated voltage is 50 % from 0.09375-s to 0.15625-s as shown in Figure 4.2 (a).

$$\begin{aligned} v(t) &= \left[u(t) - 0.5\left\{ u(t-0.09375) - u(t-0.15625) \right\} \right] \\ &\quad \times \begin{bmatrix} 100\sin(\omega t) + 50\sin(3\omega t) \\ +30\sin(5\omega t) + 20\sin(11\omega t) \end{bmatrix} \end{aligned} \tag{4.10}$$

Figures 4.2 (b), (c), (d) and (e) show the extracted fundamental, third, fifth and eleventh components using the proposed method. From the Figure 4.2 the locations of power quality disturbances are recognized clearly. Furthermore, the proposed method facilitates the visualization of the voltage sag with exact indication of starting and ending point of voltage sag.

4.3.3 Case 3: Voltage Swell with Harmonics

Voltage swell is a type of disturbance occurring in power system due to single-line-to-ground fault, which causes increase in the rated voltage of the un-faulted phases of a three-phase system. The RMS value of the voltage rises from 110 % to 180 % of the rated RMS value with duration of 0.5 cycles to one minute. To analyze the performance of the proposed scheme under swell condition, a synthetic voltage waveform is generated through MATLAB simulation for 0.2-s duration as shown in Figure 4.3 (a) according to (4.11). In this example, increase in rated voltage is 50 % from 0.09375-s to 0.15625-s.

$$\begin{aligned} v(t) &= \left[u(t) + 0.5\left\{ u(t-0.09375) - u(t-0.15625) \right\} \right] \\ &\quad \times \begin{bmatrix} 100\sin(\omega t) + 50\sin(3\omega t) \\ +30\sin(5\omega t) + 20\sin(11\omega t) \end{bmatrix} \end{aligned} \tag{4.11}$$

Figures 4.3 (b), (c), (d) and (e) show the decomposed fundamental, third, fifth and eleventh signal components obtained through the proposed technique. It can be seen from the Figure 4.3 that all the time-varying components are efficiently extracted from the distorted signal with clear visualization of beginning and ending point of swell.

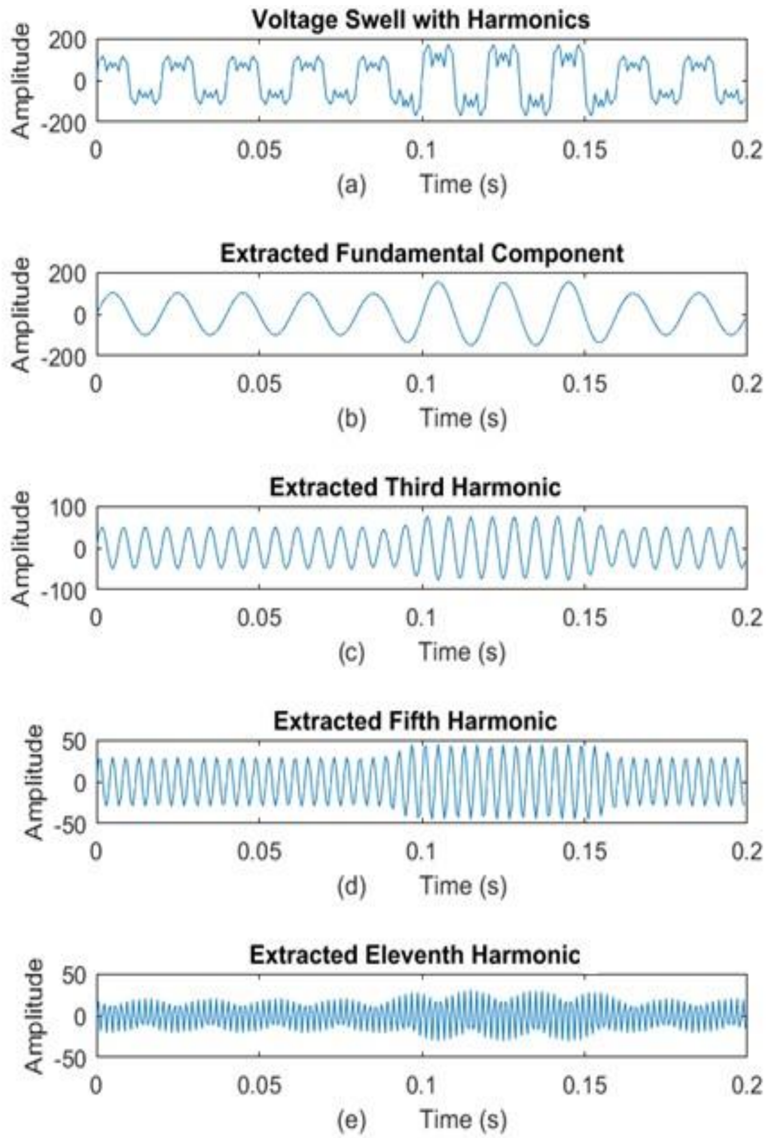

Figure 4.3. (a) Test signal-3: Synthetic signal with voltage swell and harmonics. (b) Extracted fundamental component. (c) Extracted third harmonic. (d) Extracted fifth harmonic. (e) Extracted eleventh harmonic

4.3.4 Case 4: Momentary Interruption

Voltage RMS drop of 90 % to 100 % of the original voltage enduring from half cycles to few minutes is known as momentary interruption. It occurs due to switching operations and faulty working of reclosers. For this purpose, a test-signal-4 of 0.2-s is generated by simulation of (4.12) as shown in Figure 4.4 (a).

$$v(t) = \left[u(t) - \{ u(t-0.09375) - u(t-0.15625) \} \right] \times \begin{bmatrix} 100\sin(\omega t) + 50\sin(3\omega t) \\ +30\sin(5\omega t) + 20\sin(11\omega t) \end{bmatrix} \quad (4.12)$$

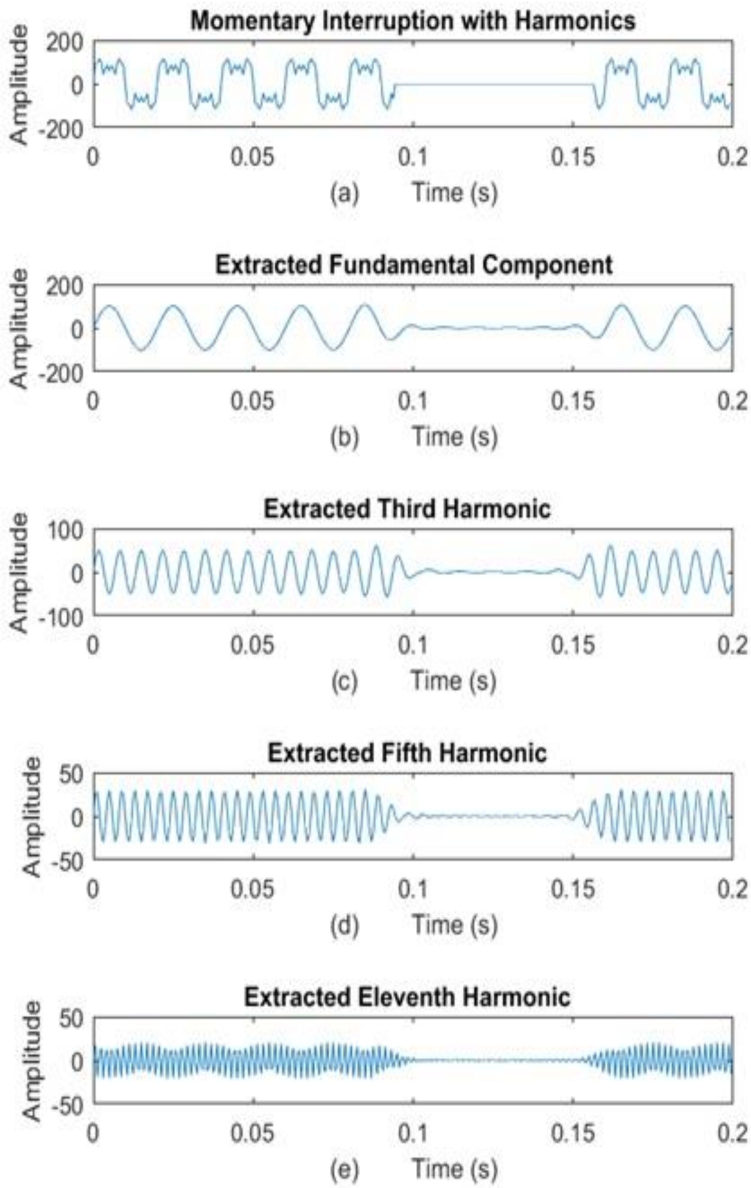

Figure 4.4. (a) Test signal-4: Simulated synthetic signal with momentary interruption and harmonics. (b) Extracted fundamental component. (c) Extracted third harmonics. (d) Extracted fifth harmonics. (e) Extracted eleventh harmonics

Simulated results are plotted in Figure 4.4 and it can be noticed that the occurrence of momentary interruption is clearly detectable. These results demonstrate the ability of the UWPT based technique for detection of the electrical disturbances in distribution system.

4.4 Conclusion

This chapter presents UWPT based scheme for detection of time-varying electrical disturbances in the time-domain using UWPT. It has been shown through MATALB simulation that the proposed approach efficiently extracts the frequency components under different type of disturbances and provides clear visualization of time-varying electrical disturbances. The proposed approach is based on the separation of the fundamental and harmonic components from the distorted signal. The proposed method can be used in monitoring and source identification of selective harmonics. In addition to these applications, this method is also suitable in area of protection, control and power quality applications.

Chapter 5

Measurement of Instantaneous Power Quality Indices Using Undecimated Wavelet Packet Transform and Hilbert Transform

5.1 Introduction

Continuous monitoring and analysis of power supply are essential aspects for both the proper operation of the electrical grid and for improving the quality of power supply. Measurement of power quality indices is a simple method for assessing the quality of power supply and electrical disturbances. The method proposed in chapter three computed the power quality indices after one cycle. Therefore, this method is not suitable for measurement of time-varying power quality indices at each sampling instant. Moreover, this method does not provide direction of power flow due to lack of phase information. Visualization of power quality disturbances is presented in chapter four. Visualization of each component in time-domain can provide only types of disturbances and its starting and ending point. For better characterization of voltage and current signal, there is need of such techniques, which can provide time-domain behavior of signal and calculate the power quality indices at each sampling instant.

Techniques based on wavelet-transform are explained in chapter one, which provide power quality indices after some pre-assumed window cycles. The work [53] proposes a technique based on DWT for locating and analysing the low-frequency oscillations in the power system. But this method is not capable to analyse all the harmonics component because of non-uniform frequency bandwidth. A method based on DWPT and SSM (Single-Sideband Modulation) is proposed in [104] for the measurement of instantaneous power quality indices. But, DWPT is time-variant transform and computationally expensive [103], which limited its ability for analysing the non-stationary signals. Moreover, it requires the large size window for the exact measurement of power quality indices, which reduces its real-time processing capability. Recently, a work reformulates the concept of the symmetrical harmonic components using DWPT and analyses the power quality indices in the three-phase system [105]. However, this technique will not allow to identify the direction of power flow due to the lack of information related to the phase parameter of each harmonic and fundamental component.

The purpose of this chapter is to propose a simple and efficient algorithm based on the UWPT and Hilbert Transform for measurement of instantaneous power quality indices. The proposed technique computes the power quality indices at every instant, thereby improving the time-resolution, real-time processing capability and providing the information about power quality indices with respect to time. Furthermore, the algorithm does not have any problem related to stability as it uses Finite Impulse Response (FIR) filters and open-loop structure. The approach of the proposed method is based on the concept of the analytic signal; thus, it also provides the direction of power flow. Moreover, the proposed algorithm does not involve any complex operations like conditional and branching operations, calculation of trigonometric functions for measurement of active and reactive power but uses basic linear algebraic operations. Considering these facts, the proposed method has been implemented on the Xilinx Virtex-6 FPGA ML-605 board after adequate analysis and synthesis on XSG/ISE design suite 14.2 and MATLAB/Simulink software platform. Finally, the simulation and experimental tests have been carried out to validate the effectiveness of the proposed method using synthetic as well as experimental voltage and current signals. The results in terms of estimation accuracy, resource utilization and timing requirements justify the performance of the proposed method for the measurement of power quality indices.

5.2 Theoretical Background

5.2.1 Hilbert Transform (HT)

Hilbert transform is generally used to convert the narrowband monocomponent signal into the analytic signal to obtain instantaneous attributes of the signal. The Hilbert Transform is defined as the convolution of continuous signal $x(t)$ with the mathematical function $1/\pi t$.

$$\tilde{x}(t) = H\left[x(t)\right] = \frac{1}{\pi}\int_{-\infty}^{+\infty}\frac{x(\tau)}{t-\tau}d\tau \tag{5.1}$$

It can be seen from (5.1) that singularity exists at $\tau = t$; hence according to Cauchy principal value theorem, (5.1) can be approximated as follows [106]:

$$H\left[x(t)\right] \simeq \frac{1}{\pi}\lim_{\varepsilon\to 0^+}\left[\int_{-\infty}^{t-\varepsilon}\frac{x(\tau)}{t-\tau}d\tau + \int_{t+\varepsilon}^{\infty}\frac{x(\tau)}{t-\tau}d\tau\right] \tag{5.2}$$

Similar to UWPT, HT is also a time-invariant transform and behaves as a linear phase shift filter. The transfer function of HT is defined as:

$$H(\omega) = \begin{cases} j & \omega > 0 \\ 0 & \omega = 0 \\ -j & \omega < 0 \end{cases} \tag{5.3}$$

Where j and ω are the imaginary units and angular frequency, respectively. HT provides a phase shift of $\pi/2$ for positive frequency components and does not change the amplitude of spectral component.

Discrete Hilbert transform can be computed using either the frequency-based method or time-based method. In the frequency-based method, HT of a signal is calculated by taking DFT and inverse DFT of the given signal, as mentioned in [107], [108]. But these methods are affected by the typical DFT limitations, hence not suitable for time-varying conditions. On the other hand, time-based methods are implemented by using digital filters (IIR and FIR). Therefore, these methods can easily capture the dynamic nature of the original signal and are more suitable for real-time applications [109]. Hence, in this chapter time-based method is adopted to implement the discrete Hilbert transform and the details about implementation are explained in the next section.

5.2.2 Instantaneous Power Quality Indices

In this section, the computation of instantaneous power quality indices based on the proposed algorithm is presented. The power quality indices are calculated for every sample providing information about power grid voltage and current signals with respect to time, therefore named instantaneous power quality indices. Following mathematical model is used for the representation of voltage and current signal in single phase system.

$$v(n)=\sum_{m=1}^{M}V_m\sin(\omega_m nT_s+\theta_m)+\xi(nT_s) \tag{5.4}$$

$$i(n)=\sum_{m=1}^{M}I_m\sin(\omega_m nT_s+\phi_m)+\xi(nT_s) \tag{5.5}$$

Where V_m, I_m, θ_m and ϕ_m are amplitudes and phase angles of the voltage and current harmonics respectively, $\omega_m = 2\pi m f_o$ is angular frequency, f_o is fundamental frequency, M is the harmonic order, ξ is the Gaussian noise and T_s is the sampling interval.

For measurement of instantaneous power quality indices, first the UWPT wavelet coefficients of voltage and current signals at the j^{th} decomposition level, n^{th} point and $2i^{th}$ node are calculated using UWPT based spectral analysis method according to equations (5.6) and (5.7). Explanation of UWPT algorithm is presented in chapter two in details.

$$X_j^{2i}(n)=\sum_{l=0}^{L-1}\tilde{h}_j(l)X_{j-1}^{i}(n-l) \tag{5.6}$$

$$X_j^{2i+1}(n)=\sum_{l=0}^{L-1}\tilde{g}_j(l)X_{j-1}^{i}(n-l) \tag{5.7}$$

Here, $\tilde{h}(l)$ and $\tilde{g}(l)$ are UWPT low-pass filter and high-pass filter, respectively.

The UWPT decomposes the distorted signal into the corresponding fundamental and harmonics component. At each node, HT is applied to the decomposed signal for getting the analytic signal. Then, instantaneous power quality indices are calculated from the analytic signal. The RMS value of voltage signal is calculated according to (5.8). Here X_j^i is UWPT wavelet coefficients of voltage signal at node i and level j respectively and

$V_j^i(n)$ is the instantaneous RMS value of voltage component at node *i* and level *j* (like $V_j^0(n)$ is the RMS value of fundamental voltage component).

$$
\begin{aligned}
&V_j^0(n)=\sqrt{\left\{X_j^0(n)\right\}^2+\left[HT\left\{X_j^0(n)\right\}\right]^2}\\
&V_j^1(n)=\sqrt{\left\{X_j^1(n)\right\}^2+\left[HT\left\{X_j^1(n)\right\}\right]^2}\\
&\ldots\ldots\ldots\ldots\\
&V_j^i(n)=\sqrt{\left\{X_j^i(n)\right\}^2+\left[HT\left\{X_j^i(n)\right\}\right]^2}
\end{aligned}
\tag{5.8}
$$

The total RMS value of the voltage signal can be obtained as follows:

$$
V_{RMS}(n)=\sqrt{\sum_{i=0}^{2^j-1}\left\{V_j^i(n)\right\}^2}
\tag{5.9}
$$

The RMS value of current signal is calculated in similar way as given in (5.10).

$$
\begin{aligned}
&I_j^0(n)=\sqrt{\left\{X_j^{*0}(n)\right\}^2+\left[HT\left\{X_j^{*0}(n)\right\}\right]^2}\\
&I_j^1(n)=\sqrt{\left\{X_j^{*1}(n)\right\}^2+\left[HT\left\{X_j^{*1}(n)\right\}\right]^2}\\
&\ldots\ldots\ldots\ldots\\
&I_j^i(n)=\sqrt{\left\{X_j^{*i}(n)\right\}^2+\left[HT\left\{X_j^{*i}(n)\right\}\right]^2}
\end{aligned}
\tag{5.10}
$$

where X_j^i is UWPT wavelet coefficients of current signal at node *i* and level *j* respectively and the total RMS value of current signal is defined as:

$$
I_{RMS}(n)=\sqrt{\sum_{i=0}^{2^j-1}\left\{I_j^i(n)\right\}^2}
\tag{5.11}
$$

According to IEEE-1459-2010, active power and reactive power are calculated using (5.12) and (5.13), respectively.

$$
P=VI\cos\delta
\tag{5.12}
$$

$$Q = VI\sin\delta \tag{5.13}$$

where, $\delta = \theta - \phi$ i.e. the angle between voltage and current signal. Evaluation of trigonometric functions such as cosine and sine are required for the computation of these indices. The implementation of these functions on a real-time hardware platform is complex, computationally demanding [110] and require more hardware resources. The proposed method overcomes these drawbacks by calculating active and reactive power using analytic signal as shown in (5.14) to (5.17). The active power at each node can be calculated according to (5.14)

$$\begin{aligned}
P_j^0(n) &= \begin{bmatrix} \left\{X_j^0(n)\right\} \times \left\{X_j^{*0}(n)\right\} + \\ \left[HT\left\{X_j^0(n)\right\} \times HT\left\{X_j^{*0}(n)\right\}\right] \end{bmatrix} \\
P_j^1(n) &= \begin{bmatrix} \left\{X_j^1(n)\right\} \times \left\{X_j^{*1}(n)\right\} + \\ \left[HT\left\{X_j^1(n)\right\} \times HT\left\{X_j^{*1}(n)\right\}\right] \end{bmatrix} \\
&\cdots\cdots\cdots\cdots\cdots \\
P_j^i(n) &= \begin{bmatrix} \left\{X_j^i(n)\right\} \times \left\{X_j^{*i}(n)\right\} + \\ \left[HT\left\{X_j^i(n)\right\} \times HT\left\{X_j^{*i}(n)\right\}\right] \end{bmatrix} \\
P_{Total} &= \sum_{i=0}^{2^j-1} \left\{P_j^i(n)\right\}
\end{aligned} \tag{5.14}$$

and the harmonic active power is calculated as

$$P_H = \sum_{i=1}^{2^j-1} \left\{P_j^i(n)\right\} \tag{5.15}$$

The reactive power at each node can be calculated according to (5.16) and the harmonic reactive power can be computed according to (5.17).

The other power quality indices are fundamental apparent power (S_1), displacement power factor (PF_1), harmonic voltages (V_H), harmonic currents (I_H), total harmonic distortion for voltage ($THDv$), total harmonic distortion for current ($THDi$) voltage distortion power (D_V), current distortion power (D_I), harmonic apparent power (S_H), nonfundamental apparent power (S_N), apparent power (S), non-active power (N) and power factor (PF). These power quality indices are derived using the equations (5.8) to (5.17) and formulas are given in chapter three, section 3.2.

$$Q_j^0(n) = \begin{bmatrix} \left[HT\left\{X_j^0(n)\right\} \times \left\{X_j^{*0}(n)\right\} \right] - \\ \left[\left\{X_j^0(n)\right\} \times HT\left\{X_j^{*0}(n)\right\} \right] \end{bmatrix}$$

$$Q_j^1(n) = \begin{bmatrix} \left[HT\left\{X_j^1(n)\right\} \times \left\{X_j^{*1}(n)\right\} \right] - \\ \left[\left\{X_j^1(n)\right\} \times HT\left\{X_j^{*1}(n)\right\} \right] \end{bmatrix}$$

$$\cdots\cdots\cdots\cdots\cdots \tag{5.16}$$

$$Q_j^i(n) = \begin{bmatrix} \left[HT\left\{X_j^i(n)\right\} \times \left\{X_j^{*i}(n)\right\} \right] - \\ \left[\left\{X_j^i(n)\right\} \times HT\left\{X_j^{*i}(n)\right\} \right] \end{bmatrix}$$

$$Q_B = \sum_{i=0}^{2^j-1} \left\{Q_j^i(n)\right\}$$

$$Q_H = \sum_{i=1}^{2^j-1} \left\{Q_j^i(n)\right\} \tag{5.17}$$

5.3 Proposed Measurement System

The block diagram of the proposed method for the measurement of instantaneous power quality indices is shown in Figure 5.1. The proposed method comprises of three distinct processes. First, the distorted power signal is decomposed into fundamental and harmonic components using the UWPT. The UWPT decomposes the input signal in such a way that the exact replica of fundamental and each harmonic component is available at the end of the decomposition level. Here, the number of decomposition levels in the UWPT decomposition tree is three and the sampling frequency is 1.6 kHz. Hence, the output nodes at the end of the decomposition level are divided into eight bands with a fixed spectrum bandwidth of 100 Hz. In this work, “db20” is selected as a mother wavelet [103].

In the second step, Hilbert transform is applied to the decomposed signals to obtain the analytic signals corresponding to fundamental and each harmonic component. The concept of the analytic signal is very similar to the approach of the phasor. Therefore, it allows us to track the amplitude and phase variation of the signal with respect to time. Analytic signals can be represented in the form of complex functions on the time-frequency plane as given in (5.18). The representation of the analytic signals in the form of complex functions is known as the Hilbert spectrum $H\ (\omega, t)$.The Hilbert spectrum preserves the instantaneous amplitude and phase information of fundamental and harmonic components as contained in the original signal.

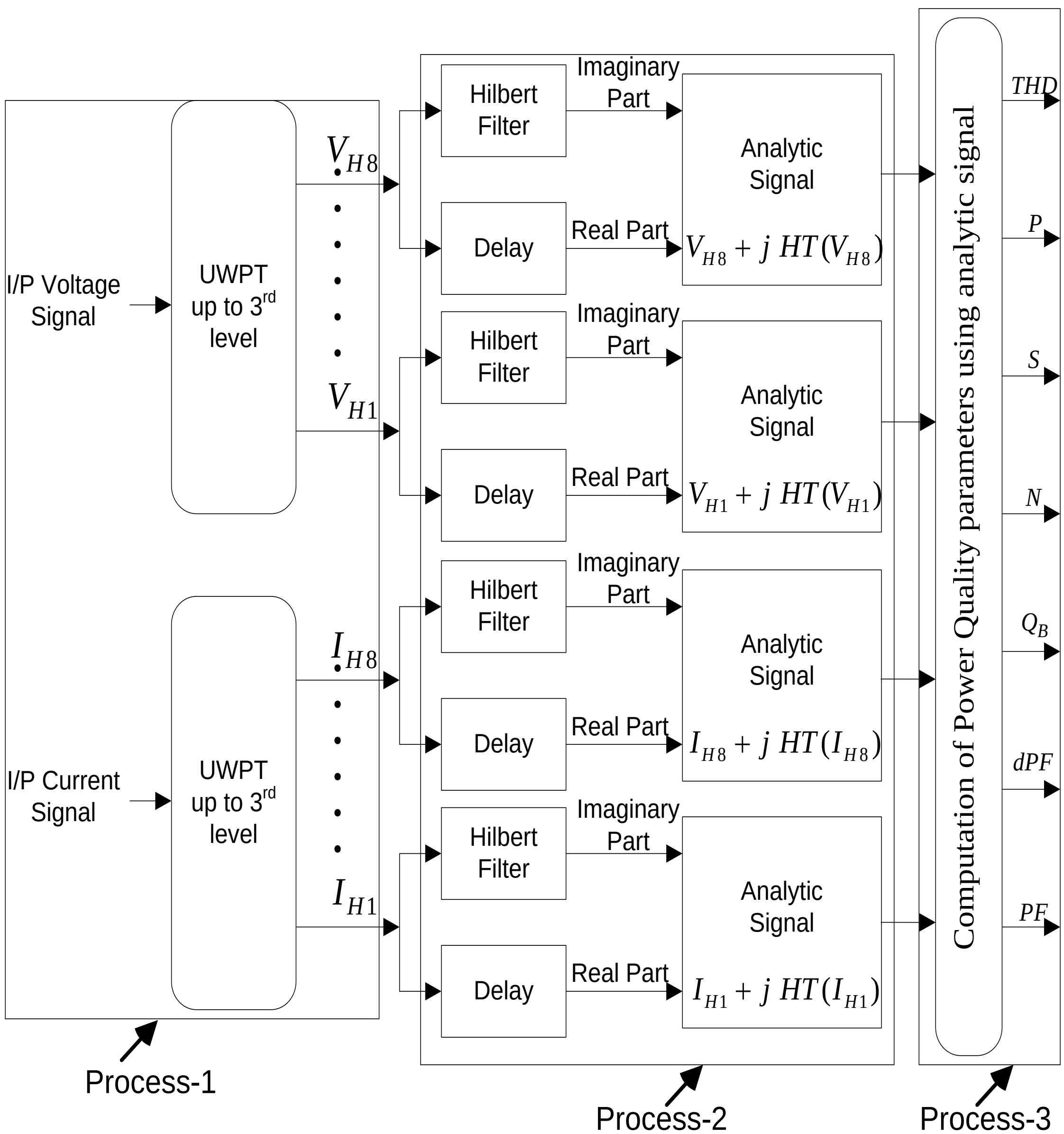

Figure 5.1. Conceptual block diagram of the proposed measurement system

$$
\begin{aligned}
&Z_1(n) = X_j^0(n) + jHT\left\{X_j^0(n)\right\} \\
&Z_2(n) = X_j^1(n) + jHT\left\{X_j^1(n)\right\} \\
&\ldots\ldots\ldots\ldots\ldots \\
&Z_i(n) = X_j^i(n) + jHT\left\{X_j^i(n)\right\}
\end{aligned}
\tag{5.18}
$$

Discrete Hilbert transform can be implemented by using IIR or FIR filters. The advantages of IIR filters are reduced computational complexity and smaller delay due to the limited number of filter coefficients. However, the drawbacks related to IIR filters are non-linear phase response and the possibility of instability due to finite word length. In comparison to IIR filters, FIR filters have inherent stability and linear phase response. Therefore, the accuracy of power quality indices is maintained. For the implementation of Hilbert transform, FIR filters of order 40, 80 and 160 are included in the analysis, which is designed by the least square technique.

Table 5.1: Hilbert filter parameters

Parameter	**HT-FIR Filter-1**	**HT-FIR Filter-2**	**HT-FIR Filter-3**
Filter Order	40	80	160
Stable	Yes	Yes	Yes
Linear phase	Yes	Yes	Yes
Transition Width (Hz)	30	30	30
Pass-band ripple (dB)	5.1516	1.5269	0.14713
Number of Multiplier	40	80	160
Number of Adder	39	79	159
Number of States	40	80	160
Multiplication per unit sample	40	80	160
Addition per unit sample	39	79	159

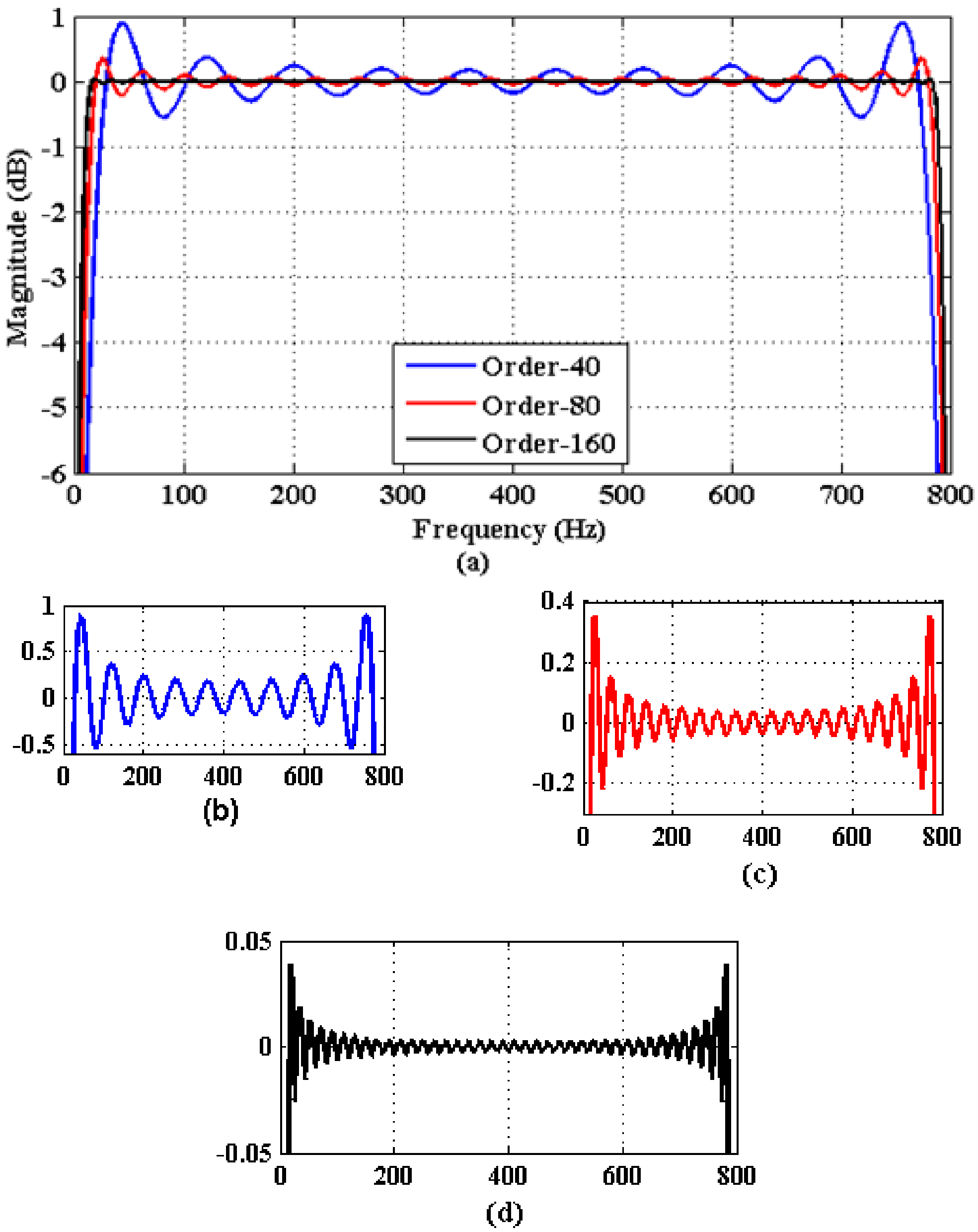

Figure 5.2. (a) Frequency response of Hilbert FIR filters. (b) Zoomed-in view of magnitude (dB) axis of (a) near unity gain for Hilbert FIR filters of order-40. (c) Zoomed-in view of magnitude (dB) axis of (a) near unity gain for Hilbert FIR filters of order-80. (d) Zoomed-in view of magnitude (dB) axis of (a) near unity gain for Hilbert FIR filters of order-160

In this context, the main objective is to choose the best order FIR filter for the measurement of instantaneous power quality indices. For this purpose, we have taken five different performance parameters, viz., passband ripple, group delay, implementation cost, computational complexity and the measurement accuracy. The transition width and sampling frequency for each filter is set to 30 Hz and 1.6 kHz, respectively. Hence, we find approximately flat passband response within the range of [50, 750] Hz. The details about performance parameters for each filter is given in Table 5.1.

The magnitude response of each filter is represented in Figure 5.2 (a) for the desired frequency bandwidth. Figure 5.2 (b), (c) and (d) show the zoomed-in view of magnitude (dB) axis of Figure 5.2 (a) near the unity gain. The fluctuations in magnitude response near the unity gain stand between -0.544 dB to 0.886 dB, -0.2145 dB to 0.3502 dB and -0.02443 dB to 0.03935 dB for filters of order 40, 80 and 160, respectively. The passband ripple is defined as the fluctuation of magnitude response with respect to unity gain in the pass bandwidth of the filter. It can be seen from Figure 5.2 (a) that as the order of filter increases, the magnitude response of filters improve due to a decrease in passband ripple. Therefore, the measurement accuracy of higher-order filters is better than lower-order filters. The group delay of the filter accounts for the time delay between input and output response. In the FIR filter, group delay is constant for all frequency components because of the linear phase response. Here, the value of group delay (in samples) for filters of order 40, 80 and 160 is found to be 20, 40 and 80, respectively.

The implementation cost and computational complexity are also significant performance parameters, specifically, during the implementation of filter on the real-time hardware platform. Performance parameters such as the number of adders, multipliers and the internal state of filter determine the implementation cost of the filter. Whereas, the number of operations (addition or multiplication) per input sample defines the computational burden of the filter. From Table 5.1, it can be noted that the implementation cost and computational complexity both are increasing with the increment of the order of the filter.

In order to evaluate the measurement accuracy of the proposed method for filters of order 40, 80 and 160, a simulation test has been performed using synthetic voltage signal. The voltage signal contains odd integer harmonics along with fundamental frequency component and is generated using (5.19) at the sampling frequency of 1.6 kHz. Table 5.2 compares the true values of absolute errors obtained in the measurement of RMS value of the fundamental and harmonic components. We can see from Table 5.2 that the measurement accuracy for filter of order 40 is less in comparison to other two filters. Filter of order 160 provides more accurate measurement in comparison to filter of order 80 due to low magnitude fluctuation near the unity gain. Although, measurement accuracy for filter of order 160 is better than the other two filters but its computational complexity and implementation cost are high.

Table 5.2: Comparison of measurement accuracy for filters of order 160, 80 and 40

HT-FIR Filter Order	Absolute Error							
	Fundamental Component	**Third Harmonic**	**Fifth Harmonic**	**Seventh Harmonic**	**Ninth Harmonic**	**Eleventh Harmonic**	**Thirteenth Harmonic**	**Fifteenth Harmonic**
160	3.04E-07	2.45E-04	3.09E-04	2.60E-03	2.74E-03	1.45E-04	7.47E-05	1.05E-07
80	4.26E-07	3.15E-03	7.34E-03	8.02E-03	7.89E-03	3.68E-03	1.59E-03	3.17E-04
40	7.18E-02	1.34E-02	1.33E-02	1.31E-02	1.25E-02	6.90E-03	6.72E-03	7.16E-03

$$\begin{aligned} v(t) &= \sin(\omega t) + 0.2\sin(3\omega t) + 0.2\sin(5\omega t) \\ &\quad + 0.15\sin(7\omega t) + 0.15\sin(9\omega t) + 0.1\sin(11\omega t) \\ &\quad + 0.1\sin(13\omega t) + 0.1\sin(15\omega t) \end{aligned} \tag{5.19}$$

From the above discussion, it can be concluded that the filter of order 160 is more demanding due to higher implementation cost and increased computations. Whereas passband ripple is more for the filter of order 40, hence it may reduce the accuracy of estimation. Therefore, in this work, filter of order 80 is selected for implementation of Hilbert transform as it provides an optimum response with respect to various performance parameters. Then, in the third step, power quality indices are computed using (5.8)-(5.17).

5.4 Performance Evaluation

5.4.1 Simulation Study

To illustrate the usefulness of the proposed method for the measurement of instantaneous power quality indices, three case studies are carried out. In the first two case studies, synthetic voltage and current signals are generated on the MATLAB platform in order to test the efficacy of the proposed technique under stationary and non-stationary conditions.

For the third case, measured real-time voltage and current signals are considered for the validation of the proposed technique. The algorithms are implemented on the MATLAB software platform running on the laptop having an Intel Core i5 2.4-GHz processor and 4-GB RAM. The sampling rate for each study case is 1.6 kHz, i.e., 32 samples per fundamental period. The performance of the proposed method is also compared with the other two similar and competitive algorithms, i.e., DWPT and STFT. In the case of DWPT, analysis is carried out with a three-level decomposition tree and "db20" is selected as the mother wavelet. In the case of STFT and DWPT, power quality indices are calculated using ten cycles windowed signal as recommended by IEEE 1459-2010 [12] and IEC 61000-4-7 [11]. Whereas, the proposed method provides the result at each instant and provides information about power quality indices with respect to time.

1) Case-1: Stationary Signal

The steady-state performance of the proposed algorithm is tested using a stationary signal. In this context, synthetic voltage and current signals in the per unit (p.u.) are generated using (5.20) & (5.21), respectively for the 1-s duration. In (5.20) & (5.21), $\omega=2\pi f$, where f is the fundamental frequency.

$$\begin{aligned} v(t) &= \sin(\omega t) + 0.2\sin(3\omega t - 70^\circ) + 0.15\sin(5\omega t) \\ &\quad + 0.1\sin(9\omega t) + 0.05\sin(13\omega t + 20^\circ) \end{aligned} \tag{5.20}$$

$$\begin{aligned} i(t) &= \sin(\omega t + 30^\circ) + 0.2\sin(3\omega t - 60^\circ) + 0.15\sin(5\omega t) \\ &\quad + 0.1\sin(9\omega t) + 0.05\sin(13\omega t + 30^\circ) \end{aligned} \tag{5.21}$$

Table 5.3 provides the performance comparison of the measured power quality indices using the proposed technique, DWPT and STFT, with the actual values obtained by IEEE Standard 1459-2010. According to phase differences in (5.20) and (5.21), the fundamental reactive power (Q_1), harmonic reactive power (Q_H) and total reactive power (Q_B) flows opposite to fundamental active power (P_1) whereas, harmonic active power (P_H), and total active power (P_1) flows in the direction of fundamental active power (P_1). It can be noticed from Table 5.3 that the proposed method provides the direction of power flow as it retains the phase information of fundamental and harmonic components. While

DWPT does not provide information about the direction of power flow due to the lack of phase information.

Table 5.3: Power quality indices for stationary signal

Power Quality Indices	IEEE-1459-2010	Proposed Method	DWPT	STFT
V_1	0.7071	0.7071	0.6879	0.7071
I_1	0.7071	0.7071	0.6818	0.7071
S_1	0.5000	0.4999	0.4691	0.5000
P_1	0.4330	0.4330	0.3984	0.4330
Q_1	-0.250	-0.2499	0.2476	-0.250
PF_1	0.8660	0.8660	0.8492	0.8660
V_H	0.1936	0.1900	0.1938	0.1936
I_H	0.1936	0.1900	0.1923	0.1936
$THDv$	0.2738	0.2688	0.2817	0.2738
$THDi$	0.2738	0.2688	0.2821	0.2738
D_V	0.1369	0.1344	0.1321	0.1369
D_I	0.1369	0.1344	0.1323	0.1369
S_H	0.0375	0.0361	0.0372	0.0375
S_N	0.1972	0.1934	0.1907	0.1972
P_H	0.0371	0.0358	0.0368	0.0371
P	0.4701	0.4688	0.4353	0.4701
Q_H	-0.0036	-0.0036	0.0046	-0.0036
Q_B	-0.2536	-0.2536	0.2522	-0.2536
S	0.5375	0.5361	0.5064	0.5375
N	0.2604	0.2600	0.2587	0.2604
PF	0.8747	0.8744	0.8596	0.8747

The absolute error as defined in (5.22) is computed for the performance comparison of the proposed method with the DWPT and STFT.

$$Absolute\ error = \left| Estimated\ value - Actual\ value \right| \tag{5.22}$$

Table 5.4 shows the values of absolute errors using the proposed method, STFT and DWPT. It can be observed that the estimation accuracy of STFT is better than the other two techniques and provides the direction of power flow. This is because the STFT outperforms in the case of a stationary signal as amplitude, phase and frequency do not fluctuate with respect to time. However, estimated indices using the proposed approach are very close to the true values, demonstrating the effectiveness of the proposed scheme in steady state.

Table 5.4: Absolute error for the stationary signal case-1

PM: Proposed Method

Method	**Absolute Error**										
	V_1	I_1	S_1	P_1	Q_1	PF_1	V_H	I_H	$THDv$	$THDi$	D_V
STFT	0.00E+00	2.22E-16	5.55E-17	1.67E-16	2.22E-16	0.00E+00	1.94E-16	1.67E-16	3.33E-16	2.78E-16	1.11E-16
DWPT	1.91E-02	2.52E-02	3.09E-02	3.46E-02	4.98E-01	1.67E-02	1.59E-04	1.29E-03	7.84E-03	8.25E-03	4.78E-03
PM	5.85E-08	5.85E-08	8.27E-08	7.16E-08	4.13E-08	1.89E-15	3.55E-03	3.55E-03	5.03E-03	5.03E-03	2.51E-03

Method	**Absolute Error**									
	D_I	S_H	S_N	P_H	P	Q_H	Q_B	S	N	PF
STFT	1.11E-16	6.94E-17	1.94E-16	1.18E-16	1.11E-16	2.11E-16	5.00E-16	0.00E+00	2.78E-16	2.22E-16
DWPT	4.59E-03	2.18E-04	6.54E-03	2.85E-04	3.49E-02	8.31E-03	5.06E-01	3.11E-02	1.70E-03	1.52E-02
PM	2.51E-03	1.36E-03	3.75E-03	1.36E-03	1.36E-03	4.54E-05	4.54E-05	1.36E-03	3.60E-04	3.11E-04

2) Case-2: Non-Stationary Signal

The intention of this experiment is to investigate the performance of the proposed method under the time-varying situation, i.e., the abrupt change in amplitude, fundamental frequency deviation, in the presence of noise and harmonics. In this context, time-varying voltage and current signals in the per unit (p.u.) are generated on the MATLAB platform

Table 5.5: Parameters (Amplitude, Frequency and Phase) of voltage signal for case-2 at different time-interval

Time Interval (s)	**Fundamental Component**			**Third Harmonic**			**Fifth Harmonic**			**Ninth Harmonic**			**Eleventh Harmonic**			**Thirteenth Harmonic**		
	V_1	f_1	θ_1	V_3	f_3	θ_3	V_5	f_5	θ_5	V_9	f_9	θ_9	V_{11}	f_{11}	θ_{11}	V_{13}	f_{13}	θ_{13}
0.0-0.2	1	50	0	0.2	150	-70	0.15	250	0	0.10	450	0	0	0	0	0.05	650	20
0.2-0.4	0.8	50.5	0	0.16	151.5	-70	0.12	252.5	0	0.08	454.5	0	0.04	555.5	20	0	0	0
0.4-0.6	1	49.5	0	0.2	148.5	-70	0.15	247.5	0	0.10	445.5	0	0	0	0	0.05	643.5	20
0.6-0.8	1.2	50.5	0	0.24	151.5	-70	0.18	252.5	0	0.12	454.5	0	0	0	0	0.06	656.5	20
0.8-1.0	0.8	49.5	0	0.16	148.5	-70	0.12	247.5	0	0.08	445.5	0	0.04	544.50	20	0	0	0
1.0-1.2	1.2	50.5	0	0.24	151.5	-70	0.18	252.5	0	0.12	454.5	0	0	0	0	0.06	656.5	20
1.2-1.4	1	50.5	0	0.2	151.5	-70	0.15	252.5	0	0.10	454.5	0	0	0	0	0.05	656.5	20
1.4-1.6	1.2	49.5	0	0.24	148.5	-70	0.18	247.5	0	0.12	445.5	0	0	0	0	0.06	643.5	20
1.6-1.64	0.8	50.5	0	0.16	151.5	-70	0.12	252.5	0	0.08	454.5	0	0.04	555.50	20	0	0	0
1.64-1.74	0.4	50.5	0	0.08	151.5	-70	0.06	252.5	0	0.04	454.5	0	0.02	555.50	20	0	0	0
1.74-1.8	0.8	50.5	0	0.16	151.5	-70	0.12	252.5	0	0.08	454.5	0	0.04	555.50	20	0	0	0
1.8-1.84	1.2	50.5	0	0.24	151.5	-70	0.18	252.5	0	0.12	454.5	0	0	0	0	0.06	656.5	20
1.84-1.94	0.6	50.5	0	0.12	151.5	-70	0.09	252.5	0	0.06	454.5	0	0	0	0	0.03	656.5	20
1.94-2.0	1.2	50.5	0	0.24	151.5	-70	0.18	252.5	0	0.12	454.5	0	0	0	0	0.06	656.5	20

using (5.23) & (5.24), respectively for a period of 2-s. In the voltage signal, the amplitudes of fundamental component and harmonics (V_1, V_3, V_5, V_9, V_{11} and V_{13}) and the frequencies of fundamental component and harmonics (f_1, f_3, f_5, f_9, f_{11} and f_{13}) are varied after some time interval according to Table 5.5. Similarly, in the current signal the amplitudes (I_1, I_3, I_5, I_9, I_{11} and I_{13}) and the frequencies (f_1, f_3, f_5, f_9, f_{11} and f_{13}) are varied after certain time interval as depicted in Table 5.6. White Gaussian noise of signal-to-noise ratio of 40 dB is added in both the signals. Resulting voltage and current signals are shown in Figure 5.3 (a) and (b), respectively.

The proposed algorithm gives the numerical value of power quality indices at each instant, i.e., sample-to-sample, whereas STFT and DWPT provide a single value for each time-window. Therefore, two types of results are discussed in this section. The first one is the variation of power quality indices with respect to time. Another one is to show the measurement accuracy of power quality indices in terms of mean and max values of absolute errors. Figure 5.3 shows the dynamic response of measured power quality indices

$$\begin{aligned} v(t) = & V_1 \sin(2\pi f_1 t + \theta_1) + V_3 \sin(2\pi f_3 t + \theta_3) \\ & + V_5 \sin(2\pi f_5 t + \theta_5) + V_9 \sin(2\pi f_9 t + \theta_9) \\ & + V_{11} \sin(2\pi f_{11} t + \theta_{11}) + V_{13} \sin(2\pi f_{13} t + \theta_{13}) \end{aligned} \tag{5.23}$$

$$\begin{aligned} i(t) = & I_1 \sin(2\pi f_1 t + \phi_1) + I_3 \sin(2\pi f_3 t + \phi_3) \\ & + I_5 \sin(2\pi f_5 t + \phi_5) + I_9 \sin(2\pi f_9 t + \phi_9) \\ & + I_{11} \sin(2\pi f_{11} t + \phi_{11}) + I_{13} \sin(2\pi f_{13} t + \phi_{13}) \end{aligned} \tag{5.24}$$

Table 5.6: Parameters (Amplitude, Frequency and Phase) of current signal for case-2 at different time-interval

Time Interval (s)	**Fundamental Component**			**Third Harmonic**			**Fifth Harmonic**			**Ninth Harmonic**			**Eleventh Harmonic**			**Thirteenth Harmonic**		
	I_1	f_1	ϕ_1	I_3	f_3	ϕ_3	I_5	f_5	ϕ_5	I_9	f_9	ϕ_9	I_{11}	f_{11}	ϕ_{11}	I_{13}	f_{13}	ϕ_{13}
0.0-0.2	1	50	30	0.2	150	-60	0.15	250	0	0.10	450	0	0	0	0	0.05	650	30
0.2-0.4	0.8	50.5	30	0.16	151.5	-60	0.12	252.5	0	0.08	454.5	0	0.04	555.5	30	0	0	0
0.4-0.6	1	49.5	30	0.2	148.5	-60	0.15	247.5	0	0.10	445.5	0	0	0	0	0.05	643.5	30
0.6-0.8	1.2	50.5	30	0.24	151.5	-60	0.18	252.5	0	0.12	454.5	0	0	0	0	0.06	656.5	30
0.8-1.0	0.8	49.5	30	0.16	148.5	-60	0.12	247.5	0	0.08	445.5	0	0.04	544.50	30	0	0	0
1.0-1.2	1.2	50.5	30	0.24	151.5	-60	0.18	252.5	0	0.12	454.5	0	0	0	0	0.06	656.5	30
1.2-1.4	1	50.5	30	0.2	151.5	-60	0.15	252.5	0	0.10	454.5	0	0	0	0	0.05	656.5	30
1.4-1.6	1.2	49.5	30	0.24	148.5	-60	0.18	247.5	0	0.12	445.5	0	0	0	0	0.06	643.5	30
1.6-1.64	0.8	50.5	30	0.16	151.5	-60	0.12	252.5	0	0.08	454.5	0	0.04	555.50	30	0	0	0
1.64-1.74	0.4	50.5	30	0.08	151.5	-60	0.06	252.5	0	0.04	454.5	0	0.02	555.50	30	0	0	0
1.74-1.8	0.8	50.5	30	0.16	151.5	-60	0.12	252.5	0	0.08	454.5	0	0.04	555.50	30	0	0	0
1.8-1.84	1.2	50.5	30	0.24	151.5	-60	0.18	252.5	0	0.12	454.5	0	0	0	0	0.06	656.5	30
1.84-1.94	0.6	50.5	30	0.12	151.5	-60	0.09	252.5	0	0.06	454.5	0	0	0	0	0.03	656.5	30
1.94-2.0	1.2	50.5	30	0.24	151.5	-60	0.18	252.5	0	0.12	454.5	0	0	0	0	0.06	656.5	30

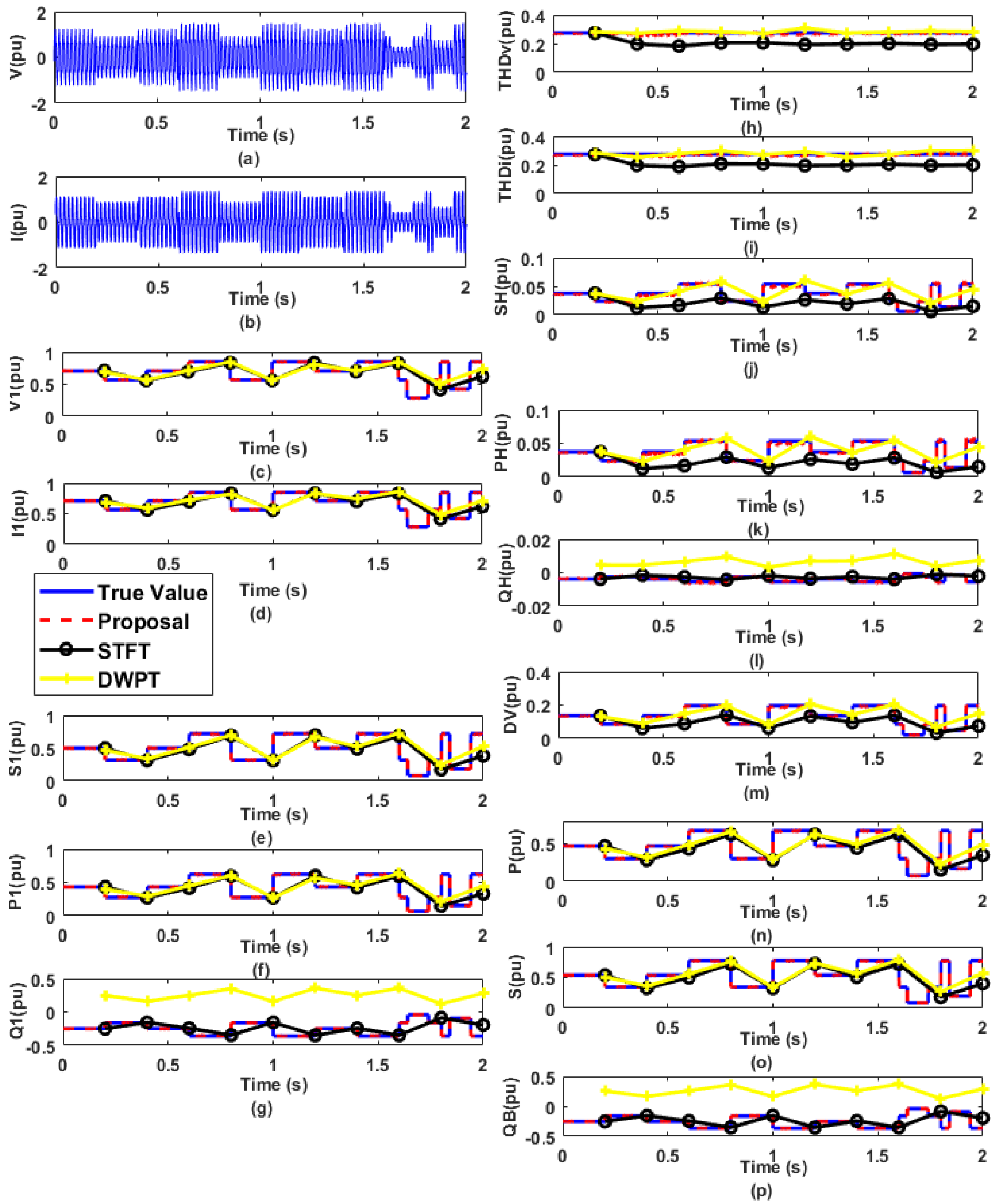

Figure 5.3. Dynamic response of measured power quality indices for case-2

with respect to time using the proposed method, STFT and DWPT. Measured power quality indices are: RMS value of fundamental voltage signal (V_1), RMS value of fundamental current signal (I_1), fundamental apparent power (S_1), fundamental active power (P_1), fundamental reactive power (Q_1), total harmonic distortion voltage ($THDv$), total harmonic distortion current ($THDi$), harmonic apparent power (S_H), harmonic active power (P_H), harmonic reactive power (Q_H), voltage distortion power (D_V), total active power (P), total apparent power (S) and total reactive power (Q_B). For each power quality parameter, the blue line indicates the true value (calculated in accordance with IEEE Standard 1459-2010 [12]) and the red line denotes the instantaneous result given by the proposed method. The black line with the circle and yellow line with the plus denote the result given by STFT and DWPT, respectively in each time-window. In case of DWPT and STFT, the length of time-window is ten cycles of the fundamental frequency according to IEC 61000-4-7 [11]. It can be observed from Figure 5.3, that the proposed method follows the path of actual value as it provides the instantaneous result while deviation from actual value is seen in the result of the STFT and the DWPT because these methods provide the average value over a time-window. Power quality indices measured by the proposed technique respond immediately to the sudden change in the parameter of voltage or current signal. For instance, when the changes occur in the parameter of voltage and current signals within time-window (1.6-s-1.8-s and 1.8-s-2-s), the proposed method tracks the actual values, while results given by STFT and DWPT are far away from the true values. Therefore, the proposed technique can capture the dynamic nature of electrical disturbances in the power system.

The proposed algorithm provides instantaneous results, i.e., sample-to-sample. Hence, for the proper and fair comparison of the proposed techniques with the other two techniques, the results provided by the proposed technique are averaged within the time-window of STFT and DWPT. Absolute errors are computed by equation (5.22). Mean and max values of absolute error found in the measurement of power quality indices are depicted in Table 5.7. In the present case, the estimation accuracy of all the techniques is affected due to the time-varying phenomenon. The proposed technique gives more accurate results in comparison to the other two techniques. It is clear from the results that the proposed technique is more accurate and consistent, justifying the effectiveness of the proposal for real-time and online applications.

Table 5.7: Mean and variance of absolute error for the non-stationary signal study case-2

PM: Proposed Method

Method		Absolute Error										
		***V*₁**	***I*₁**	***S*₁**	***P*₁**	***Q*₁**	***PF₁***	***V*H**	***I*H**	***THDv***	***THDi***	***DV***
STFT	*Mean*	1.15E-02	1.12E-02	2.26E-02	2.00E-02	1.07E-02	1.55E-03	4.91E-02	4.83E-02	6.86E-02	6.76E-02	3.83E-02
	Max	1.93E-02	1.89E-02	6.47E-02	5.68E-02	3.10E-02	2.73E-03	7.13E-02	7.00E-02	8.97E-02	8.63E-02	6.26E-02
DWPT	*Mean*	2.61E-02	3.05E-02	2.98E-02	2.89E-02	5.01E-01	1.00E-02	1.10E-02	1.18E-02	1.00E-02	1.54E-02	9.01E-03
	Max	1.06E-01	7.44E-02	7.74E-02	5.64E-02	7.17E-01	2.02E-02	3.60E-02	4.06E-02	3.39E-02	2.85E-02	2.62E-02
PM	*Mean*	1.96E-03	2.78E-03	3.12E-03	3.35E-03	7.72E-04	1.32E-03	3.91E-03	3.42E-03	4.95E-03	4.91E-03	3.03E-03
	Max	5.20E-03	4.94E-03	7.79E-03	8.54E-03	2.67E-03	2.56E-03	9.20E-03	8.28E-03	1.22E-02	1.06E-02	7.37E-03
Method		**Absolute Error**										
		DI	***SH***	***SN***	***P*H**	***P***	***QH***	***QB***	***S***	***N***	***PF***	
STFT	*Mean*	3.77E-02	1.67E-02	5.58E-02	1.66E-02	3.66E-02	1.04E-03	1.18E-02	3.93E-02	1.52E-02	4.20E-03	
	Max	6.21E-02	2.78E-02	9.15E-02	2.77E-02	7.54E-02	1.83E-03	3.23E-02	8.34E-02	3.61E-02	6.73E-03	
DWPT	*Mean*	8.75E-03	3.74E-03	1.22E-02	3.56E-03	2.99E-02	1.03E-02	5.12E-01	3.10E-02	1.03E-02	8.67E-03	
	Max	3.62E-02	1.14E-02	4.56E-02	1.10E-02	6.74E-02	1.66E-02	7.34E-01	8.89E-02	6.11E-02	1.82E-02	
PM	*Mean*	2.75E-03	1.43E-03	4.28E-03	1.43E-03	4.09E-03	1.93E-04	5.79E-04	3.83E-03	6.11E-04	1.33E-03	
	Max	7.56E-03	3.91E-03	1.11E-02	3.92E-03	9.99E-03	4.57E-04	2.22E-03	9.24E-03	2.69E-03	2.52E-03	

3) Case-3: Measured Signal

In order to assess the performance of the proposed method under the real situation, an experimental set-up is prepared in a laboratory for acquiring the real-time voltage and current signal. The experimental set-up comprises four different types of loads, i.e., mobile charging (MC), laptop charging (LC), two CFLs and a personal computer (PC). OROS-34

DAQ set up is interfaced with the laptop having Nvgate software for acquiring real-time voltage and current signal. Sigma-delta ADC of 24-bits resolution is used in the DAQ system. Measured voltage and current signals are shown in Figure 5.4. For initial 3-s, all the loads are connected to supply, then at 3-s, PC is switched off. Hence, the current is suddenly reduced as shown in Figure 5.4.

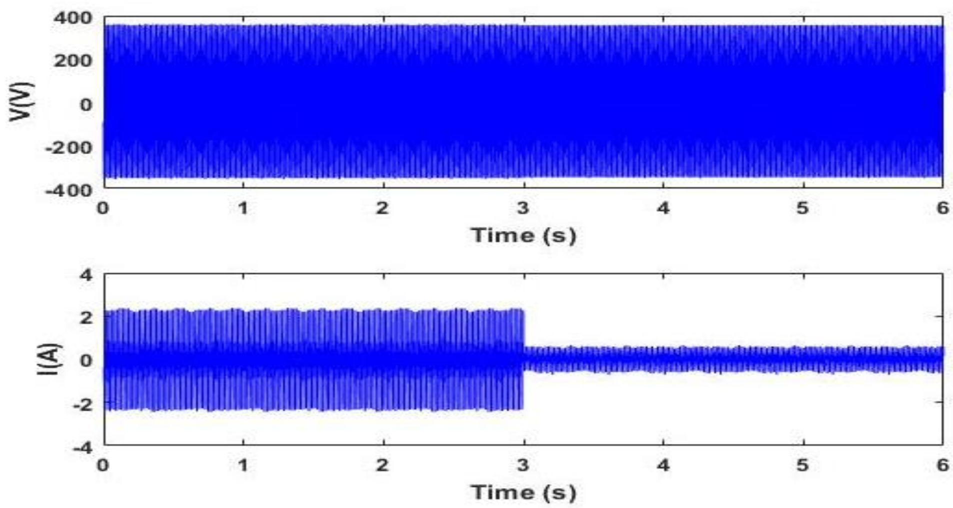

Figure 5.4. Measured voltage and current signal for case -3

Figure 5.5 shows the dynamic estimation response of power quality parameter estimation using the proposed method, the DWPT and the STFT. It can be seen from Figure 5.5 that when the signal changes suddenly (at 3-s), the proposed method quickly estimates the power quality indices after one sample while the STFT and the DWPT reflect the changes after ten cycles. Therefore, the proposed technique can provide fast detection of power quality indices when any load is connected or disconnected from the system.

5.5 FPGA Implementation of the Proposed Measurement System

In this section, the development of FPGA based digital hardware of the proposed method has been presented. The proposed methodology has been implemented on the Xilinx Virtex-6 FPGA ML-605 evaluation kit, which is connected to PC, XSG/ISE design suite 14.2, MATLAB/Simulink via JTAG interface. Figure 5.6 depicted the hardware architecture of the proposed technique, which consists of four main modules. The first and second modules compute the UWPT coefficients of voltage and current signals, respectively. The third module is responsible for the computation of analytic signals using Hilbert transform. The fourth module calculates the instantaneous power quality indices according to (5.8)-(5.17).

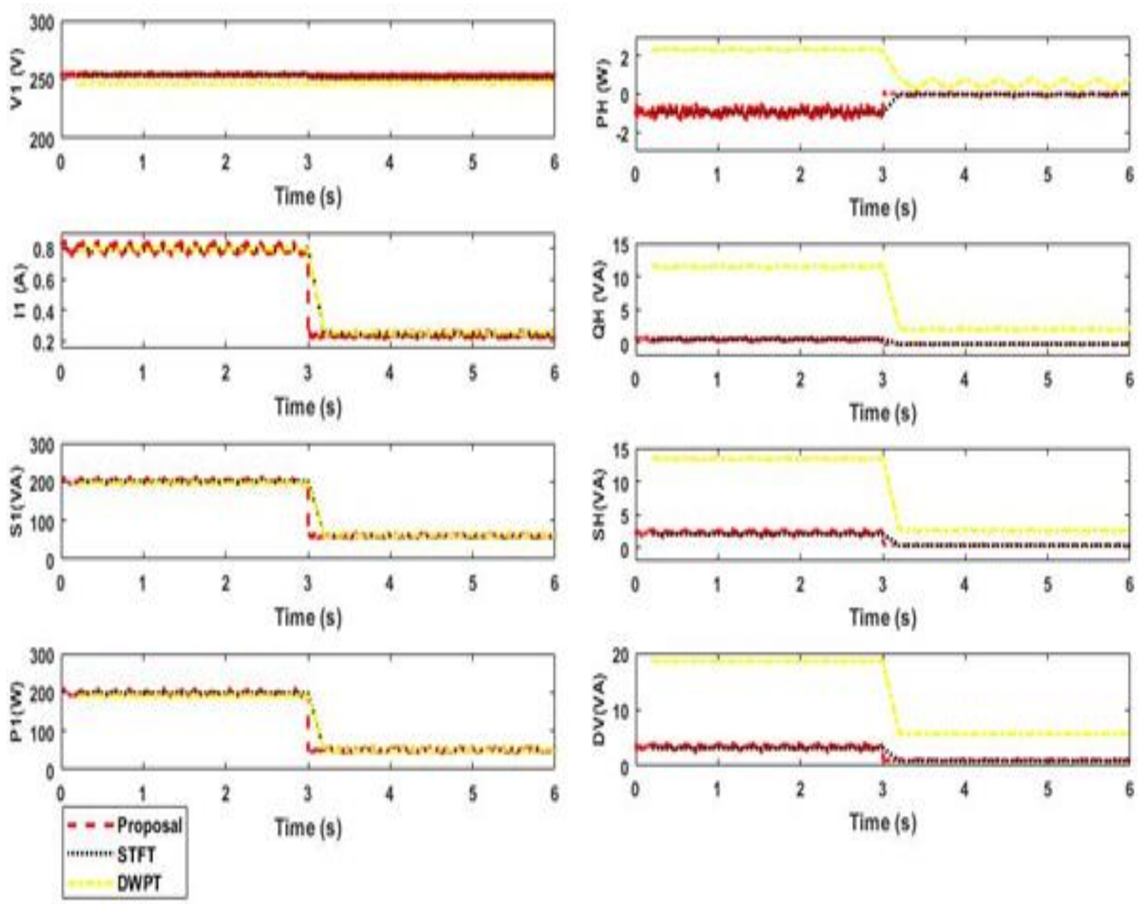

Figure 5.5. Dynamic response of measured power quality indices for case -3

The main hardware block of the proposed methodology is the FIR filter, which computes the UWPT coefficients and Hilbert transform of the signals. There are mainly two types of hardware architecture for the implementation of FIR filter, i.e., direct or transposed form and RAM-based MAC FIR filter. RAM-based MAC FIR filter consumes fewer hardware resources but at the cost of speed. Therefore, in this work RAM-based MAC FIR filter is adopted for the implementation of UWPT and Hilbert filters. Hardware architecture of the fourth module is developed using arithmetic blocks and corresponding equations. It can be seen from (5.8)-(5.17) that it involves simple mathematical operations such as addition, multiplication, subtraction, division and square root. Hence, the hardware architecture of the third module is developed using arithmetic blocks and corresponding equations. Figure 5.7 shows the digital design for the computation of active power. Table 5.8 shows the summary of resource utilization of the proposed technique on Xilinx Virtex-6 FPGA ML-605 evaluation kit.

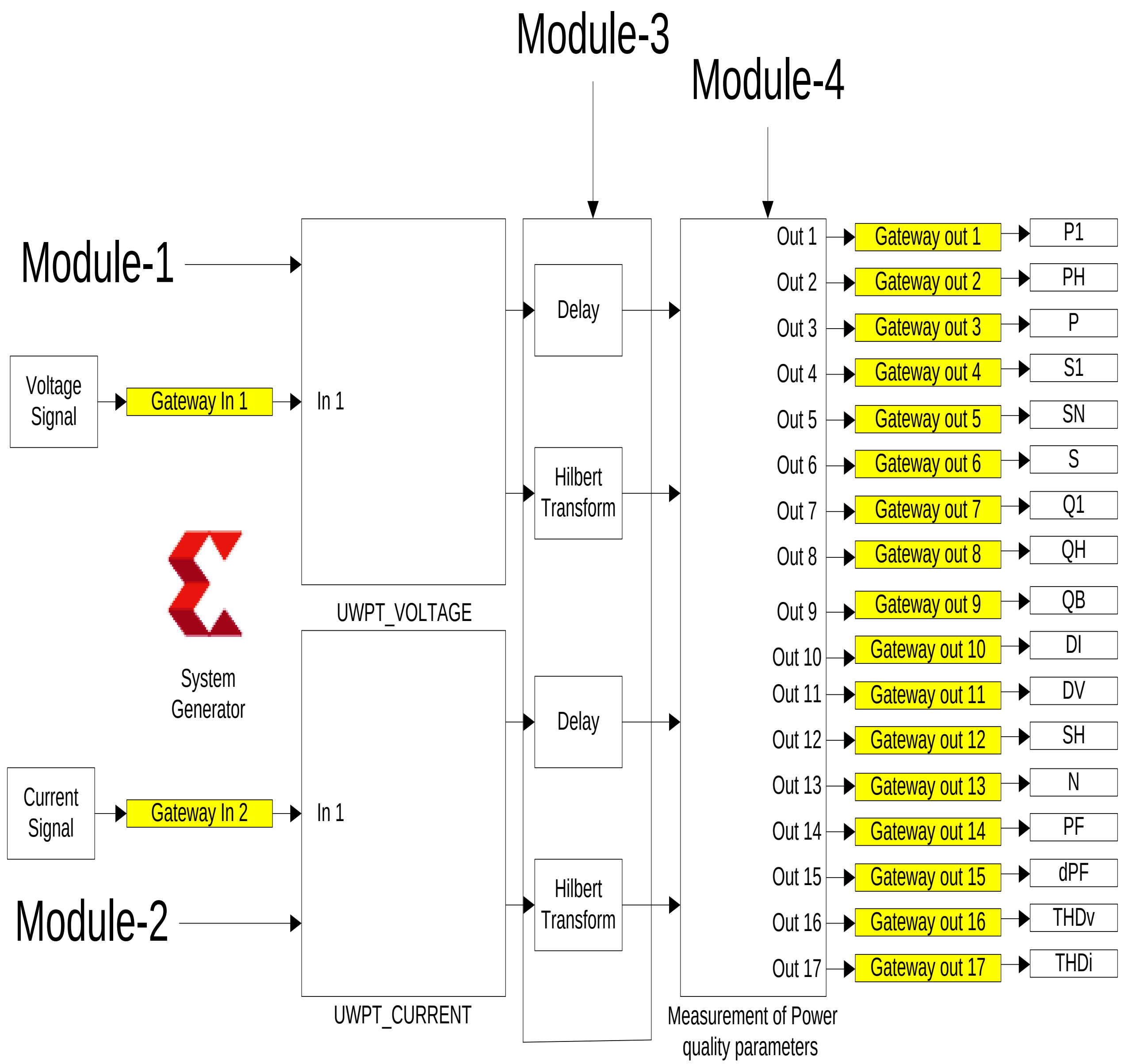

Figure 5.6. Hardware architecture of the proposed method

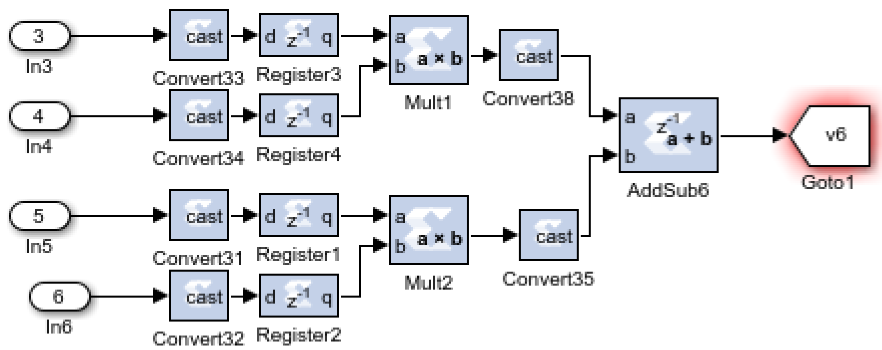

Figure 5.7. Computation of active power on XSG

Table 5.8: Resource utilization summary

Resource type	Used	Available
Number of slice registers	28,197 (9%)	301,440
Number of slice LUTs	37,109 (24 %)	150,720
Number of RAMB18E1s	44(5%)	832
Number of DSP184E1s	259 (33%)	768
Max. operating frequency	106.280 MHz	

Table 5.9: Comparison between MATLAB and FPGA results

Results	*THDv*	*THDi*	P_1	*P*	D_I	D_V	*N*	*PF*
MATLAB results	0.2688	0.2688	0.4330	0.4701	0.1344	0.1344	0.2600	0.8744
FPGA results	0.2836	0.2853	0.4292	0.4672	0.1298	0.1310	0.2543	0.8721
Absolute error	0.01480	0.0165	0.0038	0.0029	0.0046	0.0034	0.0057	0.0023

Accuracy and timing requirement of the proposed hardware is tested using the voltage and current signal of Case-1. Table 5.9 compares the estimated results of the proposed implementation with the MATLAB. Computations in MATLAB are performed in a 64-bit floating-point format. Hence, results are more accurate and taken as a reference value for comparison. In the proposed implementation data path, input and output are quantized in an 18-bit fixed-point format. Therefore, the results of the proposed implementation slightly deviate from the MATLAB results. However, the absolute errors in measurement are negligible and within acceptable limits. Table 5.10 shows the number of clock cycles required and time taken by the proposed method on the Xilinx Virtex-6 FPGA ML-605 evaluation kit at the clock frequency of 50 MHz. Performance in terms of accuracy and timing requirement shows that the proposed technique is suitable for online and real-time applications.

Table 5.10: Clock cycles required for estimation of power quality indices

Power quality indices	Clock cycles	FPGA (ms)
THDv	78,353	1.5670
THDi	78,407	1.5681
P_1	81,773	1.6356
P	82,602	1.6521
D_I	83,565	1.6713
D_V	83,402	1.6681
N	86,122	1.7224
PF	85,487	1.7097

5.6 Conclusion

A method combining the UWPT and Hilbert transform is proposed in this chapter to compute instantaneous power quality indices. Using the analytic signal, we can estimate the instantaneous power quality indices and, thus, improve the time-resolution, dynamic response and real-time processing capability of the estimation process. The proposed technique is inherently stable, does not require evaluation of trigonometric functions for the estimation of active and reactive power and also provides the direction of power flow. For the validation of the technique, three case studies are considered under different operating conditions. Results show that the proposed method is efficient in measurement and capable of tracking power quality indices. The proposed method is also implemented on the Xilinx Virtex-6 FPGA ML-605 evaluation kit for assessing the real-time performance of the technique. Estimation accuracy, resource utilization and timing requirements of the technique suggest that the proposed method is suitable for real-time applications.

Chapter 6

Conclusions

6.1 Introduction

The main focus of this thesis has been the development of hardware efficient algorithms for power quality monitoring with an objective of attaining reasonable accuracy with less computational complexity. The thesis investigates the effectiveness and suitability of two methods Undecimated Wavelet Packet Transform (UWPT) and Hilbert Transform (HT) for power quality monitoring. These two techniques are applied in this thesis for analysis of stationary as well as non-stationary power signals. Further, these techniques are implemented on Xilinx Virtex-6 FPGA ML-605 board after adequate analysis and synthesis on XSG/ISE design suite 14.2 and MATLAB/Simulink software platform.

Chapter one presented an introduction to the power quality disturbances and its causes and consequences in the emerging power system. Highlights of international standards on power quality monitoring are given with basic needs for measurement and monitoring of harmonics and power quality indices. A brief explanation of existing techniques and their limitations are presented in this section. Major challenges in the real-time estimation of harmonics and power quality indices are critically examined. The motivations behind this research work are given at the end of the chapter.

In chapter two, the UWPT is applied for the estimation of the amplitude of fundamental and harmonic components from the non-sinusoidal voltage and current signals. Limitations of the wavelet-based methods for the analysis of harmonics have been discussed. The amplitude of time-varying harmonics has been determined accurately in only one cycle of the fundamental frequency by utilizing the time-invariant property of the UWPT. The proposed method based on the UWPT reduces the computational time and improves the real-time processing capability and time-resolution. The proposed method has been tested on several time-varying voltage and current signals. The results reveal that the UWPT is outperforming the FFT and the DWPT in the case of harmonics estimation.

The proposed method has also been implemented on the Virtex-6 FPGA ML-605 board. The hardware results in terms of accuracy, resource utilization and response time confirm the utility of the proposed method.

A measurement system based on UWPT is proposed in chapter three for the estimation of power quality indices according to IEEE Standard 1459-2010. The proposed method comprises two steps. In the first step, voltage and current signals are processed in parallel for the separation of fundamental and harmonics components. In the second step, power quality indices are evaluated as per IEEE Standard 1459-2010. The proposed measurement system is developed on the FPGA platform because of its intrinsic parallelism nature and low implementation complexity. A comparative study of the proposed measurement system with DWPT and FFT has been performed to highlight the advantages. Hardware accuracy, resource utilization and timing requirement confirm that the proposed method completed the requirements of IEEE Standard 1459-2010.

A method based on UWPT is proposed in chapter four for visualization of time-varying power quality disturbances. The proposed technique accurately decomposes the distorted signal into different frequency components with exact localization of power quality disturbances. The effectiveness of the proposed method has been demonstrated through simulation results. The results authenticate that the UWPT-based scheme is suitable for detection of power quality disturbances.

In chapter five, a technique is proposed, which combines the strength of UWPT and Hilbert Transform (HT) methods. The proposed hybrid technique provides a reliable and accurate estimation of the power quality indices at every sample. The proposed method consists of three stages. Stage one for real-time separation of fundamental and harmonics components using UWPT, stage two for extraction of an envelope of different frequency components using Hilbert transform and stage three for calculation of power quality indices. The performance of the proposed technique is evaluated on stationary and time-varying power signals and compared with the conventional STFT and DWPT. The proposed method is successfully implemented on the Virtex-6 FPGA ML-605 board and accuracy of power quality indices has been verified by simulated signal.

6.2 Major Contributions of the Work

The major contributions of this thesis are summarized as follows:

1. A simple and efficient algorithm based on the UWPT has been proposed for accurate amplitude estimation of time-varying harmonics in only one fundamental cycle data. Further, the UWPT algorithm is implemented on Virtex-6 FPGA ML-605 board after proper analysis and synthesis on XSG/ISE design suite 14.2.

2. The design and implementation of a measurement system based on UWPT has been proposed for measurement of power quality indices as defined in IEEE Standard 1459-2010. To achieve higher operating frequency and save time, pipelined and parallel hardware architecture is used for implementation of the proposed technique on FPGA.

3. The time-invariant property of UWPT is utilized for detection of non-stationary electrical disturbances in the time-domain.

4. A method combining the UWPT and Hilbert transform is proposed for estimation of instantaneous power quality indices in real-time. The proposed method is also implemented on the Xilinx Virtex-6 FPGA ML-605 evaluation kit for assessing the real-time performance of the technique.

6.3 Future Scope

The research work carried out in this thesis has highlighted several new techniques that need further investigation. Some suggested new directions for future research in this area are follows:

- In this thesis, different techniques based on UWPT are proposed for the analysis of odd order frequency component up to 15^{th} order. Hence, further work can be done for the estimation of even harmonics, interharmonics and higher order harmonics by some improvements in the UWPT-based methods.

- This thesis investigates the effectiveness and suitability of the UWPT only for the measurement of harmonic components and power quality indices. The potentials of UWPT can be used for the classification of power quality disturbances.
- In recent years, the concept of the Internet of Things (IoT) is increasingly used due to the interconnection of people and objects among themselves. FPGA based smart power meter can be developed for the internet of things applications.

References

[1] M. H. J. Bollen and I. Y. H. Gu, Signal processing of power quality disturbances, vol. 30, John Wiley & Sons, 2006.

[2] *IEEE Recommended Practice and Requirements for Harmonic Control in Electric Power Systems, IEEE Std 519-2014 (Revision of IEEE Std 519-1992), pp. 1-29, 2014.*

[3] P. S. Harmonics, "Power System Harmonics: An Overview," in IEEE Transactions on Power Apparatus and Systems, vol. PAS-102, no. 8, pp. 2455-2460, Aug. 1983, doi: 10.1109/TPAS.1983.317745.

[4] B. Singh, A. Chandra and K. Al-Haddad, Power quality: problems and mitigation techniques, John Wiley & Sons, 2014.

[5] *IEEE Recommended Practice for Monitoring Electric Power Quality," in IEEE Std 1159-2019 (Revision of IEEE Std 1159-2009) , vol., no., pp.1-98, 13 Aug. 2019, doi: 10.1109/IEEESTD.2019.8796486.*

[6] A Systems View of the Modern Grid—Appendix A4: Provides Power Quality for 21st Century Needs v2.0, U.S. Dept. Energy, Nat. Energy Technol. lab.," *Available online:https://www.smartgrid.gov/document/systems_view_modern_grid_appendix_a4_ provides_ power_quality_21st_century_needs_v20*, Jan. 2007.

[7] P. Caramia, G. Carpinelli and P. Verde, Power quality indices in liberalized markets, John Wiley & Sons, 2009.

[8] V. E. Wagner, J. C. Balda, D. C. Griffith, A. Mceachern, T. M. Barnes, D. P. Hartmann, D. J. Phileggi, A. E. Emannuel, W. F. Horton, W. E. Reid and others, "Effects of harmonics on equipment," *IEEE Transactions on Power Delivery*, vol. 8, p. 672–680, 1993.

[9] APQI Report, "Economic Impact and Losses due to Poor Power Quality," *[Online]. Available: http://apqi.org/blog/economic-impact-and-losses-due-to-poor-power-quality/*, 2015.

[10] K. Koziy, B. Gou and J. Aslakson, "A low-cost power-quality meter with series arc-fault detection capability for smart grid," *IEEE Transactions on Power Delivery*, vol. 28, p. 1584–1591, 2013.

[11] *Testing and Measurement Techniques--General Guide on Harmonics and Interharmonics Measurements and Instrumentation, for Power Supply Systems and Equipment Connected Thereto, IEC Std. 61000-4-7, 2002.*

[12] *IEEE Standard Definitions for the Measurement of Electric Power Quantities Under Sinusoidal, Nonsinusoidal, Balanced, or Unbalanced Conditions, IEEE Std 1459-2010 (Revision of IEEE Std 1459-2000), pp. 1-50, 2010.*

[13] R. Flores, "Signal processing tools for power quality event classification," Ph.D. dissertation, Lic. Eng. thesis, School Elect. Eng., Chalmers Univ. Technol., Goteborg, Sweden, 2003.

[14] S. K. Jain and S. N. Singh, "Harmonics estimation in emerging power system: Key issues and challenges," *Electric power systems research,* vol. 81, p. 1754–1766, 2011.

[15] W. J. Williams, M. L. Brown and A. O. Hero III, "Uncertainty, information, and time-frequency distributions," in *Advanced Signal Processing Algorithms, Architectures, and Implementations II*, 1991.

[16] J. Barros and R. I. Diego, "Analysis of harmonics in power systems using the wavelet-packet transform," *IEEE Transactions on Instrumentation and Measurement,* vol. 57, p. 63–69, 2007.

[17] N. E. Huang, Z. Shen, S. R. Long, M. C. Wu, H. H. Shih, Q. Zheng, N.-C. Yen, C. C. Tung and H. H. Liu, "The empirical mode decomposition and the Hilbert spectrum for nonlinear and non-stationary time series analysis," *Proceedings of the Royal Society of London. Series A: mathematical, physical and engineering sciences,* vol. 454, p. 903–995, 1998.

[18] G. Rilling, P. Flandrin, P. Goncalves and others, "On empirical mode decomposition and its algorithms," in *IEEE-EURASIP workshop on nonlinear signal and image processing*, 2003.

[19] S. K. Jain and S. N. Singh, "Exact model order ESPRIT technique for harmonics and interharmonics estimation," *IEEE Transactions on Instrumentation and Measurement,* vol. 61, p. 1915–1923, 2012.

[20] R. Roy and T. Kailath, "ESPRIT-estimation of signal parameters via rotational invariance techniques," *IEEE Transactions on acoustics, speech, and signal processing,* vol. 37, p. 984–995, 1989.

[21] R. Prony, "Essai experimental–,-," *J. de l'Ecole Polytechnique*, vol. 2, 1795.

[22] G. Betta, L. Ferrigno and M. Laracca, "Cost-effective FPGA instrument for harmonic and interharmonic monitoring," *IEEE Transactions on Instrumentation and Measurement*, vol. 62, p. 2161–2170, 2013.

[23] F. Machado, P. Mariño, F. Poza, M. A. Domínguez and F. P. Fontán, "FPGA-based instrument for satellite beacon monitoring on propagation experiments," *IEEE Transactions on Instrumentation and Measurement,* vol. 63, p. 2761–2770, 2014.

[24] D. Granados-Lieberman, R. J. Romero-Troncoso, R. A. Osornio-Rios, A. Garcia-Perez and E. Cabal-Yepez, "Techniques and methodologies for power quality analysis and disturbances classification in power systems: a review," *IET Generation, Transmission & Distribution,* vol. 5, p. 519–529, 2011.

[25] C.-I. Chen and Y.-C. Chen, "Comparative study of harmonic and interharmonic estimation methods for stationary and time-varying signals," *IEEE Transactions on Industrial Electronics,* vol. 61, p. 397–404, 2013.

[26] Z. Leonowicz and T. Lobos, "Parametric Spectral Estimation for Power Quality Assessment," EUROCON 2007 - The International Conference on "Computer as a Tool", Warsaw, Poland, 2007, pp. 1641-1647, doi: 10.1109/EURCON.2007.4400304.

[27] N. C. F. Tse, "Practical application of wavelet to power quality analysis," 2006 IEEE Power Engineering Society General Meeting, Montreal, QC, Canada, 2006, pp. 5 pp.-, doi: 10.1109/PES.2006.1709311.

[28] T. Tarasiuk, "Comparative study of various methods of DFT calculation in the wake of IEC Standard 61000-4-7," *IEEE Transactions on Instrumentation and Measurement,* vol. 58, p. 3666–3677, 2009.

[29] G. Andria, M. Savino and A. Trotta, "Windows and interpolation algorithms to improve electrical measurement accuracy," *IEEE Transactions on Instrumentation and Measurement*, vol. 38, p. 856–863, 1989.

[30] F. Zhang, Z. Geng and W. Yuan, "The algorithm of interpolating windowed FFT for harmonic analysis of electric power system," *IEEE Transactions on Power Delivery*, vol. 16, p. 160–164, 2001.

[31] H. Qian, R. Zhao and T. Chen, "Interharmonics analysis based on interpolating windowed FFT algorithm," *IEEE Transactions on Power Delivery,* vol. 22, p. 1064–1069, 2007.

[32] G. W. Chang, C. I. Chen, Y. J. Liu and M. C. Wu, "Measuring power system harmonics and interharmonics by an improved fast Fourier transform-based algorithm," *IET generation, transmission & distribution,* vol. 2, p. 192–201, 2008.

[33] R. M. Hidalgo, J. G. Fernandez, R. R. Rivera and H. A. Larrondo, "A simple adjustable window algorithm to improve FFT measurements," *IEEE Transactions on Instrumentation and Measurement,* vol. 51, p. 31–36, 2002.

[34] B. Zeng, Z. Teng, Y. Cai, S. Guo and B. Qing, "Harmonic phasor analysis based on improved FFT algorithm," *IEEE Transactions on Smart Grid,* vol. 2, p. 51–59, 2010.

[35] A. Testa, D. Gallo and R. Langella, "On the processing of harmonics and interharmonics: Using Hanning window in standard framework," *IEEE Transactions on Power Delivery,* vol. 19, p. 28–34, 2004.

[36] J. Barros and R. I. Diego, "On the use of the Hanning window for harmonic analysis in the standard framework," *IEEE Transactions on Power Delivery,* vol. 21, p. 538–539, 2005.

[37] K. F. Chen and S. L. Mei, "Composite interpolated fast Fourier transform with the Hanning window," *IEEE Transactions on Instrumentation and Measurement,* vol. 59, p. 1571–1579, 2010.

[38] D. Agrez, "Weighted multipoint interpolated DFT to improve amplitude estimation of multifrequency signal," *IEEE Transactions on Instrumentation and Measurement,* vol. 51, p. 287–292, 2002.

[39] D. Belega and D. Dallet, "Amplitude estimation by a multipoint interpolated DFT approach," *IEEE Transactions on Instrumentation and Measurement,* vol. 58, p. 1316–1323, 2009.

[40] D. Belega, D. Dallet and D. Slepicka, "Accurate amplitude estimation of harmonic components of incoherently sampled signals in the frequency domain," *IEEE Transactions on Instrumentation and Measurement,* vol. 59, p. 1158–1166, 2010.

[41] T. X. Zhu, "Exact Harmonics/Interharmonics Calculation Using Adaptive Window Width," *IEEE Transactions on Power Delivery,* vol. 22, pp. 2279-2288, 2007.

[42] H. Wen, Z. Teng, Y. Wang and X. Hu, "Spectral correction approach based on desirable sidelobe window for harmonic analysis of industrial power system," *IEEE Transactions on Industrial Electronics,* vol. 60, p. 1001–1010, 2012.

[43] Y. H. Gu and M. H. J. Bollen, "Time-frequency and time-scale domain analysis of voltage disturbances," *IEEE Transactions on Power Delivery,* vol. 15, p. 1279–1284, 2000.

[44] J. Paris, J. S. Donnal, Z. Remscrim, S. B. Leeb and S. R. Shaw, "The sinefit spectral envelope preprocessor," *IEEE Sensors Journal,* vol. 14, p. 4385–4394, 2014.

[45] A. E. Emanuel and D. L. Milanez, "Clarke's alpha, beta, and zero components: a possible approach for the conceptual design of instrumentation compatible with IEEE Std. 1459–2000," *IEEE Transactions on Instrumentation and Measurement,* vol. 55, p. 2088–2095, 2006.

[46] A. Cataliotti and V. Cosentino, "A time-domain strategy for the measurement of IEEE Standard 1459-2000 power quantities in nonsinusoidal three-phase and single-phase systems," *IEEE Transactions on Power Delivery,* vol. 23, p. 2113–2123, 2008.

[47] A. Pigazo and V. M. Moreno, "Accurate and computationally efficient implementation of the IEEE 1459-2000 standard in three-phase three-wire power systems," *IEEE Transactions on Power Delivery,* vol. 22, p. 752–757, 2007.

[48] J. J. Tomic, M. D. Kusljevic and D. P. Marcetic, "An adaptive resonator-based method for power measurements according to the IEEE trial-use standard 1459–2000," *IEEE Transactions on Instrumentation and Measurement,* vol. 59, p. 250–258, 2010.

[49] S. Santoso, E. J. Powers, W. M. Grady and P. Hofmann, "Power quality assessment via wavelet transform analysis," *IEEE Transactions on Power Delivery,* vol. 11, p. 924–930, 1996.

[50] M. S. Kandil, S. A. Farghal and A. Elmitwally, "Refined power quality indices," *IEE Proceedings-Generation, Transmission and Distribution,* vol. 148, p. 590–596, 2001.

[51] J. Barros, R. I. Diego and M. De Apraiz, "Applications of wavelet transform for analysis of harmonic distortion in power systems: A review," *IEEE Transactions on Instrumentation and Measurement,* vol. 61, p. 2604–2611, 2012.

[52] W. G. Morsi and M. E. El-Hawary, "Reformulating three-phase power components definitions contained in the IEEE standard 1459–2000 using discrete wavelet transform," *IEEE Transactions on Power Delivery,* vol. 22, p. 1917–1925, 2007.

[53] S. Avdaković and N. Čišija, "Wavelets as a tool for power system dynamic events analysis–State-of-the-art and future applications," *Journal of Electrical Systems and Information Technology,* vol. 2, p. 47–57, 2015.

[54] A. Domijan, A. Hari and T. Lin, "On the selection of appropriate wavelet filter bank for power quality monitoring," *Int. J. Power Energy Syst,* vol. 24, p. 46–50, 2004.

[55] E. Y. Hamid, R. Mardiana and Z.-I. Kawasaki, "Method for RMS and power measurements based on the wavelet packet transform," *IEE Proceedings-Science, Measurement and Technology,* vol. 149, p. 60–66, 2002.

[56] J. L. Willems, "Reflections on apparent power and power factor in nonsinusoidal and polyphase situations," *IEEE Transactions on Power Delivery,* vol. 19, p. 835–840, 2004.

[57] L. Eren, M. Unal and M. J. Devaney, "Harmonic analysis via wavelet packet decomposition using special elliptic half-band filters," *IEEE Transactions on Instrumentation and Measurement,* vol. 56, p. 2289–2293, 2007.

[58] W. G. Morsi and M. E. El-Hawary, "Novel power quality indices based on wavelet packet transform for non-stationary sinusoidal and non-sinusoidal disturbances," *Electric Power Systems Research,* vol. 80, p. 753–759, 2010.

[59] V. K. Tiwari and S. K. Jain, "Hardware implementation of polyphase-decomposition-based wavelet filters for power system harmonics estimation," *IEEE Transactions on Instrumentation and Measurement,* vol. 65, p. 1585–1595, 2016.

[60] J. Bruna and J. J. Melero, "Selection of the most suitable decomposition filter for the measurement of fluctuating harmonics," *IEEE Transactions on Instrumentation and Measurement,* vol. 65, p. 2587–2594, 2016.

[61] S.-W. Sohn, Y.-B. Lim, J.-J. Yun, H. Choi and H.-D. Bae, "A filter bank and a self-tuning adaptive filter for the harmonic and interharmonic estimation in power

signals," *IEEE Transactions on Instrumentation and Measurement,* vol. 61, p. 64–73, 2011.

[62] W. G. Morsi and M. E. El-Hawary, "Wavelet packet transform-based power quality indices for balanced and unbalanced three-phase systems under stationary or nonstationary operating conditions," *IEEE Transactions on Power Delivery,* vol. 24, p. 2300–2310, 2009.

[63] C. F. Norman, J. Y. C. Chan, W.-H. Lau and L. L. Lai, "Hybrid wavelet and Hilbert transform with frequency-shifting decomposition for power quality analysis," *IEEE Transactions on Instrumentation and Measurement,* vol. 61, p. 3225–3233, 2012.

[64] M. J. Afroni, D. Sutanto and D. Stirling, "Analysis of nonstationary power-quality waveforms using iterative Hilbert Huang transform and SAX algorithm," *IEEE Transactions on Power Delivery,* vol. 28, p. 2134–2144, 2013.

[65] P. K. Dash, B. K. Panigrahi and G. Panda, "Power quality analysis using S-transform," *IEEE Transactions on Power Delivery,* vol. 18, p. 406–411, 2003.

[66] M. Biswal and P. K. Dash, "Estimation of time-varying power quality indices with an adaptive window-based fast generalised S-transform," *IET Science, Measurement & Technology,* vol. 6, p. 189–197, 2012.

[67] K. Thirumala, A. C. Umarikar and T. Jain, "Estimation of single-phase and three-phase power-quality indices using empirical wavelet transform," *IEEE Transactions on Power Delivery,* vol. 30, p. 445–454, 2014.

[68] K. Thirumala, T. Jain, A. C. Umarikar and others, "Visualizing time-varying power quality indices using generalized empirical wavelet transform," *Electric power systems research,* vol. 143, p. 99–109, 2017.

[69] A. Bracale, G. Carpinelli, Z. Leonowicz, T. Lobos and J. Rezmer, "Measurement of IEC groups and subgroups using advanced spectrum estimation methods," *IEEE Transactions on Instrumentation and Measurement,* vol. 57, p. 672–681, 2008.

[70] I. Y.-H. Gu and M. H. J. Bollen, "Estimating interharmonics by using sliding-window ESPRIT," *IEEE Transactions on Power Delivery,* vol. 23, p. 13–23, 2007.

[71] C. I. Chen, G. W. Chang, R. C. Hong and H. M. Li, "Extended real model of Kalman filter for time-varying harmonics estimation," *IEEE Transactions on Power Delivery,* vol. 25, p. 17–26, 2009.

[72] S. K. Singh, N. Sinha, A. K. Goswami and N. Sinha, "Several variants of Kalman Filter algorithm for power system harmonic estimation," *International Journal of Electrical Power & Energy Systems*, vol. 78, p. 793–800, 2016.

[73] M. S. Reza, M. Ciobotaru and V. G. Agelidis, "Instantaneous power quality analysis using frequency adaptive Kalman filter technique," in *Proceedings of The 7th International Power Electronics and Motion Control Conference*, 2012.

[74] G. W. Chang, C.-I. Chen and Q.-W. Liang, "A two-stage ADALINE for harmonics and interharmonics measurement," *IEEE Transactions on Industrial Electronics*, vol. 56, p. 2220–2228, 2009.

[75] H. C. Lin, "Intelligent neural network-based fast power system harmonic detection," *IEEE Transactions on Industrial Electronics*, vol. 54, p. 43–52, 2007.

[76] G. W. Chang, C.-I. Chen and Y.-F. Teng, "Radial-basis-function-based neural network for harmonic detection," *IEEE Transactions on Industrial Electronics*, vol. 57, p. 2171–2179, 2009.

[77] C.-I. Chen, "A two-stage solution procedure for digital power metering according to IEEE standard 1459-2010 in single-phase system," *IEEE Transactions on Industrial Electronics*, vol. 60, p. 5550–5557, 2012.

[78] S. K. Jain and S. N. Singh, "Low-order dominant harmonic estimation using adaptive wavelet neural network," *IEEE Transactions on Industrial Electronics*, vol. 61, p. 428–435, 2013.

[79] M. Artioli, G. Pasini, L. Peretto, R. Sasdelli and F. Filippetti, "Low-cost DSP-based equipment for the real-time detection of transients in power systems," *IEEE Transactions on Instrumentation and Measurement*, vol. 53, p. 933–939, 2004.

[80] C. Gherasim, J. Van den Keybus, J. Driesen and R. Belmans, "DSP implementation of power measurements according to the IEEE trial-use standard 1459," *IEEE Transactions on Instrumentation and Measurement*, vol. 53, p. 1086–1092, 2004.

[81] M. E. Salem, A. Mohamed, S. A. Samad and R. Mohamed, "Development of a dsp-based power quality monitoring instrumentfor real-time detection of power disturbances," in *2005 International Conference on Power Electronics and Drives Systems*, 2005.

[82] D. Gallo, C. Landi and N. Rignano, "Real-time digital multifunction instrument for power quality integrated indexes measurement," *IEEE Transactions on Instrumentation and Measurement,* vol. 57, p. 2769–2776, 2008.

[83] C. A. Sepúlveda, J. A. Muñoz, J. R. Espinoza, M. E. Figueroa and C. R. Baier, "FPGA v/s DSP performance comparison for a VSC-based STATCOM control application," *IEEE Transactions on Industrial Informatics,* vol. 9, p. 1351–1360, 2012.

[84] A. Cardenas, C. Guzman and K. Agbossou, "Real-time evaluation of power quality using FPGA based measurement system," in *2010 IEEE International Symposium on Industrial Electronics*, 2010.

[85] T. Tarasiuk and M. Gorniak, "Simple method of fundamental reactive power measurement for ASIC application," *IET Generation, Transmission & Distribution,* vol. 11, p. 2393–2402, 2017.

[86] M. Lopez-Ramirez, L. M. Ledesma-Carrillo, A. L. Martinez-Herrera, E. Cabal-Yepez and H. Miranda-Vidales, "FPGA-based reconfigurable unit for real-time power quality index estimation," in *2014 International Conference on ReConFigurable Computing and FPGAs (ReConFig14)*, 2014.

[87] S. Jaiswal and M. S. Ballal, "FDST-based PQ event detection and energy metering implementation on FPGA-in-the-loop and NI-LabVIEW," *IET Science, Measurement & Technology,* vol. 11, p. 453–463, 2017.

[88] G. P. Nason and T. Sapatinas, "Wavelet packet transfer function modelling of nonstationary time series," *Statistics and Computing,* vol. 12, p. 45–56, 2002.

[89] J.-C. Pesquet, H. Krim and H. Carfantan, "Time-invariant orthonormal wavelet representations," *IEEE Transactions on Signal Processing,* vol. 44, p. 1964–1970, 1996.

[90] G. D'Antona, C. Muscas, P. A. Pegoraro and S. Sulis, "Harmonic source estimation in distribution systems," *IEEE Transactions on Instrumentation and Measurement,* vol. 60, p. 3351–3359, 2011.

[91] M. S. Hamad, M. I. Masoud, K. H. Ahmed and B. W. Williams, "A shunt active power filter for a medium-voltage 12-pulse current source converter using open loop control compensation," *IEEE Transactions on Industrial Electronics,* vol. 61, p. 5840–5850, 2014.

[92] M. A. M. Radzi and N. A. Rahim, "Neural network and bandless hysteresis approach to control switched capacitor active power filter for reduction of harmonics," *IEEE Transactions on Industrial Electronics,* vol. 56, p. 1477–1484, 2009.

[93] N. Locci, C. Muscas and S. Sulis, "Investigation on the accuracy of harmonic pollution metering techniques," *IEEE Transactions on Instrumentation and Measurement,* vol. 53, p. 1140–1145, 2004.

[94] A. T. Walden, "Wavelet analysis of discrete time series," in *European Congress of Mathematics*, 2001.

[95] E. Pardo, M. A. Rodríguez-Hernández and J. J. Pérez-Solano, "Narrowband interference suppression using undecimated wavelet packets in direct-sequence spread-spectrum receivers," *IEEE Transactions on Signal Processing,* vol. 54, p. 3648–3653, 2006.

[96] H. Keskes and A. Braham, "Recursive undecimated wavelet packet transform and DAG SVM for induction motor diagnosis," *IEEE Transactions on Industrial Informatics,* vol. 11, p. 1059–1066, 2015.

[97] H. Taşmaz and E. Erçelebi, "Speech enhancement based on undecimated wavelet packet-perceptual filterbanks and MMSE–STSA estimation in various noise environments," *Digital Signal Processing,* vol. 18, p. 797–812, 2008.

[98] A. V. Oppenheim, Discrete-time signal processing, Pearson Education India, 1999.

[99] I. Carugati, C. M. Orallo, P. G. Donato, S. Maestri, J. L. Strack and D. Carrica, "Three-phase harmonic and sequence components measurement method based on mSDFT and variable sampling period technique," *IEEE Transactions on Instrumentation and Measurement,* vol. 65, p. 1761–1772, 2016.

[100] Model-Based DSP Design using System Generator, UG897 (v2014.3), October 1, 2014, Xilinx May 18, 2008.

[101] W. G. Morsi, C. P. Diduch, L. Chang and M. E. El-Hawary, "Wavelet-based reactive power and energy measurement in the presence of power quality disturbances," *IEEE Transactions on Power Systems,* vol. 26, p. 1263–1271, 2010.

[102] R. Shariatinasab, M. Akbari and B. Rahmani, "Application of wavelet analysis in power systems," in *Advances in Wavelet Theory and their applications in Engineering, Physics and Technology*, IntechOpen, 2012.

[103] V. K. Tiwari, A. C. Umarikar and T. Jain, "Fast amplitude estimation of harmonics using undecimated wavelet packet transform and its hardware implementation," *IEEE Transactions on Instrumentation and Measurement,* vol. 67, p. 65–77, 2017.

[104] I. Urbina-Salas, J. R. Razo-Hernandez, D. Granados-Lieberman, M. Valtierra-Rodriguez and J. E. Torres-Fernandez, "Instantaneous power quality indices based on single-sideband modulation and wavelet packet-Hilbert transform," *IEEE Transactions on Instrumentation and Measurement,* vol. 66, p. 1021–1031, 2017.

[105] P. A. Karafotis, V. A. Evangelopoulos and P. S. Georgilakis, "Evaluation of harmonic contribution to unbalance in power systems under non-stationary conditions using wavelet packet transform," *Electric Power Systems Research,* vol. 178, p. 106026, 2020.

[106] P. Henricci, *Applied and Computational Complex Analysis, Volume 1: Power Series Integration Conformal Mapping Location of Zero*, Wiley-Blackwell, 1997.

[107] V. Cizek, "Discrete hilbert transform," *IEEE Transactions on Audio and Electroacoustics,* vol. 18, p. 340–343, 1970.

[108] M. Vetterli, J. Kovačević and V. K. Goyal, Foundations of signal processing, Cambridge University Press, 2014.

[109] M. Sabri and W. Steenaart, "Discrete Hilbert transform filtering," *IEEE Transactions on Acoustics, Speech, and Signal Processing,* vol. 25, pp. 452-454, 1977.

[110] D. Das, K. Mukhopadhyaya and B. P. Sinha, "Implementation of four common functions on an LNS co-processor," *IEEE Transactions on Computers,* vol. 44, p. 155–161, 1995.

[111] Z. Remscrim, J. Paris, S. B. Leeb, S. R. Shaw, S. Neuman, C. Schantz, S. Muller and S. Page, "FPGA-based spectral envelope preprocessor for power monitoring and control," in *2010 Twenty-Fifth Annual IEEE Applied Power Electronics Conference and Exposition (APEC),* 2010.

[112] C. Muscas, "Power quality monitoring in modern electric distribution systems," *IEEE Instrumentation & Measurement Magazine*, vol. 13, p. 19–27, 2010.